Photodynamics of a flavin based blue-light regulated phosphodiesterase protein and its photoreceptor BLUF domain

Dissertation

Zur Erlangung des Doktorgrades der Naturwissenschaften

(Dr. rer. nat.)

der Naturwissenschaftlichen Fakultät II – Physik

der Universität Regensburg

vorgelegt von

Amit Tyagi

aus

Hapur, India

Regensburg 2009

Diese Arbeit wurde angeleitet von: Prof. Dr. A. Penzkofer.

Promotionsgesuch eingereicht am: 20.01.2009

Promotionskolloquium am: 20.03.2009

Prüfungsausschuss:

Vorsitzender: Prof. Dr. I. Morgenstern

1. Gutachter: Prof. Dr. A. Penzkofer

2. Gutachter: Prof. Dr. J. Zweck

Weiterer Prüfer: Prof. Dr. J. Repp

Dedicated to my Parents

Table of Contents

1   Introduction

Light plays a crucial role for life on earth. It is one of the most important environmental factors for the living organisms. The energy of the sun is converted to chemical energy by plants and several micro-organisms via photosynthesis. In addition, light also functions as an information carrier, for example in vision and regulation of day and night cycles. This information is then used to change the behaviour or physiology. Hence, to be able to monitor their light environment and respond to changes in the light-climate, organisms have developed elaborate systems for perception and transduction of light signals, allowing them to adjust growth and development optimally to the prevailing light conditions. Photosensory receptors are the elegant molecular machines responsible for this. These photoreceptors are not only able to distinguish between light on and off, but they can also use the total information that is present in the light. This information includes (i) irradiance, (ii) the colour or spectral distribution, (iii) the direction of light and (iv) the polarization of light [Bat03].

1.1   Photoreceptors

Photoreceptors are the molecular machines used by organisms to detect light. All photoreceptors known till now consist of a protein moiety with one or several chromophores (called co-factor) which are covalently or non-covalently bound to the protein. The chromophore absorbs the photons and the protein moiety is required to transduce the primary light signal to downstream components. The absorption of light by the chromophore may result in a change of its configuration and/or the protein binding pocket of the chromophore, which initiates a series of events that result in a transient change in the tertiary structure of the photoreceptor protein. This light-induced meta-stable state of the receptor protein, generally referred to as the signaling state, communicates the process of photon-absorption from the

1

receptor part to the signal transduction protein part, ultimately resulting in a response of the organism.

There are six major families of photoreceptors known: the rhodopsins, the phytochromes, the xanthopsins, the cryptochromes/photolyases, the phototropins and the BLUF proteins. Only a small number of chromophore classes have been found in these photoreceptors. These chromophore classes are: retinals- present in rhodopsins; linear tetrapyrroles - present in phytochromes, thiol-ester linked 4-hydroxy - cinnamic acid (p-coumaric acid) - present in xanthopsins, the flavins - present in BLUF proteins, cryptochromes and phototropins; the folate derivative 5, 10-methenyltetrahydrofolate - present as second chromophore in cryptochromes/photolyases [Bat03].

1.1.1 Photo-isomerisation based photoreceptors

In the photoisomerisation based photoreceptors light absorption causes an isomerisation of the light sensitive chromophore. To the photoisomerisation based photoreceptors belong the rhodopsins (chromophore retinal) which respond to green light (green light photoreceptor), the phytochromes (chromophore tetrapyrrole) which respond to red light (red light photoreceptor) and the xanthopsin (chromophore p-coumaric acid) which respond to blue light (blue light photoreceptor).

The rhodopsins are the family of photoreceptors that has been characterized in most detail with respect to structure, function and mechanisms of activation and signal transduction. Rhodopsins are green light photoreceptors. Rhodopsins are found in the microorganisms - prokaryotes (cells with no nucleus) as bacteria (archea and eubacteria), eukaryotes (cells with nucleus) as algae, fungi and in animals (vertebrates and invertebrates). Rhodopsin serves as the primary light receptor protein in the visual system of all animals investigated so far, independent of the structural and functional complexity, of the optical apparatus, or of the neuronal networks which animals have developed to analyze and process the information

2

encoded in a light signal [Ben03]. The visual rhodopsins have 11-*cis*-retinal as receptor state cofactor which changes to all-*trans*-retinal in the signaling state by photoisomerisation [Rid07]. One form of rhodopsins, the channelrhodopsins, work as light-gated ion channels (pores which open or close in response to light and establish and control the small voltage gradient across the membrane of living cells by allowing the flow of ions down their electrochemical gradient). Some other forms e.g. bacteriorhodopsin, proteorhodopsin, halorhodopsin act as proton pumps i.e. they capture light energy and use it to move protons across the membrane out of the cell. The resulting proton gradient is subsequently converted into chemical energy. The channelrhodopsin, bacteriorhodopsin and proteorhodopsin contain all *trans*-retinal as the receptor state cofactor which on excitation turns to 13-*cis*-retinal by photoisomerisation [Nag03, Kre02]. Several new members of the rhodopsin family have been identified recently in algae [Sin02], proteobacteria [Bej00] cyanobacteria [Jun03]. The structure of bacteriorhodopsin, containing a seven-transmembrane helix motif, was resolved as the first molecular structure of a membrane protein [Hen75].

The chromophore, retinal, consists of a β-ionylidene ring bonded to a five double bonded polyene chain. It is covalently linked via protonated Schiff base to Lysine located in the transmembrane helix seven. Figure 1.1(a) shows an all *trans* structure of the retinal. The
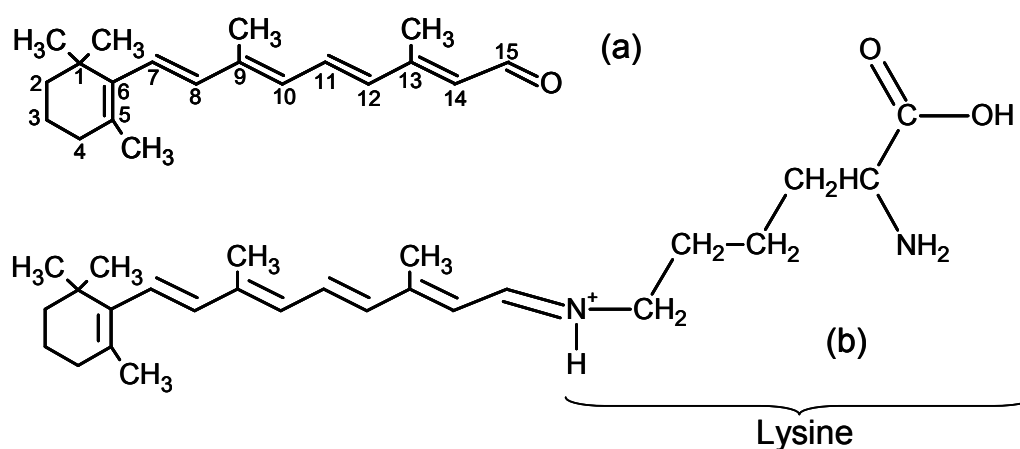
Figure 1.1   (a) All *trans* configuration of retinal, (b) Binding of retinal as protonated Schiff base to the amino acid lysine in visual rhodopsin.

part (b) shows how the retinal is bound to the protein by connecting to the amino acid, lysine.

The photocycle of different rhodopsins occur via photoisomerisation from *trans* to *cis* or from *cis* to *trans* at different places along the polyene chain. The photocycle goes through many intermediates and is completed within 1 μs to 100 ms [Xia 00, Yan91].

The phytochromes are the photoreceptors responsible for red/far-red light reversible plant responses. They are the red-light photoreceptors. Important plant responses regulated by phytochromes are seed germination, photoperiodic flowering, plant stem elongation, chloroplast movement, leaf senescence (aging of a leaf) and leaf abscission (shedding of a leaf). The chromophore responsible for the activity of phytochrome is a linear tetrapyrrole [Yeh98]. Red light triggers a photoisomerisation of red absorbing "Pr" (absorption peak at 666 nm) to far-red absorbing "Pfr" conformation (absorption peak at 730 nm). The Pfr form is the active form that initiates biological responses.

$$\text{Pr} \underset{\text{far red}}{\overset{\text{red}}{\rightleftharpoons}} \text{Pfr} \longrightarrow \text{Biological Activity}$$
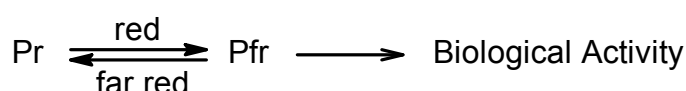
The Pfr form can revert back to Pr form in the dark over a time scale of hours or almost instantaneously via absorption of far red light (photoinduced back transfer). During these transitions, structural changes take place in the protein that lead to the initiation of the response. The structure of the linear tetrapyrrole is shown in Fig 1.2. It is attached to the
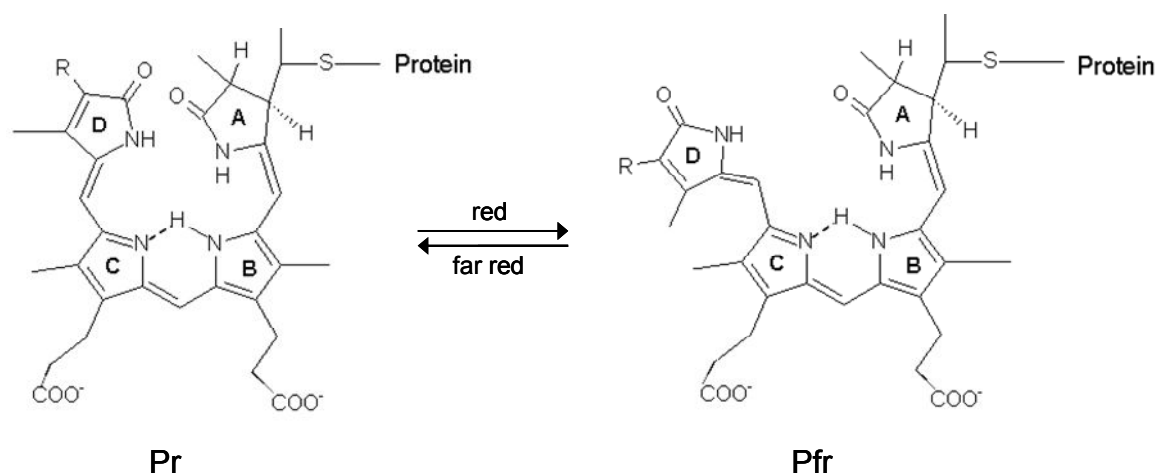
Figure 1.2   Structure of linear tetrapyrrole in the Pr and Pfr forms of phytochromes.

phytochrome protein through a sulphur linkage. The absorption spectra of phytochromes in Pr and Pfr states is shown in Fig.1.3
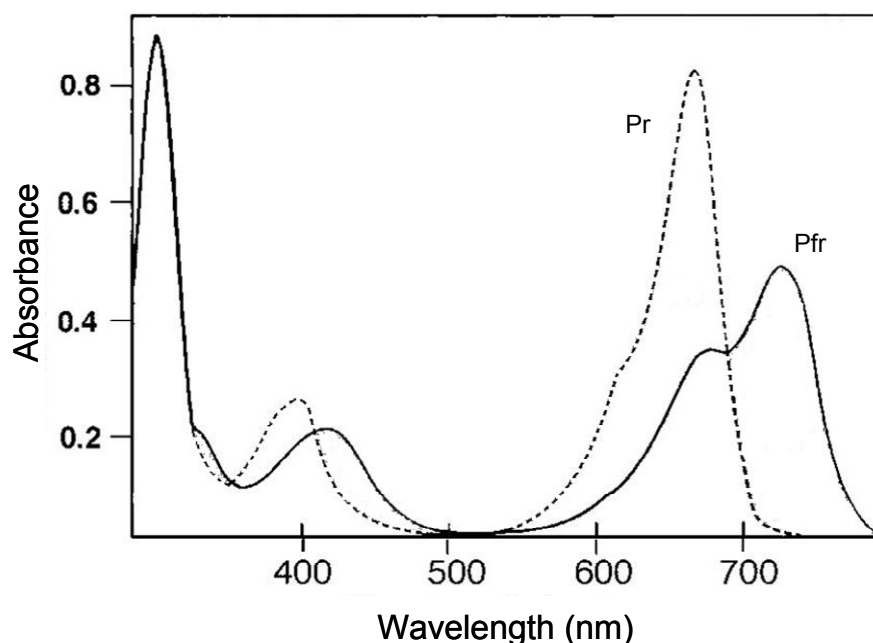
Figure 1.3   Absorption spectra of the two forms (Pr and Pfr) of phytochromes [Wan02]. The Pr form absorbs maximally at 666 nm, while the Pfr form absorbs maximally at 730 nm.

The most studied member of **xanthopsins** is Photoactive Yellow Protein (PYP), a yellow coloured protein isolated for the first time from halophillic phototropic bacterium *Halorhodospira halophila* [Mey85] and later found in many other proteobacteria. They are blue light photoreceptors. PYP is responsible for the negative phototactic response (moving out of the illuminated region) of the *H. halophila*. The chromophore in xanthospins is a covalently bound *trans*-p-hydroxy cinnamic acid (also called p-coumaric acid) cysteine thioester. On photon absorption the chromophore undergoes *trans-cis* isomerization. Afterwards a proton is transferred from a nearby amino acid (glutamine) to the chromophore [Kor96, Xie96, Ima97] and a global conformation change of the protein moiety takes place which leads to formation of signaling state [Bre95, Rub98, Hof99, Ohi01]. More detailed information on the photocycle and other aspects of xanthopsins is given in the chapter 5 on

blue light photoreceptors. An absorption spectra of PYP in receptor state and in signaling state is shown in Fig. 1.4
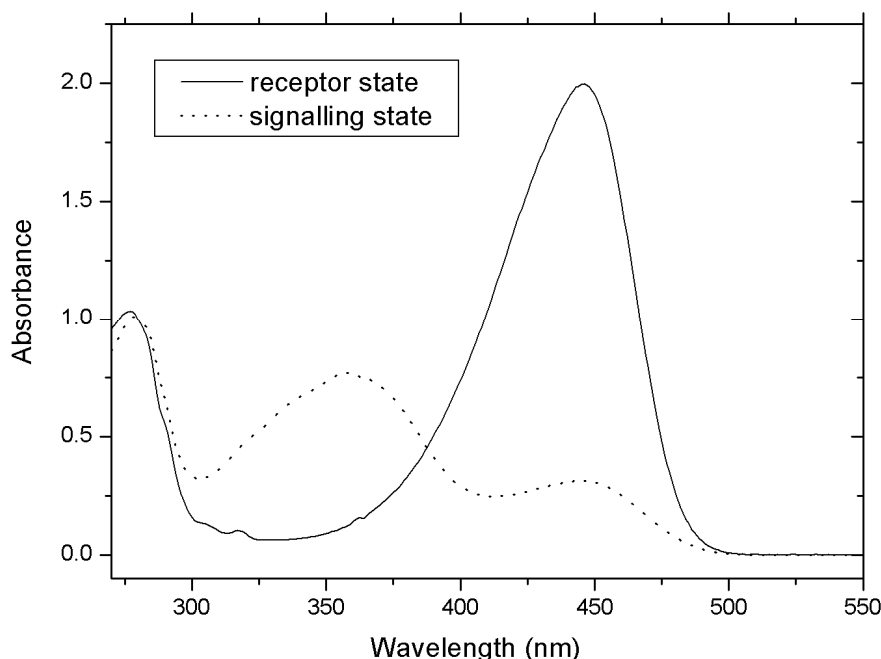
Figure 1.4   Absorption spectra of PYP from *E. halophilla* in receptor state and of M100A mutant (exposed to 450 nm light) in signaling state [Ghe97].

1.1.2 Redox based blue light photoreceptors using flavin chromophore

In contrast to their functional diversity, the rhodopsins, phytochromes and xanthopsins share the same mechanism of activation: Light-induced E/Z isomerization of a particular double bond in their chromophore. The cryptochromes, phototropins and BLUF proteins all contain a flavin as their chromophore, which lacks an isomerizable double bond. Accordingly, other mechanisms underlie activation of these blue-light photoreceptors

Flavins play an important role in many biological systems. Flavo-enzymes have the capability of catalyzing a wide range of biological reactions like dehydrogenation of a variety of metabolites, one- and two- electron transfer processes to and from redox centers and hydroxylation reactions [Mas95]. The tricyclic isoalloxazine system is the reactive part of the flavins, capable of undergoing reversible oxidation and reduction. The molecules when

6

oxidized have a bright yellow color due to the absorption of blue light ($\lambda_{max} \approx 450$ nm). An overview of the flavins is given in chapter 3.

During the last 15 years three families of photoreceptors have been discovered which use flavin molecules as their chromophore namely- the cryptochromes [Ahm93], the phototropins [Hua97] and the BLUF proteins [Gom02].

The cryptochromes are found in both lower and higher eukaryotes including mammals (like *Homo sapiens),* insects *(Drosophila),* plants, algae *(Chlamydomonas)* and in one prokaryote *(Synechocystis).* They are involved in processes like synchronization of the circadian clock, seed germination and regulation of pigment synthesis [Lin03]. These proteins contain two non-covalently bounded chromophores in their binding pocket, FAD (flavin-adenine dinucleotide) as key cofactor and the folate derivative 5,10-methenyltetrahydrofolate (MTHF) as light antenna [San00, Pok05]. The photocycle of cryptochromes is based on changes in the FAD redox state [Bou07, Son06]. Detailed information on the structure and photocycle of cryptochromes is given in chapter 5.

The photoropins are another class of blue light photoreceptors getting their name because of their involvement in phototropism in plants (bending of plants towards the light) [Chr99]. Phototropins also control other blue light regulated activities in plants like stomatal opening, leaf expansion etc. [Chr01]. The light sensitive domain that is responsible for the photoresponse of phototropins is referred to as LOV domain (Light-Oxygen-Voltage domain) [Hua97]. It non-covalently binds oxidized flavin mononucleotide (FMN) as chromophore [Chr99, Sal00].

The photocycle of LOV domains is based on the formation of a covalent adduct between the C4 atom of the isoalloxazine ring and the sulfur of a conserved nearby cysteine amino acid (see chapter 5). The covalent adduct subsequently thermally decays relatively slowly to the ground-state, with rates varying between 10^{-1} and 10^{-4} s^{-1} [Ken03, Kot03, Swa01, Hol04]. Adduct formation results in disruption of the planar configuration of the flavin, which

leads to conformational changes in the LOV domain [Cro02, Fed03, Sal01]. More detailed information on the structure and photocycle of phototropins is given in chapter 5.

The BLUF protein family is the most recently discovered family of blue light photoreceptors [Gom02]. BLUF stands for "Blue Light sensing Using FAD" since the chromophore involved is FAD, bound non-covalently in the protein binding pocket. The proteins of this family have been found to be involved in photophobic responses in *Euglena gracilis* (PAC protein, [Ise02]) and *Synechocystis* (Slr1694 protein, [Oka05]) and transcriptional regulation in *Rhodobacter sphaeroides* (AppA protein, [Mas02]).

Blue-light excitation of a dark-adapted BLUF domain (receptor state) leads to a red-shifted signalling state, which recovers to the initial absorption behaviour in the dark. The signaling state formation is understood to be due to electron transfer from a neighbouring
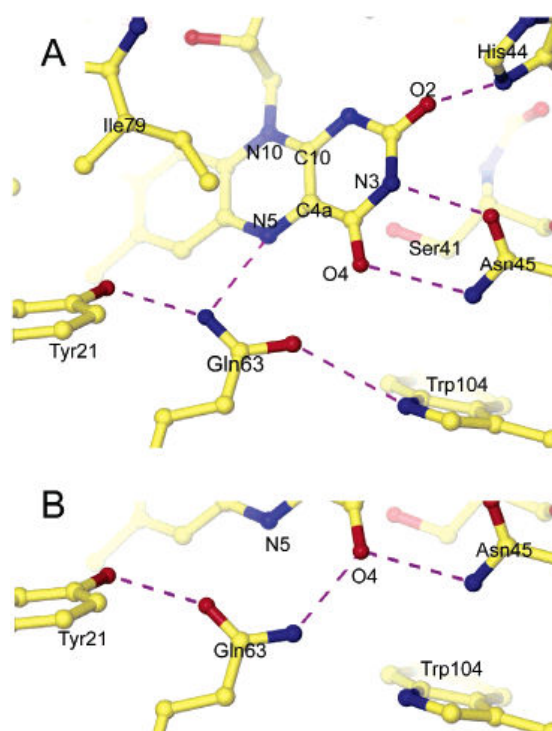
Figure 1.5   Hydrogen bond network to the flavin in AppA crystal. Hydrogen bonds are shown as dashed lines. (A) Hydrogen bond network in dark state orientation of Gln63 (B) Alternate hydrogen bond network with rearrangement of hydrogen bonds network after illumination with blue light. [And05].

amino acid (generally tyrosine) to the flavin followed by hydrogen bond restructuring around the flavin. The crystal structure of AppA in light and dark state is shown in Fig. 1.5. The BLUF proteins are explained in more details in chapter 5.

1.2   Aims and Outline

The study of BLUF proteins is currently an active field of research. The BLUF domains of a few BLUF proteins have been cloned, overexpressed, purified, and spectroscopically investigated. These include, AppA and BlrB from *R. sphaeroides* [Gom98, Bra02, Mas02, Jun05, Zir06], Tll0078 (also called TePixD) from *Thermosynechococcus elongatus* [Oka06, Tak07, Fuk05, Kit05], Slr1694 (also called PixD) from *Synechocystis* sp. PCC6803 [Has04, Has05, Mas04, Mas04, Oka05, Gau06, Zir07a], photoactivated adenylyl cyclase PAC from the unicellular flagellate *Euglena gracilis* [Ise02], and protein YcgF (BlrP) from *Escherichia coli* [Gom98, Raj04, Mas05, Has06]. Crystal structures have been published for the BLUF domains AppA [And05], a mutant of AppA, AppA-C20S [Jun06], BlrB [Jun05], Tll0078 [Kit05], and Slr1694 [Yua06].

Here a recently expressed BLUF domain and a BLUF-EAL domain from the enteric (intestinal) bacterium *Klebsiella pneumoniae* is studied by optical spectroscopic methods in some detail and the photocycle dynamics is revealed experimentally and analysed theoretically.

Klebsiella pneumoniae is an enteric bacterium present in the gastrointestinal tracts, primarily in the colon (or "large" bowel) of humans and many other animals. *K. pneumoniae* contains two BLUF proteins namely, BlrP1 and BlrP2 (BlrP stands for <u>b</u>lue <u>l</u>ight-<u>r</u>egulated phosphodiesterase). The BlrP1 protein from the enteric bacterium *Klebsiella pneumoniae* consists of a BLUF and an EAL domain (EAL domain contains: glutamic acid (E), alanine (A), leucine (L)). It is predicted to activate c-di-GMP phosphodiesterase (an enzyme

responsible for breaking a phosphodiester bond) upon activation by blue-light. This protein has been cloned, overexpressed and purified by M. Gomelsky and I. Schlichting [Tya08]. Both, the BlrP1 BLUF domain and the full length BlrP1 protein containing the BLUF and EAL domain have been expressed. Since the protein with only the BLUF domain may behave differently compared to a full protein that consists of both BLUF and EAL domain, the full protein (denoted as BlrP1) and the BLUF domain alone (denoted as BlrP1_BLUF) have been studied in this work.

In contrast to other BLUF domains studied so far, BlrP1_BLUF contains no tryptophan (Trp or W). Trp was discussed to play a crucial role in the photocycle dynamics of previously studied BLUF domains. This work has shown that the essential photocycle dynamics remains even in the absence of Trp.

The present work is structured as: Chapter 2 deals with the fundamentals of photophysics, photochemistry and photobiology which are needed to understand and analyse the results of the experiments. Since the BLUF proteins have flavin as chromophore, some knowledge of the flavins and their photochemistry is needed. This has been provided in chapter 3. Chapter 4 presents a brief description of proteins so as to give a biological background for understanding of BLUF proteins. Chapter 5 gives some characterization of the different blue light photoreceptor families including the BLUF proteins. The experimental methods which were employed are explained in Chapter 6. The experimental results of the investigated samples (BlrP1 protein and the BlrP_BLUF from *K. pneumoniae*) together with a developed theoretical dynamics model and analysis are given in chapter 7. Chapter 8 compares the investigated proteins with other BLUF proteins and gives a generalized model description applicable to photodynamics of all BLUF domains studied so far. A short summary and the outlook in chapter 9 end the dissertation.

2 Photophysical, photochemical and photobiological fundamentals

The absorption of light resulting in the excitation of an electron from a lower to a higher molecular quantum state is the first step towards some final photochemical product. The excited molecule is energetically unstable with respect to the ground state. If the excited molecule does not rearrange or fragment, it will lose its excitation energy and will return to the ground state. There are a number of de-excitation pathways and the ones which are most favourable depend on the type of the molecule and nature of the electronic states involved. This chapter deals with these processes which are fundamental to understanding the photophysics, photochemistry and photobiology discussed in the following chapters.

2.1 Absorption of light

The efficiency of light absorption at a wavelength λ by an absorbing medium is characterized by the absorbance $A(\lambda)$ or the transmittance $T(\lambda)$ defined as

$$A(\lambda) = \log(\frac{I_\lambda^0}{I_\lambda}) = -\log[T(\lambda)]$$
$$T(\lambda) = \frac{I_\lambda}{I_\lambda^0}$$

(2-1)

where I_λ^0 and I_λ are the light intensities of the beams entering and leaving the absorbing medium, respectively. At low excitation intensities, the absorbance of a sample follows the Lambert-Beer law

$$A(\lambda) = \varepsilon(\lambda) l C$$

(2-2)

where $\varepsilon(\lambda)$ is the molar decadic extinction coefficient (common unit: liter $mol^{-1}cm^{-1}$ = 1 M $^{-1}cm^{-1}$ with 1 liter=1 dm^3 and 1 M = 1 mol dm^{-3}), C is the concentration (in mol $liter^{-1}$) of the absorbing species and l is the path length through the absorbing medium (in cm).

The absorption coefficient is defined as

$$\alpha(\lambda) = \frac{1}{l}\ln\left(\frac{I_\lambda^0}{I_\lambda}\right) \qquad \text{or} \qquad I_\lambda = I_\lambda^0 e^{-\alpha(\lambda)l} \qquad\qquad (2\text{-}3)$$

The absorption coefficient is proportional to the number density, N, of molecules in the absorbing medium (unit: cm^{-3}). The proportionality constant is the molecular absorption cross-section, $\sigma(\lambda)$, characterizing the photon capture area of a molecule;

$$\sigma(\lambda) = \frac{\alpha(\lambda)}{N} \qquad\qquad (2\text{-}4)$$

2.2 Intramolecular photophysical processes

2.2.1 De-excitation of electronically excited molecules

The energy gained by a molecule when it absorbs a photon causes an electron to be promoted to a higher electronic energy level. The intramolecular transitions can be illustrated graphically by the Perrin-Jablonski diagram (Fig. 2.1). In Fig. 2.1, the symbols S_0, S_1, S_2 refer to the ground electronic singlet state, first excited singlet state, second excited singlet state, and triplet states are denoted with T_1, T_2 …. Thicker lines represent the lowest vibrational level of each state and the thinner lines are vibrational levels of that state. The boxes detail the electronic spins in the considered orbital with electrons shown as up and down arrows to distinguish their spin direction. Nearly all organic and biological molecules (a few
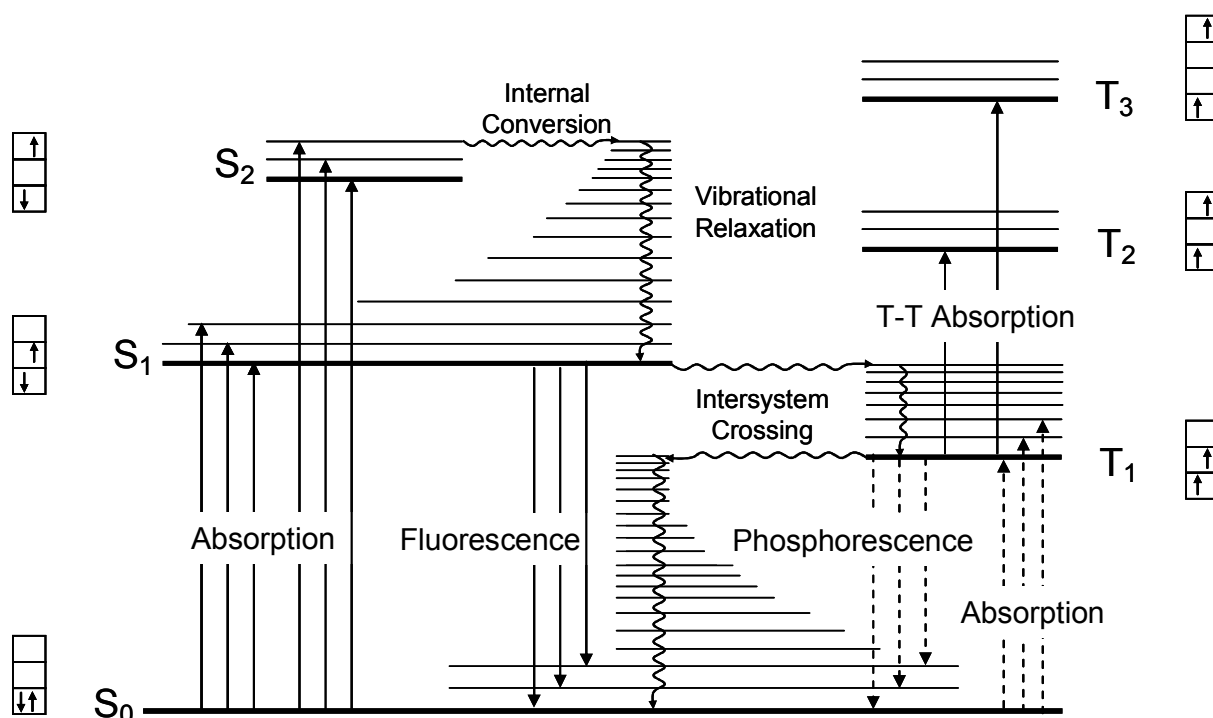
Figure 2.1 Perrin-Jablonski Diagram – It is a term diagram for a molecule with singlet and triplet systems, explaining the most important radiative and non-radiative processes. The boxes show the spins of electrons in the singlet states (opposite orientation) and the triplet states (same orientation) [Hak04].

exceptions exist) have a singlet ground state. The absorption of a photon is extremely fast ($\approx 10^{-15}$ s) with respect to all other processes, so the positions of the nuclei are unchanged in the molecular entity and its environment during the excitation process (Franck-Condon Principle) [Hak04]. Absorption of a photon brings a molecule to one of the vibrational levels of S_1, S_2... followed by different de-excitation processes: fluorescence, internal conversion, intersystem crossing, phosphorescence, delayed fluorescence [Lak99, Val 02].

 Internal Conversion is an iso-energetic transition between two electronic states of the same multiplicity. When a molecule is excited to a higher singlet state (S_n, $n \geq 2$), internal conversion and vibrational relaxation leads the excited molecule towards the lowest vibrational level of the S_1 state in $\approx 10^{-13}$ s. The excess vibrational energy is transferred to the solvent during collisions of the excited molecule with the solvent molecules. The efficiency of

13

internal conversion decreases with increasing energy gap between the electronic states involved. Thus the internal conversion $S_1 \rightarrow S_0$ is much less efficient than the $S_2 \rightarrow S_1$ internal conversion, the gap between S_1 and S_0 being much larger than the other. [Lak99, Val 02]. Internal conversion combined with subsequent vibrational relaxation is sometimes simply named internal conversion.

Fluorescence is defined as radiative transition from an excited electronic state (usually the first singlet excited state, S_1) to a lower lying state of the same spin multiplicity (usually the singlet ground state of the molecule, S_0) [Lak99]. The fluorescence spectrum is located at higher wavelengths (lower energy) than the absorption spectrum because of energy loss in the excited state due to the vibrational relaxation (Fig. 2.1) and because of the vibrational level population in the (Franck Condon) ground level. The gap between the maximum of the first absorption band and the maximum of the fluorescence band is called the Stokes shift. According to the Boltzmann law, at room temperature a small fraction of molecules is in vibrational levels higher than level 0, both in the ground state and in the excited state, therefore, the short wavelength fluorescence tail overlaps with the long wavelength absorption tail [Lak99, Val 02].

Intersystem crossing is an isoenergetic transition between two electronic states having different spin multiplicities. As is shown in Fig. 2.1, an excited molecule in 0 vibrational level of S_1 state can move to an isoenergetic vibrational level of the T_n triplet level; then vibrational relaxation (if $T_n = T_1$) or combined internal conversion ($T_n \rightarrow T_{n-1}$, ……) and vibrational relaxation brings it to the lowest vibrational level of T_1. Intersystem crossing is forbidden by the spin conservation law, but spin - orbit coupling slightly breaks the selection rule and makes it slightly allowed. The efficiency of spin-orbit coupling increases with the fourth power of the atomic number, therefore intersystem crossing is favoured by the presence of heavy atoms (called heavy atom effect) [Val 02].

Phosphorescence is the radiative de-excitation from an excited state involving a change of spin multiplicity. The most relevant phosphorescence is due to $T_1 \rightarrow S_0$ emission. Because the transition $T_1 \rightarrow S_0$ is forbidden (but made possible by spin-orbit coupling), the corresponding radiative rate constant is generally very low. A molecule which has been excited to a higher triplet state loses its energy, via a rapid series of non-radiative processes (internal conversion and vibrational relaxation bringing it to the T_1 state). When it arrives at the lowest triplet state T_1, it may release its remaining excitation energy radiatively by $T_1 \rightarrow S_0$ phosphorescence emission and non-radiatively by $T_1 \rightarrow S_0$ intersystem crossing followed by S_0 state vibrational de-excitation. The lowest triplet state is metastable, its lifetime (phosphorescence decay time) may be up to minutes [Val 02].

Delayed Fluorescence occurs due to reverse intersystem crossing $T_1 \rightarrow S_1$ that may occur if the energy difference between S_1 and T_1 is small. This results in a delayed fluorescence emission, but with a longer decay time constant than the direct fluorescence emission because molecules stay for some time in the triplet state before emitting from S_1 [Val 02].

2.2.2 Fluorescence lifetime

As seen in the previous section, de-excitation of an excited molecule occurs via several processes, radiative and non-radiative ones. The rate constants are denoted as:

k_r: rate constant for radiative deactivation $S_1 \rightarrow S_0$ with emission of fluorescence

k_{ic}: rate constant for internal conversion $S_1 \rightarrow S_0$.

k_{isc}: rate constant for intersystem crossing $S_1 \rightarrow T_1$.

k_F: rate constant of excited-state deactivation (inverse of fluorescence lifetime).

The total rate constant of non-radiative decay is denoted as k_{nr}, and given by $k_{nr} = k_{ic} + k_{isc}$. After excitation, let $[^1A^*]$ number density of molecules be in the excited state S_1 at time 0.

These excited molecules return to S_0 either radiatively or non-radiatively. The rate of decrease of the number density of excited molecules is given by

$$\frac{-d\left[{}^1A^*\right]}{dt} = (k_r + k_{nr})\left[{}^1A^*\right]$$

(2-5)

If $\left[{}^1A^*\right]_0$ is the number density of excited molecules at time 0 after excitation then solving eq.2-5 gives

$$\left[{}^1A^*(t)\right] = \left[{}^1A^*\right]_0 \exp(\frac{-t}{\tau_F}),$$

(2-6)

where $\tau_F = k_F^{-1}$ is the lifetime of the excited state S_1 given by

$$\tau_F = \frac{1}{k_r + k_{nr}}$$

(2-7)

If the only way of de-excitation from S_1 to S_0 were fluorescence emission, the lifetime would be $\frac{1}{k_r}$ which is called the radiative lifetime, τ_{rad}. The radiative lifetime can be calculated theoretically from the absorption cross-section spectrum and fluorescence spectrum using the Strickler-Berg relation [Str62, Bir63] which is derived from the Einstein A coefficient for spontaneous emission and the Einstein B coefficient for absorption and stimulated emission. The relation reads

$$\frac{1}{\tau_{rad}} = \frac{8\pi c_0 n_F^3}{n_A} \frac{\int_{em} E_F(\lambda)d\lambda}{\int_{em} E_F(\lambda)\lambda^3 d\lambda} \int_{abs} \frac{\sigma_a(\lambda)}{\lambda}d\lambda$$

(2-8)

n_F is the average refractive index in the fluorescence region, n_A is the average refractive index in the region of the first absorption band, $E_F(\lambda)$ is the fluorescence quantum distribution, and $\sigma_a(\lambda)$ is the absorption cross section spectrum. The integrals extend over the fluorescence region (em) and over the $S_0 \rightarrow S_1$ absorption band (abs).

2.2.3 Fluorescence quantum yield

The fluorescence quantum yield, ϕ_F, is the ratio of the number of intrinsically emitted photons over the whole wavelength region to the number of absorbed photons [Pen87, Hol99]:

$$\phi_F = \frac{\int_{em} S_i(\lambda)d\lambda}{S_{abs}} = \frac{h\nu_L \int_{em} S_i(\lambda)d\lambda}{W_L(1-T_L)} \tag{2-9}$$

where $S_i(\lambda)$ is the intrinsic spectral fluorescence photon density distribution, T_L is the transmittance, W_L is the input excitation energy and $\nu_L = \dfrac{c_0}{\lambda_L}$ is the excitation frequency.

The fluorescence quantum distribution, $E_F(\lambda)$, is defined as the spectral fluorescence photon density distribution $S_i(\lambda)$ over the total number of absorbed photons, i.e.

$$E_F(\lambda) = \frac{S_i(\lambda)}{S_{abs}} \tag{2-10}$$

The fluorescence quantum yield is given by

$$\phi_F = \int_{em} E_F(\lambda)d\lambda \tag{2-11}$$

The measured spectral fluorescence photon density distribution $S_m(\lambda)$ is proportional to the intrinsic spectral fluorescence photon density distribution $S_i(\lambda)$, the proportionality

factor depending on the fluorescence absorption, re-emission, reflection and the instrumental conditions. To avoid measuring all these factors, a reference dye of known fluorescence quantum yield and similar transmission is measured under the same instrumental conditions. The quantum yield for the measured sample in the case of fixed input energy W_L is given by

$$\phi_F = \frac{\int_{em} S_{i,S}(\lambda)d\lambda}{\int_{em} S_{i,R}(\lambda)d\lambda} \frac{(1-T_{L,R})}{(1-T_{L,S})} \phi_R = \frac{\int_{em} S_{m,S}(\lambda)d\lambda}{\int_{em} S_{m,R}(\lambda)d\lambda} \frac{(1-T_{L,R})}{(1-T_{L,S})} \frac{n_{F,R}^2}{n_{F,S}^2} \phi_R \qquad (2\text{-}12)$$

where $S_{i,S}(\lambda)$ and $S_{i,R}(\lambda)$ are the intrinsic spectral fluorescence photon density distribution for the sample and the reference, $S_{m,S}(\lambda)$ and $S_{m,R}(\lambda)$ are the measured spectral fluorescence photon density distribution for the sample and the reference, and $T_{L,S}$ and $T_{L,R}$ represent the transmittance of the samples and the reference respectively. The refractive index quotient takes care of different collection solid angles of the detector depending on the sample refractive index (refraction angle is refractive index dependent) [Pen87].

In the case of excitation of an absorbing medium with only one absorbing species and only photophysical relaxation (no excited state chemistry), the fluorescence quantum yield is given by the ratio of the rate constant of emission of photons to the total rate constant of de-excitation [Lak99]:

$$\phi_F = \frac{k_r}{k_r + k_{nr}} = \frac{k_r}{k_F} \qquad (2\text{-}13)$$

This ratio is equal to

$$\phi_F = \frac{\tau_F}{\tau_{rad}} \qquad (2\text{-}14)$$

2.3 Intermolecular photophysical processes

Along with the intramolecular interactions (or the intrinsic pathways) of de-excitation of an excited molecule M^* there may be intermolecular interactions responsible for de-excitation of molecules. These interactions also lead to a reduction of the fluorescence quantum yield. The process of reduction of fluorescence of an excited molecule by other molecules is called fluorescence quenching. The species responsible for the quenching is called a quencher. The main intermolecular photophysical processes responsible for de-excitation of molecules are collisional (or dynamic) quenching, excimer formation, exciplex formation, electron transfer, proton transfer and energy transfer.

In collisional (or dynamic) quenching, the excited fluorophore gives its excitation to the quencher (Q) in near distance. This leads to a decrease in the fluorescence quantum yield and shortens the fluorescence lifetime. This process may be diffusion controlled in liquids and gases. For efficient quenching the excited molecule has to move to a quencher or a quenching molecule has to move to the excited molecule within the excited-state lifetime.

In static quenching, the quencher is already in near contact to the fluorophore (within a sphere of effective quenching, the fluorophore and quencher form a ground state non-fluorescent complex) and deactivates the excitation non radiatively. In the ideal case of static fluorescence quenching the fluorescence quantum yield of the fluorophore-quencher complex is zero. The sphere of effective quenching extends over a radius R_q. The system exhibits a biphasic behaviour, all the molecules with a quencher within R_q do not fluoresce ($\tau_{F,q}= 0$, $\phi_{F,q} = 0$), and the other molecules with quencher outside R_q behave normal fluorescing and follow the dynamic quenching behaviour (τ_F normal, ϕ_F normal).

The formation of a non-fluorescent complex is given by the reaction

$$M+Q \rightleftharpoons MQ \tag{2-15}$$

The fluorescence intensity of M in a solution decreases upon addition of Q [Lak99].

Exciplexes are excited-state complexes formed between an excited state molecule and a different ground state molecule. The complex is held together by favourable orbital interactions as well as Coulombic binding forces. The electronic excitation is shared by the donor and the acceptor molecules

$$D^* + A \rightleftharpoons (DA)^* \tag{2-16}$$

$$A^* + D \rightleftharpoons (DA)^*$$
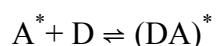
Excimers are excited state complex formed between an excited state molecule and a ground state molecule of the same species. They are formed by collision between an excited molecule and an identical unexcited molecule.

$$M^* + M \rightleftharpoons (MM)^* \tag{2-17}$$

The electronic excitation is delocalized over the two moieties [Lak99, Val 02].

Energy transfer and electron transfer between a donating molecule and an accepting molecule may occur by photo-excitation according to

$$D^* + A \rightleftharpoons D + A^* \text{ (excitation or energy transfer)},$$

$$D^* + A \rightleftharpoons D^+ + A^- \text{ (oxidative electron transfer)},$$

$$D + A^* \rightleftharpoons D^+ + A^- \text{ (reductive electron transfer)}.$$
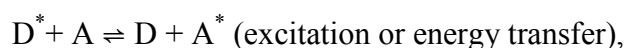
These processes are dealt with in the following sections.

2.3.1 Excitation energy transfer

Energy transfer is an important mechanism responsible for quenching of molecular emission of a donor molecule by transfer of the excitation energy from an excited donor (D^*)

to an initially un-excited acceptor (A) which may emit or non-radiatively relax. This bimolecular reaction is given by

$$D^* + A \rightarrow D + A^* \tag{2-18}$$

The excitation energy provided initially to D by photon absorption appears in A. For this kind of reaction to occur, the energy level difference between A^* and A must be lower than or equal to the energy level difference between D^* and D. Different energy transfer processes can be distinguished:

1. Radiative (or trivial) energy transfer

2. Non-radiative resonant energy transfer

   - Coulombic (Förster type) energy transfer.

   - Exchange interaction (Dexter type) energy transfer.

1. *Radiative energy transfer*

In this process the emission from D^* is reabsorbed by A.

$$D^* \rightarrow D + h\nu, \ \ A + h\nu \rightarrow A^* \tag{2-19}$$

This process is called the trivial energy transfer. It requires that the emission spectrum of D* and absorption spectrum of A overlap.

Radiative energy transfer results in a decrease of the donor fluorescence intensity in the region of spectral overlap with the absorption of the acceptor. This is called inner filter effect. The fraction, a, of the photons emitted by D which are absorbed by A is given by [Val02]

$$a = \frac{1}{\phi_D^0} \int_0^\infty E_{F,D}(\lambda)(1 - 10^{-\varepsilon_A(\lambda)C_A l}) d\lambda \tag{2-20}$$

where C_A is the concentration of acceptor molecules (in mol dm^{-3}), $\phi_D^0 (= \int_{em} E_{F,0}(\lambda)d\lambda)$ is the fluorescence quantum yield of the donor molecules in the absence of an acceptor, l is the sample thickness, $E_{F,D}(\lambda)$ is the fluorescence quantum distribution of the donor and $\varepsilon_A(\lambda)$ is the extinction coefficient of the acceptor. If $\varepsilon_A(\lambda)C_A l$ is large, then the term in the parentheses is ≈ 1 and there is near unit probability that the excited photon will be absorbed by A. If $\varepsilon_A(\lambda)C_A l$ is moderate, equation 2-20 may be simplified by Taylor series expansion

$10^{-x} = e^{-2.3026x} = 1 - 2.3026x + \ldots\ldots$ and keeping only the first two terms of the expression.

This truncation gives,

$$a = \frac{2.3026 C_A l}{\phi_D^0} \int_0^\infty E_{F,D}(\lambda)\varepsilon_A(\lambda)d\lambda = \frac{2.3026 C_A l}{\phi_D^0} J \qquad (2\text{-}21)$$

The integral $J = \int_0^\infty E_{F,D}(\lambda)\varepsilon_A(\lambda)d\lambda$ is called overlap integral [Gil91]. The overlap integral J expresses the degree of spectral overlap between the donor emission and the acceptor absorption.

For most organic molecules A, the S_0-T excitation coefficient spectrum is weak (because the transition is spin forbidden). Therefore singlet-triplet radiative transfer is negligible (J→0, a→0). The inner filter effect (trivial energy transfer) becomes large if the S_0-S_n (n ≥ 1) absorption spectrum of an acceptor A overlaps with the fluorescence spectra of D (large overlap integral), the sample length, ℓ, is long, and the acceptor concentration is high.

2. *Non-radiative energy transfer*

Non-radiative energy transfer requires the presence of a specific interaction between D* and A. Two different mechanisms may be acting termed as long range Coulombic

interaction and short range electron exchange interaction. The initial and final electronic states in the energy donor and the acceptor molecules are coupled through an electrostatic interaction with Coulomb potential, $V = \dfrac{e^2}{4\pi\varepsilon_0 r}$. A description of the excitation energy transfer is found in [Spe96]. The transfer rate may be described by the Fermi Golden rule

$$k_{ET} = \frac{2\pi}{\hbar} V_{ET}^2 \rho \qquad (2\text{-}22)$$

where V is the interaction matrix element $\langle \psi_i | \hat{V}_{ET} | \psi_f \rangle$ and ρ is the Franck - Condon factor between the ground state wavefunction ψ_i and the excited-state wavefunction ψ_f. V is the Coulomb interaction potential given by

$$\hat{V}_{ET} = \frac{e^2}{4\pi\varepsilon_0 \varepsilon_s r_{AD}} \qquad (2\text{-}23)$$

where ε_s is the static dielectric constant of the solvent and r_{AD} is the distance between the interacting electrons (here ground state electron of acceptor A and excited electron of donor D^*).

The wavefunctions ψ_i and ψ_f in the excitation transfer $D^* + A \rightarrow D + A^*$ are described by two-electron antisymmetric wavefunctions

$$\psi_i = \frac{1}{\sqrt{2}} \left[\psi_{D^*}(1)\psi_A(2) - \psi_{D^*}(2)\psi_A(1) \right]$$

and $\qquad\qquad\qquad\qquad\qquad\qquad\qquad\qquad\qquad\qquad (2\text{-}24)$

$$\psi_f = \frac{1}{\sqrt{2}} \left[\psi_D(1)\psi_{A^*}(2) - \psi_D(2)\psi_{A^*}(1) \right]$$

where ψ denotes the total wavefunction. In Born-oppenheimer approximation ψ my be separated in an electronic part ϕ and a vibrational part χ, i.e.

$$\psi = \phi \chi \qquad (2\text{-}25)$$

The interaction matrix element for the donor acceptor excitation transfer becomes

$$V_{ET} = \langle \psi_i | V | \psi_f \rangle = \langle \psi_{D*}(1) \psi_A(2) | V | \psi_D(1) \psi_{A*}(2) \rangle - \langle \psi_{D*}(1) \psi_A(2) | V | \psi_D(2) \psi_{A*}(1) \rangle \quad (2\text{-}26)$$

The first term gives the classical coulomb integral J (electron 1 remains at the donor molecule and electron 2 remains at the acceptor molecule in the excitation energy transfer). The second term gives the quantum mechanical electron exchange integral K (initial excited electron 1 in the donor molecules change to the acceptor and brings the acceptor to the excited state, the initially unexcited electron 2 in the acceptor molecules changes over to the ground state level of the donor). The Coulomb integral J remains large even if the interacting donor electron and acceptor electron do not overlap (decrease is determined by the $1/r_{AD}$ dependence of Coulomb interaction potential $\hat{V}$).

The excitation energy transfer due to the Coulomb interaction is given by

$$k_{ET,Coulomb} = \frac{2\pi}{\hbar} J^2 \rho \qquad (2\text{-}27)$$

When the distance r_{AD} is larger than the sum of the donor and acceptor molecule radii, then the electron wavefunction do not overlap, the exchange excitation transfer dies out, and the Coulomb integral may be approximated by the dipole dipole interaction term leading to

$$k_{ET,d-d} = \frac{2\pi}{\hbar} V^2_{ET,d-d} \rho \qquad (2\text{-}28)$$

with

$$V_{ET,d-d} = \frac{1}{4\pi\varepsilon_0 \varepsilon_s r^3_{AD}} \left[\vec{M}_D \cdot \vec{M}_A - \frac{3}{r^2_{AD}} (\vec{r}_{AD} \cdot \vec{M}_D)(\vec{r}_{AD} \cdot \vec{M}_A) \right] \qquad (2\text{-}29)$$

where by

$$\vec{M}_D = \sqrt{2}\langle\phi_D|e\vec{r}_D|\phi_{D*}\rangle$$

and

$$\vec{M}_A = \sqrt{2}\langle\phi_A|e\vec{r}_A|\phi_{A*}\rangle$$

(2-30)

are the transition dipole moments of the donor and the acceptor. The energy transfer was first described by Förster and is therefore called Förster-type energy transfer [För59].

The excitation energy transfer due to the exchange integral is given by

$$k_{ET,exchange} = \frac{2\pi}{\hbar}K^2\rho$$

(2-31)

K is given by

$$K = \frac{1}{4\pi\varepsilon_0\varepsilon_s}\langle\phi_{D*}(1)\phi_A(2)|\frac{e^2}{r_{AD}}|\phi_D(2)\phi_{A*}(1)\rangle$$

(2-32)

This excitation transfer was described by Dexter [Dex53] and hence is called Dexter-type energy transfer.

2.3.1.1 Long-range Coulombic energy transfer (Förster-type energy transfer)

It is dominated by long range dipole-dipole interaction (Coulomb matrix element J) which cause perturbation of the donor and acceptor electron orbitals. These perturbations are transmitted by the electromagnetic fields of D[*] and A molecules, in which dipole oscillation of D[*] induces a corresponding oscillation in A. The resulting dipole dipole interaction leads to the excitation of electrons of A. Thus D[*] gets de-excited and returns to the ground electronic state with a simultaneous excitation of A to A[*]. Energy is transferred from D[*] to A despite the fact that the two species do not come into direct contact and no electrons are transferred between them. This process may take place over large intermolecular separations (upto to the order of 10 nm). It is illustrated in the top part of Fig. 2.2

Coulombic Energy Transfer

Exchange Energy Transfer
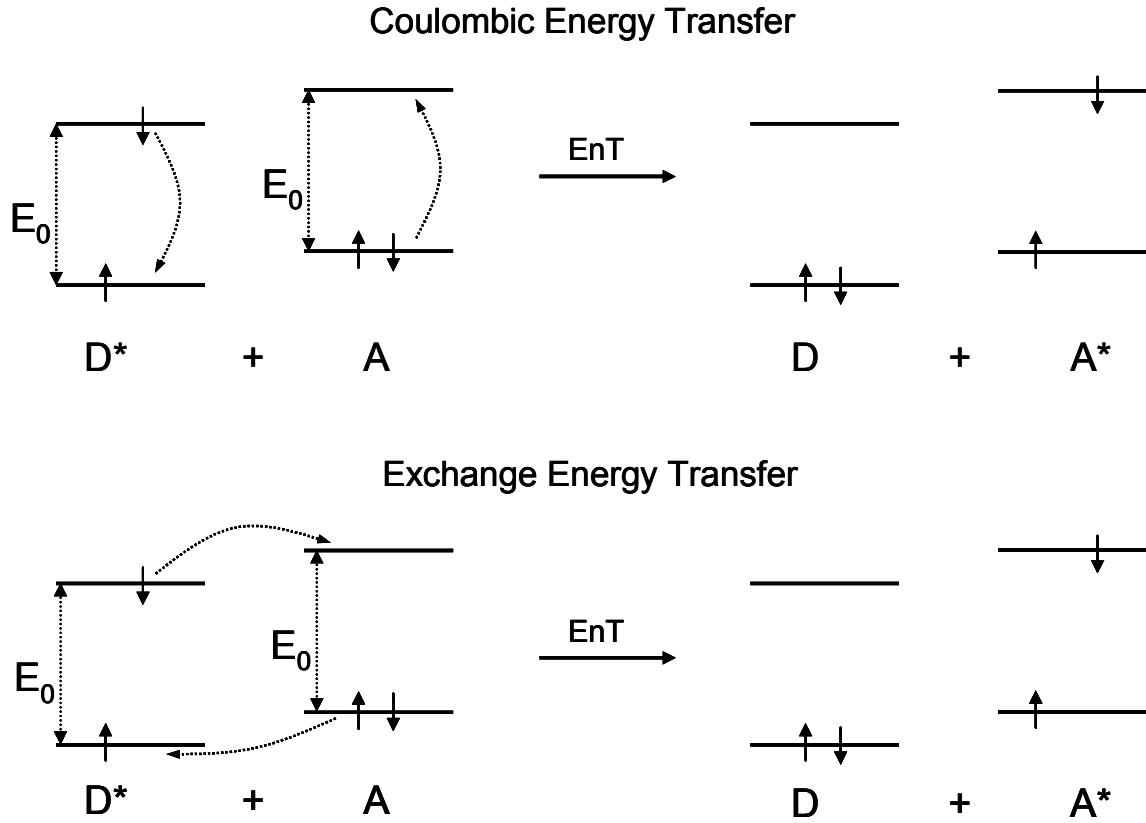
Figure 2.2 Energy level diagrams showing (top) electron movements in long-range Coulombic energy transfer (Förster-type energy transfer), (bottom) electron transfer steps in electron exchange energy transfer (Dexter type energy transfer) [Val02]

Long range Coulombic dipole dipole energy transfer was formulated by Förster (hence called Förster-type energy transfer, or Förster transfer, or Förster resonance energy transfer 'FRET'). The energy transfer rate is given by [För59]:

$$k_{dd} = k_{F,D}^0 \left[\frac{R_0}{r} \right]^6 = \frac{1}{\tau_{F,D}^0} \left[\frac{R_0}{r} \right]^6 \qquad (2\text{-}33)$$

where $k_{F,D}^0$ and $\tau_{F,D}^0$ are emission rate constant and fluorescence lifetime of donor in the absence of acceptor, r is the distance between donor and acceptor (assumed to remain constant during the excited-state lifetime of the donor) and R_0 is the critical transfer distance or Förster

radius, i.e. the distance at which energy transfer rate k_{dd} and undisturbed fluorescence emission rate, $k_{F,D}^0$ of the excited donor are equally probable. R_0 is given by [För59]

$$R_0^6 = \frac{9\kappa^2}{128\pi^5 n^4} \int_0^\infty E_{F,D}(\lambda)\sigma_A(\lambda)\lambda^4 d\lambda = \frac{9\kappa^2 \phi_D^0}{128\pi^5 n^4} J_F \qquad (2\text{-}34)$$

κ is an orientation factor which accounts for the directional nature of the dipole-dipole interaction. κ^2 can have values between 0 (perpendicular transition moments, ($\uparrow\rightarrow$)) and 4 (collinear transition moments ($\rightarrow\rightarrow$)). When the transition moments are parallel ($\uparrow\uparrow$), $\kappa^2 = $ 1.When the molecules are free to rotate at a rate that is much faster than the de-excitation rate of donor (isotropic dynamic averaging), the average value is $\kappa^2 = 2/3$ [Val02]. J_F is the spectral Förster overlap integral.

The energy transfer efficiency is defined as

$$\phi_{ET} = \frac{k_{dd}}{k_{dd} + k_{F,D}^0} = \frac{1}{1 + k_{F,D}^0 / k_{dd}} = \frac{1}{1 + \dfrac{\tau_{F,D}}{\tau_{F,D}^0}} = \frac{1}{1 + (r/R_0)^6} \qquad (2\text{-}35)$$

This equation implies that the transfer efficiency is 50% when the donor-acceptor distance is equal to Förster critical radius. Thus the distance between donor and acceptor can be determined by measuring the efficiency of transfer. In the case of small energy transfer efficiency ($\phi_{ET}\ll 1$) the transfer energy may be approximated by

$$\phi_D = \frac{1}{1 + \dfrac{\tau_{F,D}}{\tau_{F,D}^0}} \approx 1 - \frac{\tau_{F,D}}{\tau_{F,D}^0} \qquad (2\text{-}36)$$

where $\tau_{F,D}^0$ and $\tau_{F,D}$ are the donor excited state lifetime in the absence and presence of acceptor, respectively.

2.3.1.2 Short range electron exchange energy transfer (Dexter-type energy transfer)

When the wavefunctions of the excited donor electron and the ground state acceptor electron overlap then the exchange excitation transfer (Dexter - type energy transfer) becomes important. It is illustrated in the lower part of Fig. 2.2.

According to Dexter, who first formulated this type of transfer [Dex53] the rate constant for exchange interaction energy transfer can be expressed as

$$k_T^{ex} = \frac{2\pi}{\hbar} Z^2 \frac{\int\limits_0^\infty E_{F,D}(\lambda)\varepsilon_A(\lambda)d\lambda}{\int\limits_0^\infty E_{F,D}(\lambda)d\lambda \int\limits_0^\infty \varepsilon_A(\lambda)d\lambda} = \frac{2\pi}{\hbar} Z^2 J_D \qquad (2\text{-}37)$$

where Z is a parameter related to the matrix element for electron exchange,

$$J_D = \int E'_{F,D}(\lambda)\varepsilon'_A(\lambda)d\lambda \text{ with } E'_{F,D} = E_{F,D}(\lambda)/\int\limits_0^\infty E_{F,D}(\lambda)d\lambda \text{ and } \varepsilon'_A(\lambda) = \varepsilon_A(\lambda)/\int\limits_0^\infty \varepsilon_A(\lambda)d\lambda$$

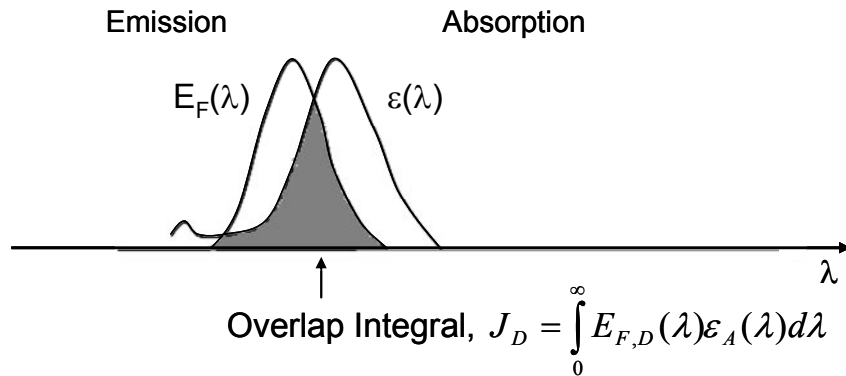is the Dexter overlap integral. It is shown in Fig. 2.3.

Figure 2.3 Schematic description of spectral Dexter overlap integral J_D and its relation to an experimental absorption and emission spectrum. The shaded portion corresponds to the overlap [Val02].

Dexter found

$$Z^2 = \kappa e^{-2r/l} \qquad (2\text{-}38)$$

where r is the distance between donor and acceptor molecules (center to center) and l is the van der Waals radius of the donor-acceptor pair (i.e. the sum of the van der Waals radii of donor and acceptor molecules).κ is the coupling constant at donor - acceptor overlap (electron exchange overlap integral). Z^2 diminishes exponentially with the distance between the molecules.

2.3.2 Electron transfer

The transfer of an electron from one molecular entity (electron donor) to another one (electron acceptor) or between two localized sites in the same molecular entity is called electron transfer. If the electron transfer is triggered by absorption of a photon then it is known as photoinduced electron transfer. The oxidative and reductive properties of molecules are enhanced in the excited state [Kav93]. Oxidative and reductive photoinduced electron transfer processes occur according to the following relations

Oxidative electron transfer: $D^* + A \rightarrow D^+ + A^-$

Reductive electron transfer: $A^* + D \rightarrow A^- + D^+$ (2-39)
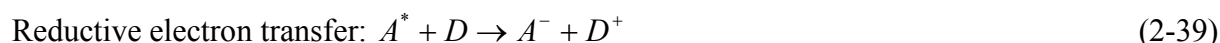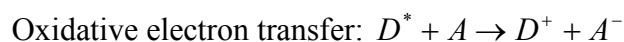
Fig. 2.4 shows the two processes schematically.

2.3.2.1 Fundamentals of electron transfer (Markus Theory)

In order to understand the electron transfer a brief discussion of the theoretical aspects is given.

Let us consider a one-electron transfer, for example when an electron is transferred from a reduced (or electron rich) species, R´, to an oxidized (or electron deficient) species, O.

Oxidative Electron Transfer

$$D^* \quad + \quad A \longrightarrow D^{\bullet+} \quad + \quad A^{\bullet-}$$

LUMO

LUMO

HOMO

HOMO

excited
flurophore

quencher

oxidised
flurophore

reduced
quencher

Reductive Electron Transfer

$$A^* \quad + \quad D \longrightarrow A^{\bullet-} \quad + \quad D^{\bullet+}$$

HOMO

LUMO

LUMO

HOMO

excited
flurophore

quencher

reduced
flurophore

oxidised
quencher

Figure 2.4 Oxidative electron transfer (excited molecule acts as electron donor) (top). Reductive electron transfer (excited molecule acts as electron acceptor) (bottom) [Val02].

$$R' - e \rightarrow R$$
$$O + e \rightarrow O'$$

$$(2\text{-}40)$$

Combining the two

$$O + R' \rightarrow R + O'$$

$$(2\text{-}41)$$

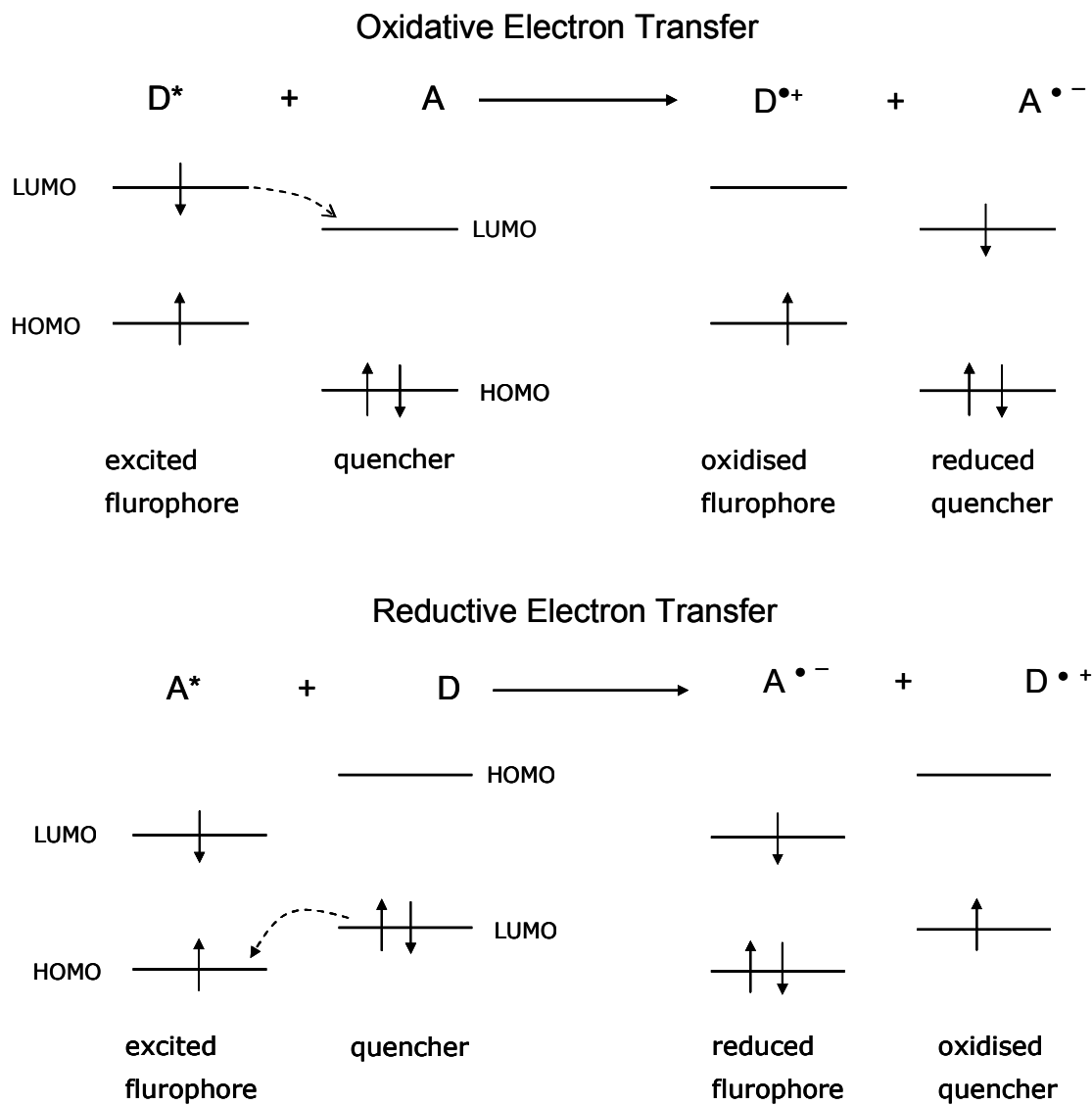This reaction typically proceeds by the two reacting species coming together with R′ and O closely associated in an 'encounter complex', to enable the transfer of an electron. In the theory of electron transfer by Marcus [Mar56, Mar85], the nuclear configuration of the reactant encounter pair is imagined to fluctuate due to vibrational motions and changes in the positions, orientation and polarization of the solvent molecules which surround the encounter pair. The many dimensional potential energy surface on which all of this motion occurs can be represented as a simple quadratic curve in many-dimensional configuration space. A similar curve for the products can be drawn. The intersection of these two curves (Fig. 2.5(a)) represents the configuration at which reactants are indistinguishable from products. It is at this point that the electron transfer can happen with no change in the nuclear configuration of the reactant "supermolecule" (and hence can proceed within the constraints of the Franck-Condon principle). The intersection point is reached from the reactant encounter pair by stretching and/or compressing of bonds and the reorientation and repolarisation of solvent molecules. After electron transfer, the configurations relax to their lowest energy states [Cha95].
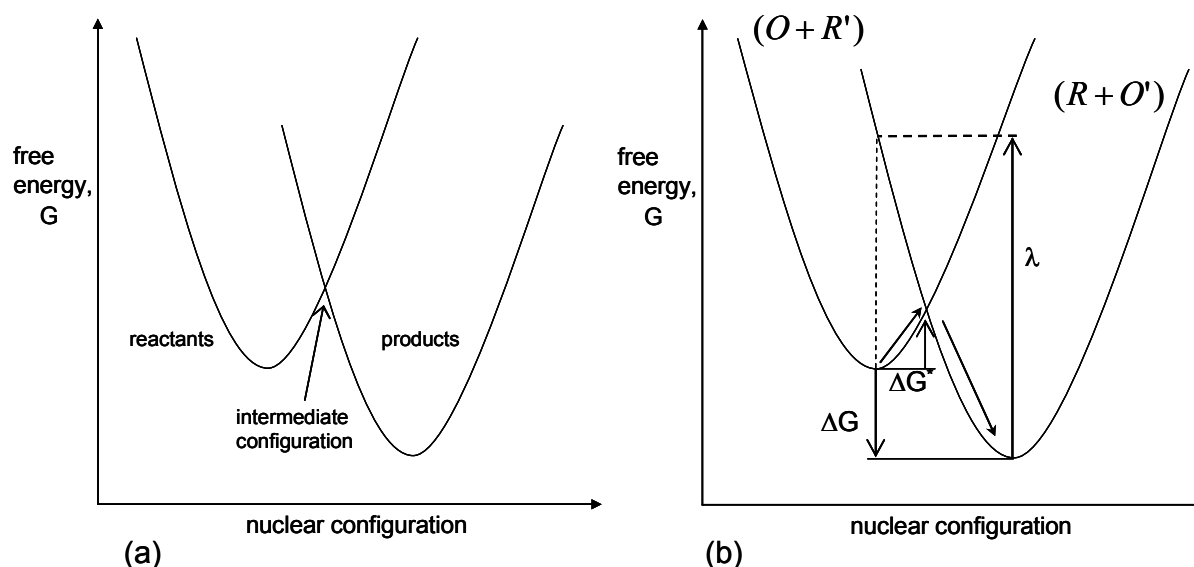
Figure 2.5 (a) A typical free energy (G) *vs*. nuclear configuration diagram for reactants and products. Electron transfer occurs at the intermediate configuration shown. (b) Analogous energy diagram for electron transfer between two different redox centers. The left hand curve is for reactants (O+R′) and the right hand curve for products (R+O′). Reaction proceeds *via* the route shown with solid arrows. The free -energy vectors illustrate the sign and magnitude of ΔG, ΔG^*, and λ.

When there is electron transfer between two different redox centers, then the changes in the combined nuclear configurations of either the (O + R′) reactants or the (R + O′) products must be considered and these can be represented in a way as shown in Fig. 2.5(b). One curve shows variation in the configuration of the reactants and the other shows variation for the products and so the reaction rate can be given by the same theoretical treatment as given for the reactant or the products separately. In this case, the electron-transfer rate depends upon the difference in energy between the bottom of the reactant and product curves, ΔG, and the amount of energy required to change the nuclear configuration of the product to that of the reactant, λ, as shown. The constant λ is called as the reorganization energy and ΔG is the driving force (which is proportional to the difference in the redox potentials, ΔE^0, of the two redox-active species). The activation barrier height of the reaction is given by, ΔG^*,

$$\Delta G^* = (\Delta G + \lambda)^2 / 4\lambda \qquad (2\text{-}42)$$

λ is always positive, $(\Delta G + \lambda)$ determines the rate of reaction. Three cases can be distinguished: $(\Delta G + \lambda)$ greater than zero, equal to zero, and less than zero. These cases are displayed in Figure 2.6 (a), (b), and (c) and are termed the normal, activationless, and inverted regions. According to Marcus theory, the electron-transfer rate, k_{ET}, is given by

$$k_{ET} = \frac{2\pi}{\hbar} V_0^2 \exp(-\beta R_{ed}) \frac{1}{\sqrt{(4\pi\lambda k_B T)}} \exp\left[\frac{-\Delta G^*}{k_B T}\right] \qquad (2\text{-}43)$$

where V_0^2 is the donor-acceptor (here reactant-product) coupling constant (square of wave-function overlap integral, V_0, of donor and acceptor state at donor–acceptor contact i.e. at R_{ed} = 0), R_{ed} is the edge to edge distance between the donor and acceptor, β is the distance coefficient (value: $\beta \approx 14$ nm^{-1} [Mos92]). Using Equations (2-42) and (2-43), the variation in
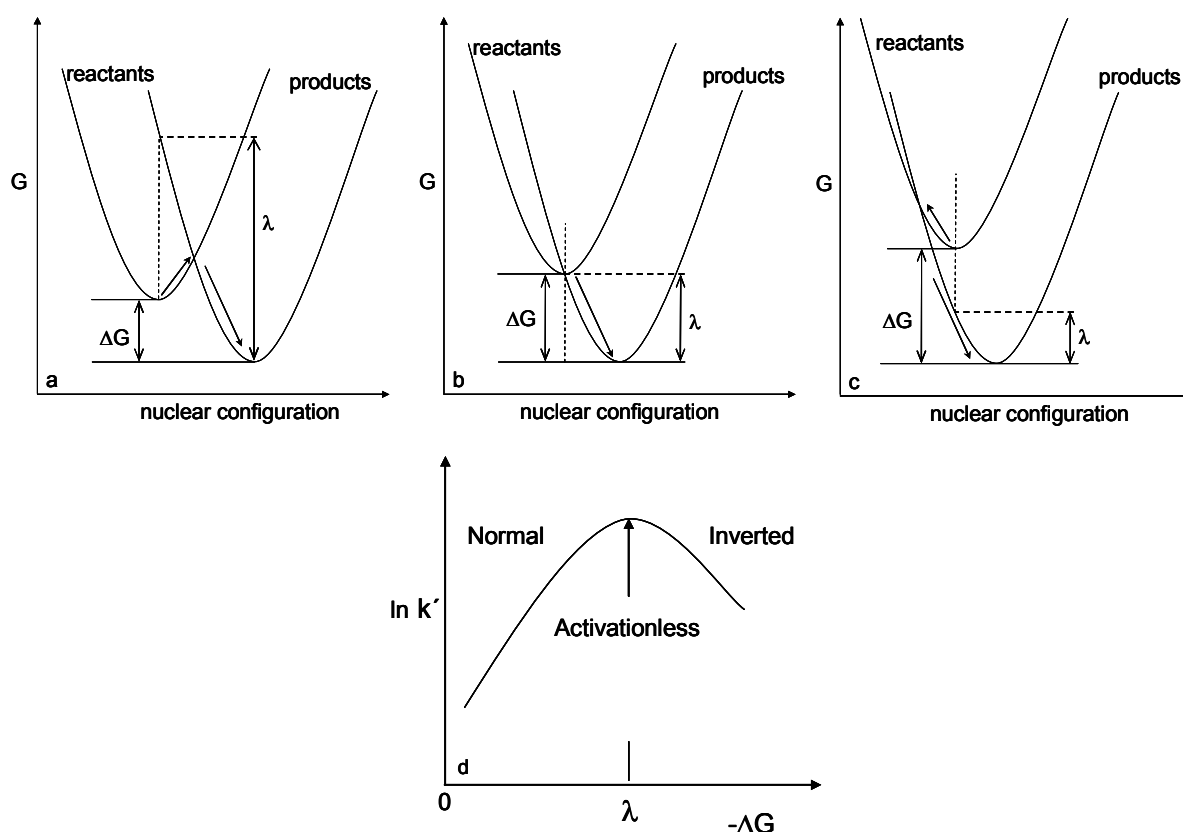
Figure 2.6 The three regimes for energy transfer (a) normal ($\Delta G + \lambda > 0$), (b) activationless ($\Delta G + \lambda = 0$) where the maximum electron transfer rate is obtained, and (c) inverted ($\Delta G + \lambda < 0$). The arrows denote the reaction pathway, (d) the variation of logarithm of electron transfer rate constant (k') with free energy between reactants and products (ΔG) as predicted by the theory

k_{ET} with ΔG can be calculated. Figure 2.6(d) illustrates this variation. When $-\Delta G < \lambda$, we are in the normal region, and an increase in $-\Delta G$ (an increase in the thermodynamic driving force) will lead to a less-positive ΔG^* and an increased electron-transfer rate. The rate will reach a maximum when $-\Delta G = \lambda$ as at this point $\Delta G^* = 0$. The reaction is therefore activationless. If $-\Delta G$ is increased still further, ($\Delta G + \lambda$) becomes increasingly negative, and from Equation (2-42), ΔG^* becomes increasingly positive. Thus, in contrast to the normal region, the activation barrier increases as the thermodynamic driving force increases. Therefore in this region k_{ET} falls as ΔG becomes more negative. This is the inverted region. This happens because the

33

curves intercept at a value more positive than the bottom of the reactant curve, seen in Figure 2.6(c), and so activation energy is required for the reaction to proceed.

## 2.3.2.2 Electron transfer in proteins

Biological electron transfer in proteins, DNA (deoxyribonucleic acid), and photosynthetic system has fundamental features in common with the small molecule electron transfer. As in simple reactions, biological systems undergo vibrational and environmental changes during the reaction and the rates depend on λ and ΔG. But the macromolecules are more complex and relevant structural information, conformational information and the environmental information is often missing. Changes in the macromolecular conformations may precede or follow the electron transfer. Nevertheless, Marcus theory has been helpful in understanding the biological electron transfer. In proteins, electron transfer was theoretically explained in terms of electron tunneling [DeV80]. Through-space electron transfer between biological redox centers involves an electron in an orbital on one redox centre transferring to a vacant orbital on the other redox centre. The electron tunnels through the higher energy intervening medium and the efficiency of this process will depend upon the overlap of the two electronic wave functions. The larger the overlap, the more favoured will be the electron transfer and the faster the rate. Since electronic wave functions decrease exponentially with distance, the overlap efficiency and hence the electron-transfer rate decrease exponentially with the distance between the redox centres. In long range electron transfer ($\geq$ 3nm), electronic states of the intervening bridge mediate the transfer. The tunneling-pathway model [Ber89, Ber90, Ber91] explains increased long distance electron transfer rates. According to this model, the medium between the donor and the acceptor is decomposed into smaller subunits linked by covalent bonds, hydrogen bonds, or through-space jumps. There may be many possible pathways for electron transfer, and a longer pathway may have a greater stabilization of the electronic wave functions, which may lead to a greater electron transfer

rate than for the shortest electron transfer route. It is suggested that different protein secondary structures mediate electronic coupling with different efficiencies. Thus the β-sheet structures may act as conducting pathways through proteins, while α-helices may provide insulation against long range electron transfer [Gra96].

2.4 Hydrogen bonding

A hydrogen bond is the attractive force that arises between the covalent pair X—H in which a hydrogen atom H is bound to a more electronegative atom X, and other neighbour electronegative atom A in a molecule A—Y.

The electron formally associated with the hydrogen atom is involved in the covalent X–H bond. Its center of mass is displaced relative to the hydrogen atom position in the direction of the center of the bond. This gives rise to a dipole with a positive charge at the hydrogen end of the X–H bond, irrespective of whether X carries a net charge. It is the Coulombic interaction of the dipole with the excess electron density at the acceptor atoms that forms the hydrogen bond interaction [Jef91].
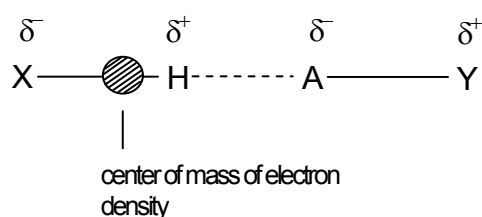
Hydrogen bonds can be strong (e.g. FH····F with bond energy = 155 kJmol^{-1}), or moderately strong (e.g.OH····N, bond energy = 29 kJmol^{-1}) or very weak such as in N–H····O (bond energy = 8 kJmol^{-1}). Strong hydrogen bonds are of minor importance in biological structures.

Moderate to weak hydrogen bonds are different from covalent bonds in two important aspects:

1. They are 'soft' bonds which are easily deformed by other intermolecular interactions, which may be other hydrogen bonds, or van der Waals forces.

The stretching and bending force constants of hydrogen bonds are about 15 times smaller than for the covalent bonds. Therefore, from a structural point of view, the hydrogen-bond length or hydrogen-bond angles observed in any particular molecular structure are dependent on the environment in which they are measured. In any crystal structure, the hydrogen bond $XH\cdots A$ geometries will be compressed or expanded by up to 20% of their equilibrium distances, that is between 1.4 and 2.1 Å for an equilibrium bond length of 1.8 Å. Therefore the characteristic of a particular type of hydrogen bond is the most probable hydrogen bond length, obtained by statistical surveys of a large number of structures in which they occur.

2. Hydrogen bonds do not have atom pair properties but group pair properties.

Covalent bonds have atom-pair properties. They are almost unaffected by the environment of the molecules considered because compression/expansion effects in bond distances seldom exceed 2% and valence angles vary over only a few degrees. Hydrogen bonds are group properties, depending not only upon the first neighbour atoms of both X and A, but also upon the sequential nature of the total pattern of the bonding [Jef91].

2.4.1 Hydrogen bonding in proteins

In proteins, different amino acids are linked in specific sequence by peptide bonds to form linear polypeptides of molar mass in the range of a few thousand to several hundred thousand Dalton (1 Dalton =1 Da = 1g mol^{-1}). If a protein contains cysteines, these can cross-link by oxidation to form disulphide bridges. Besides these covalent bonds, the main stabilization of the very complex three-dimensional structure which is characteristic of each protein is by hydrophobic forces, van der Waals forces, and even more important by hydrogen bonds.

The amino acid sequence or primary structure is responsible for the higher level structure and biological function of a protein. The secondary structure defines the conformation of the polypeptide backbone (the 'main chain') with the typical repetitive elements, α-helix and β-pleated sheet. In addition, there are bends in the polypeptide chain called β-turns and Ω-loops which give rise to sharp hairpin-like folds. The arrangement in three dimensional space of the regions with secondary structure elements and the region of irregular polypeptide conformation is called tertiary structure. This gives the proteins their characteristic shape. It describes the folding of the polypeptide chains into functionally active sites and is essential for the specific biological properties of a protein. In multi-subunit proteins, the individual subunits are combined in certain arrangements to form quaternary structures. They represent the highest level of organization in protein assembly and are not held together by covalent forces.

The secondary structure is stabilised only by main-chain to main-chain inter-peptide $N–H\cdots O=C$ hydrogen bonds (bond energy ~ 8 kJ mol^{-1}). Tertiary and quaternary structures are held together by hydrogen bonds of the type main-chain to main-chain, main-chain to residue, residue to residue. Besides this, there are also interactions between water and main polypeptide chain or amino acid residues. The residues (20 different amino acids) have a variety of functional groups which can act as hydrogen bond donors and acceptors [Jef 91].

Hydrogen bonds have functional properties that are essential for life purposes. They are weak interactions relative to covalent or ionic bonds and can therefore be switched on or off with energies which are within the range of thermal fluctuations at life temperatures. Thus, the processes that require fast intermolecular recognition and reaction can easily occur. Stronger interactions, with bonding energies well in excess of those attained by hydrogen bonding, would seriously impede the flow of biological information and events. On the other hand, the weakness of the individual bonds is such that it is often not sufficient to provide the

strength and specificity necessary for biological processes. This can be overcome because hydrogen bonds have vectorial properties and are sensitive to stereochemistry. If hydrogen-bond donors and acceptors are arranged in particular geometries, the hydrogen-bonding interactions become specific, with additive and often cooperative strengths [Jef91]

In photoreceptor proteins the chromophore is held inside a binding pocket. The chromophore may be covalently bound or non-covalently bound with the help of a hydrogen bond network. When the chromophore absorbs a photon, there occurs a change in the hydrogen bond network and the protein comes into a new conformation that helps in passing the information to another part in the signal transduction pathway ultimately resulting in a response of the organism. Fig. 2.7 illustrates the hydrogen bonding of the chromophore in AppA, a sensor for blue light. It also shows the changes in the hydrogen bonding that occur on sensing the light [And05].
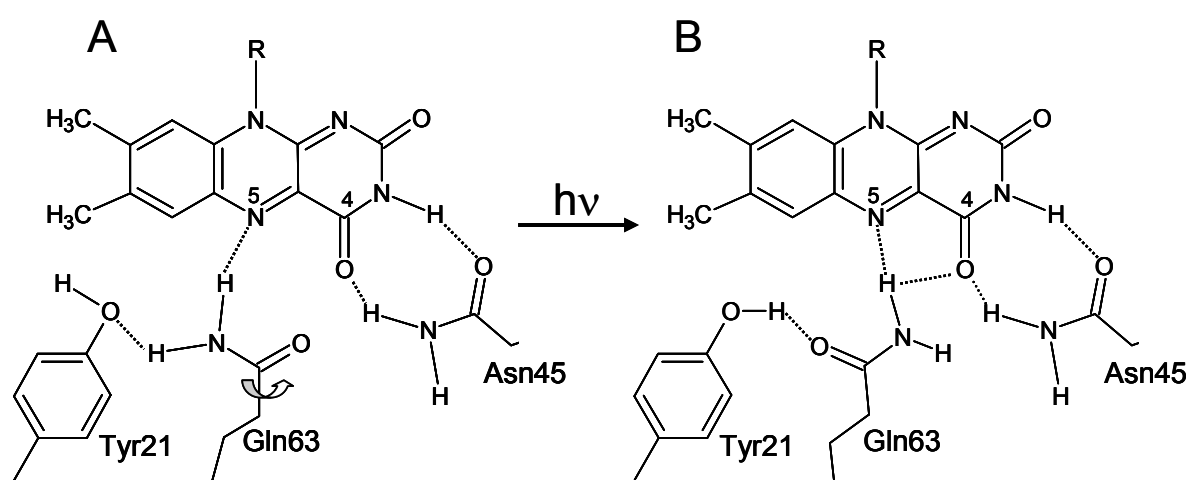

Figure 2.7 Hydrogen bond network to the flavin in AppA. Hydrogen bonds are shown as dashed lines. (A) Hydrogen bond network in dark state orientation of Gln63.(B) Alternate hydrogen bond network with rearrangement of hydrogen bonds network after illumination with blue light. [And05].

3   Flavins

The derivatives of the dimethylisoalloxazine (7,8-dimethylbenzo[*g*] pteridine-2,4(3*H*,10*H*)-dione) skeleton, with a substituent on the 10 position are known as Flavins. Flavins are redox active yellow coloured compounds ubiquitously found in nature and take part in many biochemical reactions as coenzyme in enzymes and as cofactor in photoreceptors. Riboflavin (vitamin B$_2$) is the most abundant flavin compound found in nature. Riboflavin is found in milk, yeast, meat, beans, peas [Mas00]. Its deficiency leads to growth disturbances, skin diseases and hair loss [Fri88]. Riboflavin acts as precursor molecule for riboflavin-5´-phosphate, commonly called as flavin mononucleotide (FMN) and for flavin adenine dinucleotide (FAD). FMN is the cofactor in the phototropins of plants [Bri02] which are the blue light sensitive photoreceptors responsible for phototropism (bending response of plant towards or away from light source) [Iin01], chloroplast movement [Hau99] and many other functions. FMN is non-covalently bound in phototropin. FAD (flavin adenine dinucleotide) contains a isoalloxazine (flavin) moiety conjugated with an adenosine diphosphate. It is found as a redox cofactor in many enzymes which are involved in several important reactions in metabolism. FAD together with 8-hydroxy-7,8-didemethyl-5-deazariboflavin (8-HDF) or methenyl tetrahydrofolate (MTHF) are the chromophores in DNA photolyases [San03]. The cofactors of cryptochromes are FAD and MTHF [Lin95]. FAD is also the redox and light sensitive, non-covalently bound chromophore in the BLUF proteins [Gom02] (see details in chapter5). The flavins have been described here to some extent since FAD is the cofactor in the here investigated BLUF blue light photoreceptor BlrP1 in the bacteria *K. pneumoniae*.

3.1   Physical and chemical properties of flavins

The structural formulae of FAD, FMN, Riboflavin, Lumichrome and Lumiflavin along with the internationally accepted numbering system of the isoalloxazine moiety are shown in
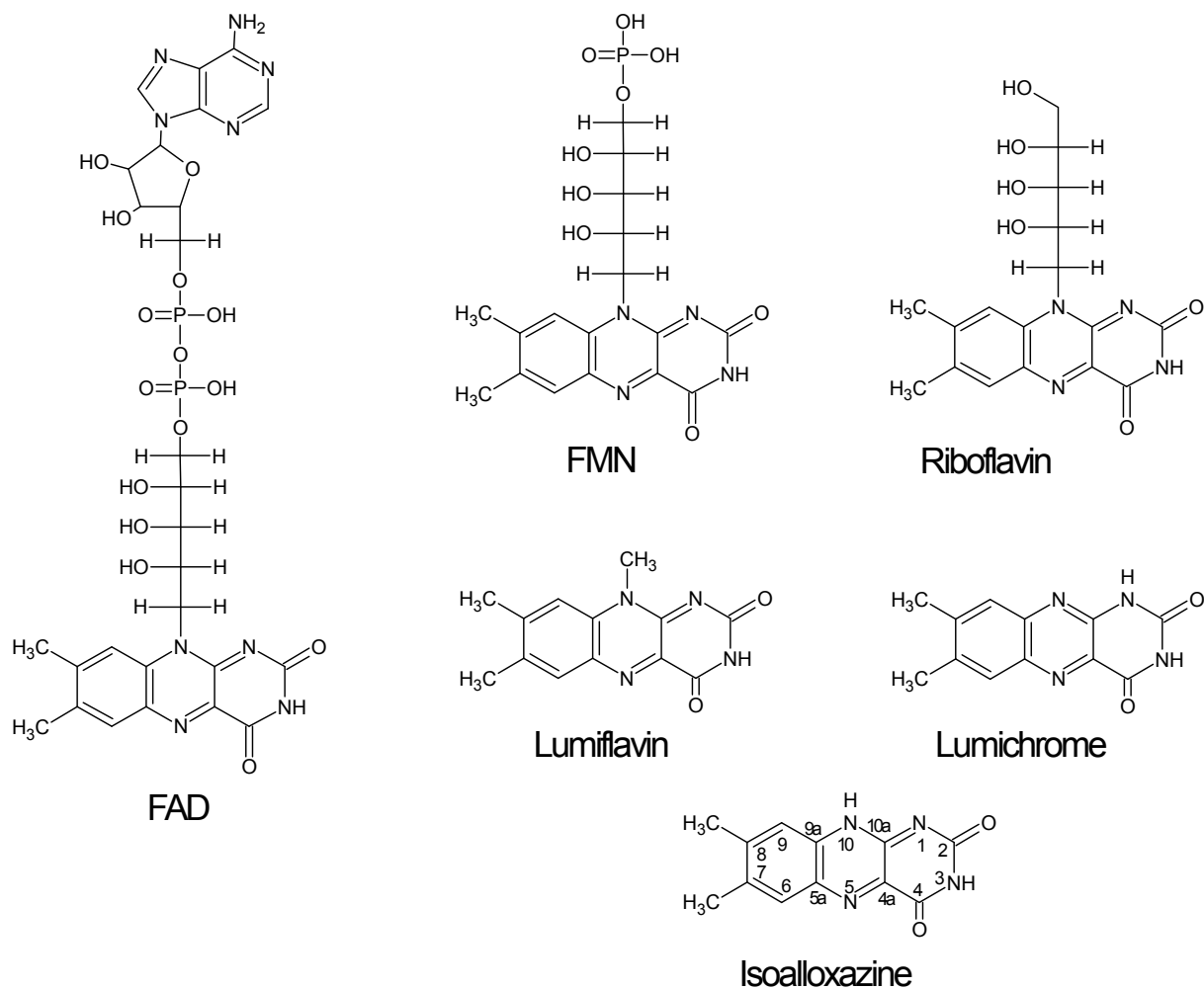
Figure 3.1 The structural formulae of FAD, FMN, Riboflavin, Lumichrome amd Lumiflavin along with the structure (IUPAC recommendations 1995) of the isoalloxazine moiety [Mül87].

Fig. 3.1. Lumichrome and Lumiflavin are photodegradation products of FAD, FMN and riboflavin [Hol05].

The chemical entity responsible for the diverse biological activity of flavin is the isoalloxazine moiety. It exists in three redox states: 1) the oxidized or quinone state, 2) the one-electron reduced or semiquinone (radical) state, and 3) the two-electron reduced (fully reduced) or hydroquinone state. Flavin is an amphoteric molecule existing as neutral, anionic and cationic species in all the three redox states. The different structures of the various redox forms of flavin are discussed in section 3.2.

The absorption spectrum of flavins in the visible wavelength region is caused by the isoalloxazine ring [Whi53]. For FAD, in the UV spectral region adenine also contributes to the absorption spectrum [Mil68]. The absorption spectra of Riboflavin, FAD, FMN, Lumichrome and Lumiflavin are displayed in Fig. 3.2.
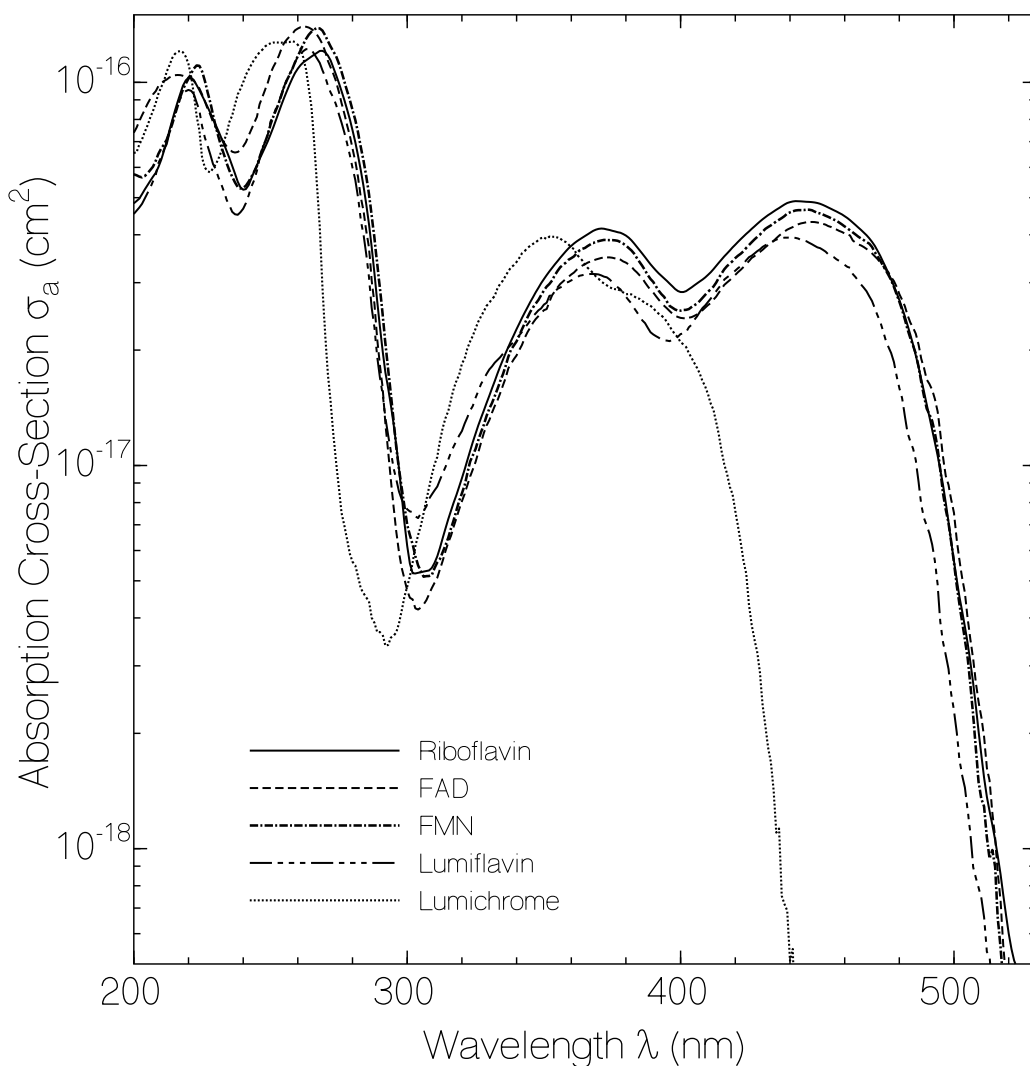
Figure 3.2 Absorption cross-section spectra for Riboflavin, FAD, FMN, Lumiflavin in aqueous solutions at pH 7 and lumichrome in bi-distilled water [Drö02, Isl03b, Hol05].

The fluorescence spectral shapes of FAD, FMN and riboflavin are also determined by the isoalloxazine ring and are similar [Bar73]. But depending on the solvent conditions the fluorescence quantum efficiency and the fluorescence lifetime of FAD are different from that

of riboflavin and FMN [Web50, Mil68, Vis84, Berg02]. The fluorescence quantum yields in aqueous solution buffered to pH 8 are about 0.26 (riboflavin), 0.037 (FAD), 0.23 (FMN), 0.235 (lumiflavin) and 0.049 (lumichrome) [Drö02, Isl03b, Hol05]. The normalized fluorescence quantum distributions of riboflavin, FAD, FMN, lumiflavin and lumichrome in aqueous solution are shown in Fig. 3.3.

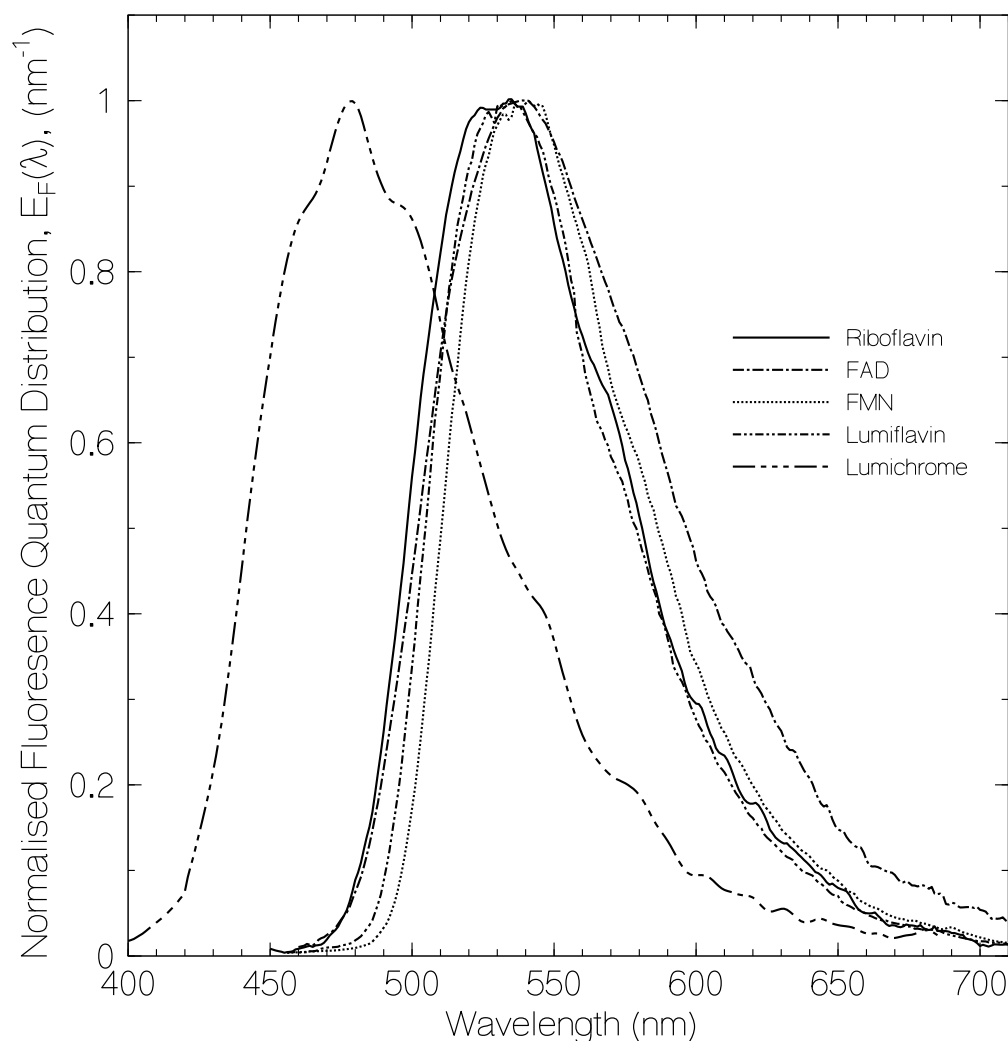**Figure 3.3** Normalized Fluorescence quantum distribution of Riboflavin, FMN, FAD, Lumichrome in aqueous solution at pH 8 and FAD in pH 7 [Drö02, Isl03b, Hol05]

The lower fluorescence quantum yield of FAD has been explained to be due to the formation of an intramolecular complex between the adenine and isoalloxazine moieties of FAD. This form is called as non-fluorescent stacked (closed) form of FAD. The stacked form

is in equilibrium with a fluorescent un-stacked (open) form of FAD in which isoalloxazine and adenine moieties are not in contact and are separated by the ribityl bridge [Web50, Isl03b]. The FAD molecules in aqueous solution at neutral pH are predominantly in the stacked conformation. The mole fraction of stacked FAD molecules in the ground state causes static fluorescence quenching and is responsible for the low fluorescence quantum yield of FAD in neutral aqueous solution. The shorter fluorescence lifetime of FAD compared to the fluorescence lifetime of riboflavin or FMN is due to photoisomerisation of unstacked FAD molecules to stacked FAD molecules within the excited state lifetime which occurs in few nanoseconds (dynamic fluorescence quenching). The stacked FAD is non-fluorescent because of photo-induced electron transfer between the adenine moiety and the isollaoxazine moiety [Ber02]. For the un-stacked form of FAD no electron transfer happens since the distance between the electron acceptor group (isoalloxazine) and the electron donor (adenine) is too large and the ribytyl bridge favours no electron transfer [Ber02].

3.2 The flavin redox system

As stated earlier, flavins are found in three different redox states and each of these states can exist in cationic, anionic and neutral form (Fig 3.4). Any redox reaction carried out with flavin is influenced by the pH of the solution used.

The naturally occurring flavins are found in oxidized form, also called as flavoquinone ($Fl_{ox}H$). At pH values between 1 and 9, the flavoquinone is in the neutral form. The proton at N(3) dissociates with a pK value of about 10. The cation is formed at pH values < 0. In aqueous solution of riboflavin, the cationic form has been found to be non fluorescent ($\phi_F < 5 \times 10^{-5}$), the fluorescence quantum yield of the neutral form is pH independent ($\phi_F \approx 0.26$) and the fluorescence quantum yield of the anionic form is weak ($\phi_F \sim 0.00115$) [Drö02].
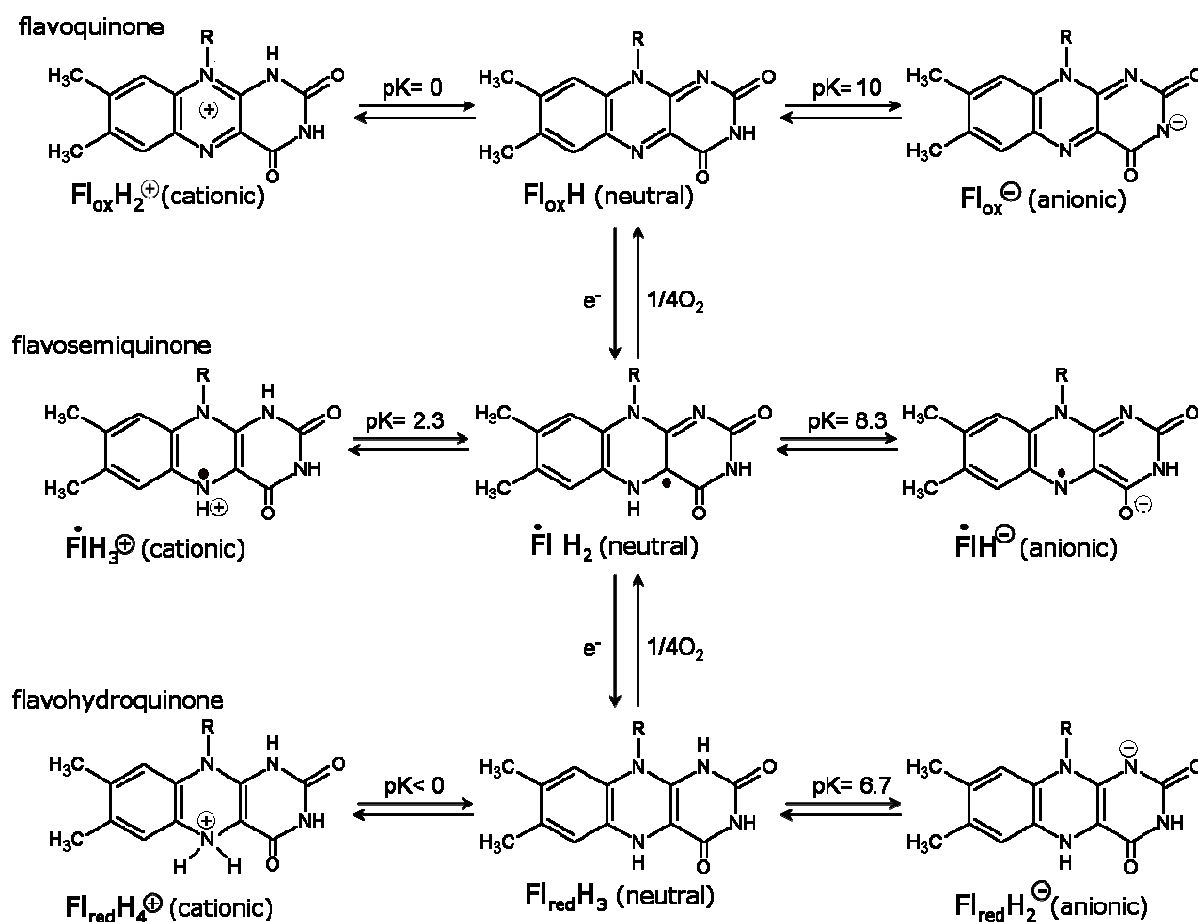
Figure 3.4 The structures of the neutral, anionic and cationic flavin species in the three redox states [Hee82, Mül87].

The reduction of flavoquinone by one electron gives flavosemiquinone (Fl•H$_2$). The proton in the neutral molecule is bound to the N(5) atom [Mül70]. The solution of the neutral flavosemiquinone is blue or green coloured, depending on the polarity of the solvent [Mül72]. The anionic flavosemiquinone deprotonates with a pK of 8.3. It possesses a red colour [Mül91].The neutral flavoquinone protonates with a pK value of 2.3. Cationic semiquinone is rather stable towards oxygen compared to the neutral and anionic species.

The two electron reduced flavin is called flavohydroquinone (Fl$_{red}$H$_3$). Protonation occurs at N(5) with a pK<0.The most acidic position is N(1) with a pK of about 6.7 [Mül91].

All the forms of flavin are not biologically relevant. Only neutral flavoquinone, neutral and anionic flavosemiquinone, neutral and anionic flavohydroquinone may be present under physiological conditions [Mül87].

Excitation of the flavins causes some photodegradation of the molecules. The main products of photodegradation are lumichrome and derivatives of lumiflavin. FAD is found to have a higher photostability because of the reductive photo-induced electron-transfer from adenosine moiety to isoalloxazine ring and subsequent non-radiative recombination leading to a short lifetime in excited state. This short effective excited-state lifetime of FAD seems to be responsible for the higher FAD photo-stability compared to FMN and riboflavin [Hol05].

4   Proteins

Proteins are the most versatile macromolecules in living systems and serve crucial functions in essentially all biological processes. They function as catalysts, they transport and store other molecules such as oxygen, they provide mechanical support and immune protection, they generate movement, transmit nerve impulses, and control growth and differentiation [Ber07b, Nel04].

Proteins are polymers built up from monomer units called amino acids. An amino acid consists of a central carbon atom (the alpha carbon C_{alpha}) and an amino group (NH_2), a hydrogen atom (H), a carboxy group (COOH) and a side group (R) which are bound to the C_{alpha}. With four different groups connected to the tetrahedral α-carbon atom, amino acids are chiral; the two mirror-image forms are called the l isomer and the d isomer. The l and d isomers are mirror images of each other. Only l amino acids are constituents of proteins [Ber07b].

Different side groups (R_i) make up different amino acids with different physico-chemical properties There are twenty different side groups varying in size, shape, charge, hydrogen bonding capacity, hydrophobic character and chemical reactivity commonly found in proteins. The amino acids with their letter codes and molecular structures are shown in the appendix A.1.

4.1   Protein structure organisation

The structural organization of protein can be divided into four levels: primary, secondary, tertiary, quaternary.

46

4.1.1 Primary structure

The protein sequence, or amino acid sequence, in a polypeptide chain defines the primary structure of a protein. Proteins are linear polymers formed by linking the α-carboxyl group of one amino acid to the α -amino group of another amino acid with a peptide bond (also called amide bond).The formation of a dipeptide from two amino acids is accompanied by the loss of a water molecule. The equilibrium of this reaction lies on the side of hydrolysis, i.e. on the left side of the following reaction, and hence biosynthesis of peptide bonds requires an input of free energy [Ber07b].

$$H_2N-\underset{\underset{H}{|}}{\overset{\overset{R_1}{|}}{C}}-\underset{O}{\overset{OH}{C}} \quad + \quad H_2N-\underset{\underset{H}{|}}{\overset{\overset{R_2}{|}}{C}}-\underset{O}{\overset{OH}{C}} \quad \xrightarrow{\Delta G} \quad H_2N-\underset{\underset{H}{|}}{\overset{\overset{R_1}{|}}{C}}-\boxed{\underset{O}{\overset{}{C}}-\underset{|}{\overset{H}{N}}}-\underset{\underset{H}{|}}{\overset{\overset{R_2}{|}}{C}}-\underset{O}{\overset{OH}{C}} \quad + H_2O$$
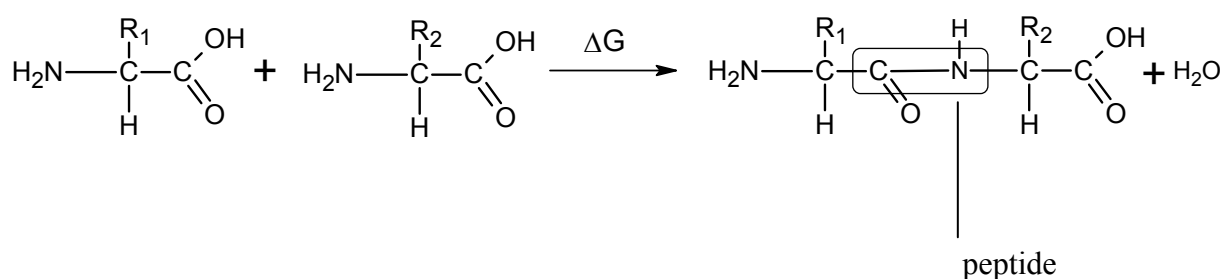
peptide

A series of amino acids joined by peptide bonds form a polypeptide chain. Each amino acid unit in a polypeptide is called a residue. A polypeptide chain has polarity because its ends are different with an amino group at one end and a carboxyl group at the other. By convention, the amino end (N- terminal) is taken to be the beginning of a polypeptide chain and hence the sequence of amino acids in a polypeptide chain is written starting with the amino-terminal residue [Ber07, Nel04].

A polypeptide chain consists of a regularly repeating part, called the main chain or backbone, and a variable part, comprising of distinctive side groups, R_i ,of the amino acids (Fig. 4.1). The polypeptide backbone is rich in hydrogen-bonding potential. Each residue contains a carbonyl group, which is a good hydrogen-bond acceptor and a NH group (with the exception of proline), which is a good hydrogen-bond donor. These groups interact with each other and with functional groups from side groups to stabilize particular structures.
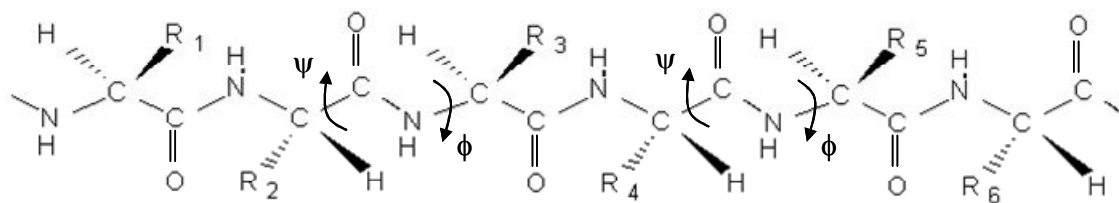
Figure 4.1 A polypeptide chain consisting of a constant backbone and variable side chains. Also shown in the figure are torsion angles of the backbone.

The peptide bond has some double bond character (40%) due to the resonance which occurs with amides. As a result of this, the peptide bond cannot rotate and this constrains the conformation of the peptide backbone and therefore the peptide bonds are almost planar. The C-N distance in a peptide bond is typically 1.32 Å, which is between the values expected for a C-N single bond (1.49 Å) and a C=N double bond (1.27 Å).

Two configurations are possible for a planar peptide bond. In the *trans* configuration, the two α-carbon atoms are on opposite sides of the peptide bond. In the *cis* configuration, these groups are on the same side of the peptide bond. Almost all peptide bonds in proteins are *trans*. This preference for *trans* over *cis* is because of the steric clashes between groups attached to the α-carbon atoms hinder formation of the *cis* form.

In contrast with the peptide bond, the bonds between the amino group and the α-carbon atom and between the α-carbon atom and the carbonyl group are pure single bonds. The two adjacent rigid peptide units may rotate about these bonds, taking on various orientations. This freedom of rotation about two bonds of each amino acid allows proteins to fold in many different ways. The rotations about these bonds can be specified by dihedral angles. The angle of rotation about the bond between the nitrogen and the α-carbon atoms is called phi (ϕ), see Fig 4.1. The angle of rotation about the bond between the α-carbon and the carbonyl carbon atoms is called psi (ψ), see Fig 4.1. A clockwise rotation about either bond as viewed from the front of the back group corresponds to a positive value. The ϕ and ψ angles

determine the path of the polypeptide chain. The rigidity of the peptide unit and the restricted set of allowed ϕ and ψ angles limits the number of structures accessible to the unfolded form sufficiently to allow protein folding to occur [Ber07].

4.1.2 Secondary structure

Polypeptide chains can fold into structures such as the α-helix, the β pleated sheet, β turn and omega (Ω) loop. α helices and β sheets are periodic structures. The common turn or loop structures are also well defined (although not periodic) and contribute with α helices and β sheets to form the final protein structure.

4.1.2.1 Alpha helix

The α –helix is a rodlike structure. A tightly coiled backbone forms the inner part of the rod and the side groups extend outward in a helical array (Fig 4.2). The α helix is
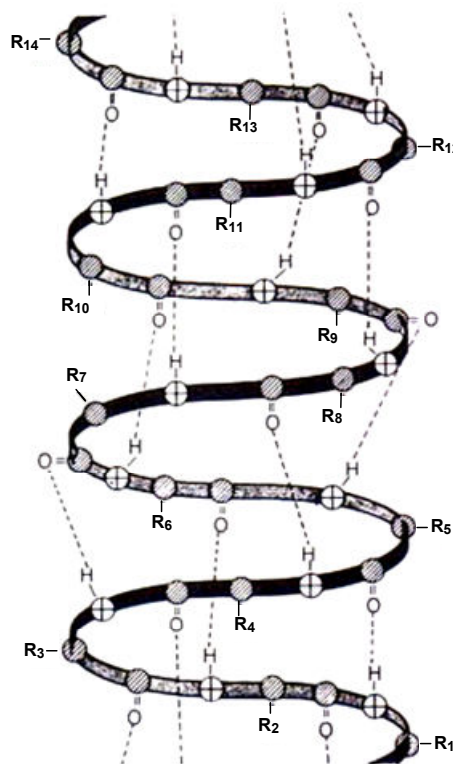

Figure 4.2   Structure of an α-helix. Nitrogen atoms are shown as ⊕ and carbon atoms are shown as ⊘.

stabilized by hydrogen bonds between the NH and CO groups of the main chain. In particular, the CO group of each amino acid (n) forms a hydrogen bond with the NH group of the amino acid that is situated four residues ahead in the sequence (n+4).

Thus, except for amino acids near the ends of an α helix, all the main-chain CO and NH groups are hydrogen bonded. Each residue is related to the next one by a rise of 1.5 Å along the helix axis and a rotation of 100 degrees, which gives 3.6 amino acid residues per turn of helix. Thus, amino acids spaced three and four apart in the sequence are spatially quite close to one another in an α helix. The amino acids two apart in the sequence are situated on opposite sides of the helix and so are unlikely to make contact. The *pitch* of the α helix (the product of the translation (0.15 nm) and the number of residues per turn (3.6)) is 0.54 nm. The screw sense of a helix can be right-handed (clockwise) or left-handed (counterclockwise).

4.1.2.2 Beta sheets

β-sheets are composed of two or more different regions of stretches of at least 5-10 amino acids. The folding and alignment of stretches of the polypeptide backbone aside one another to form β-sheets is stabilized by H-bonding between amide nitrogens and carbonyl carbons. However, the H-bonding residues are present in adjacently opposed stretches of the polypetide backbone as opposed to a linearly contiguous region of the backbone in the α-helix. β-sheets are said to be pleated. This is due to positioning of the α-carbons of the peptide bond which alternates above and below the plane of the sheet. β-sheets can be either parallel, antiparallel or mixed. In parallel sheets adjacent peptide chains proceed in the same direction (i.e. the direction of N-terminal to C-terminal ends is the same), whereas in antiparallel sheets adjacent chains are aligned in opposite directions. In the mixed sheets some strands are parallel and some are antiparallel. Parallel sheets are less twisted than the antiparallel ones and are always buried. In contrast, antiparallel sheets can withstand greater distortions and greater exposure to solvent, implying that antiparallel sheets are more stable than parallel ones.

Fig. 4.3 shows an antiparallel β-strand and a parallel β-strand. The hydrogen bonds between the NH and CO groups are shown with dashed lines. The directions of the strands are shown with arrows pointing in the direction from N to C terminal.
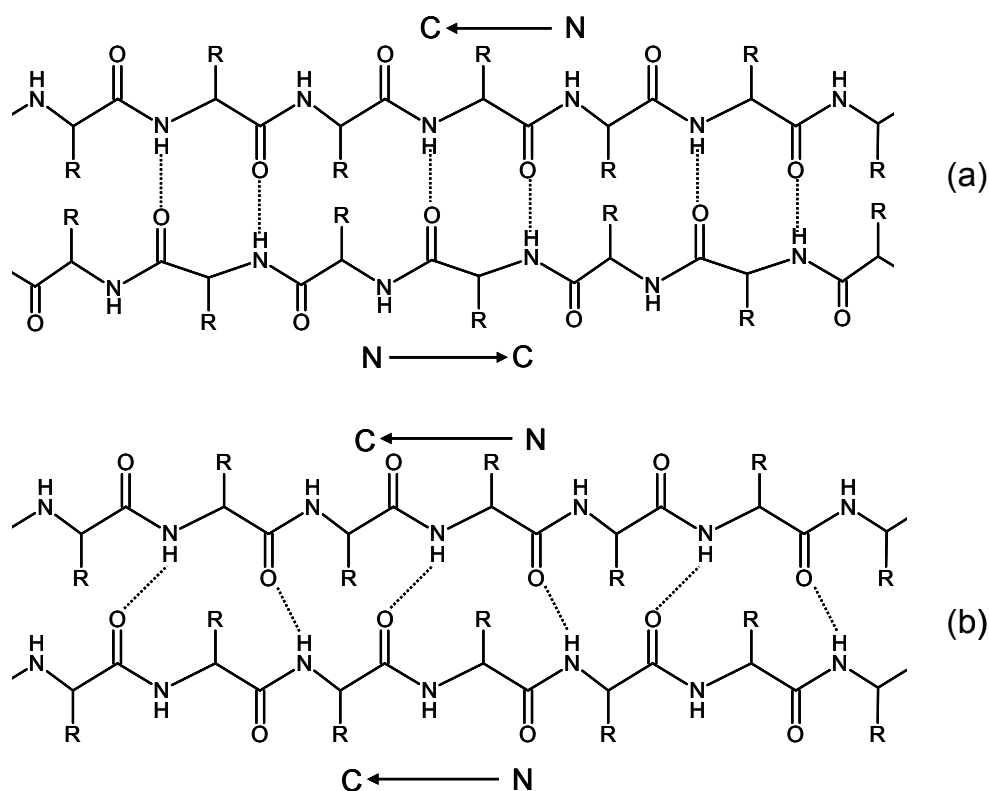

Figure 4.3 (a) An antiparallel β sheet. Adjacent β strands run in opposite directions. Hydrogen bonds between NH and CO groups connect each amino acid to a single amino acid on an adjacent strand, stabilizing the structure. (b) A parallel β Sheet. Adjacent β strands run in the same direction. Hydrogen bonds connect each amino acid on one strand with two different amino acids on the adjacent strand. Hydrogen bonds are shown with dashed lines (.....).

Usually, β strands are depicted by broad arrows pointing in the direction of the carboxyl-terminal end to indicate the type of β sheet formed—parallel or antiparallel.

4.1.2.3 Beta turns and Omega loops

Most proteins have compact, globular shapes, requiring reversals in the direction of their polypeptide chains. Many of these reversals are accomplished by a common structural element called the β turn (also known as the reverse turn or hairpin bend). In many reverse

turns, the CO group of residue n, of a polypeptide is hydrogen bonded to the NH group of residue n + 3. This interaction stabilizes abrupt changes in direction of the polypeptide chain. In many cases, structures called as Ω loops (omega loops) are responsible for chain reversals. Unlike α helices and β strands, loops do not have regular, periodic structures. Nonetheless, loop structures are often rigid and well defined. Turns and loops lie on the surfaces of proteins and thus often participate in interactions between proteins and other molecules. The distribution of α helices, β strands, and turns along a protein chain is referred to as its secondary structure [Ber07].

4.1.3 Tertiary structure

Tertiary protein structure refers to the complete three dimensional folding of a protein. Included in this description is the spatial relationship of different secondary structures to one another within a polypeptide chain and how these secondary structures themselves fold into the three-dimensional form of the protein. Secondary structures of proteins often constitute distinct domains. Therefore, tertiary structure also describes the relationship of different domains to one another within a protein. Stabilization of a protein's tertiary structure may involve interactions between amino acids located far apart along the primary sequence. These may include:

- weak interactions such as hydrogen bonds and Van der Waals interactions.
- ionic bonds involving negatively charged and positively charged amino acid side- groups.
- disulfide bonds, covalent linkages that may form as the thiol groups of two cysteine residues are oxidized to a disulfide: $2 \text{ R–SH} \rightarrow \text{R–S–S–R}$.

Interactions with the aqueous solvent, known as the hydrophobic effect, results in residues with non-polar side-groups typically being buried in the interior of a protein. Conversely, polar amino acid side-groups tend to be on the surface of a protein where they are exposed to the aqueous milieu. There are, however, many exceptions in which polar residues

are buried or non-polar residues exposed on the surface of a protein. Such atypical locations might be stabilized, e.g. by interaction of amino acid side- groups with enzyme prosthetic groups or other ligands, by interactions between amino acid side- groups, or by association of proteins with lipid membranes, etc.

4.1.4 Quaternary structure

Quaternary protein structure refers to the regular association of two or more polypeptide chains, called subunits, to form a complex. A variety of bonding interactions including hydrogen bonding, salt bridges, and disulfide bonds hold the various chains into a particular geometry. The simplest sort of quaternary structure is a dimer consisting of two identical subunits.

Generally speaking, all functions of the living organisms are related with proteins. Each protein or group of proteins is responsible for its own specific function. Proteins can be classified on the basis of their functions as:

- Enzymes: proteins catalyzing chemical and biochemical reactions with in living cells and outside. For example, hydrolases catalyze the hydrolysis of various bonds.

- Hormones: proteins responsible for regulation of many processes in organisms. An example is insulin.

- Transport proteins: proteins transporting or storing some chemical compounds or ions.

- Antibodies: proteins involved into immune response of the organism against foreign molecules.

- Structural proteins: proteins maintaining the structures of other biological components like cells and tissues.

- Receptors proteins: proteins responsible for signal detection and translation into other type of signal. For example, rhodopsin-light detecting protein.

- Signalling proteins: proteins involved into signaling translation proteins. Usually they significantly change conformation in presence of some signaling molecules. These proteins can act as enzymes. Some can interact with receptors.

5   Blue light photoreceptors

Light in the blue region of the spectrum is an ubiquitous environmental signal. Blue light can penetrate marine water to a depth greater than all other wavelengths, up to the limits of the photic zone ($\approx$ 1,500 m depth) [Los08] and may be linked to the evolution of photosynthesis [Rag04]. Blue light is also potentially dangerous because it is readily absorbed by intracellular photosensitizers (e.g., porphyrin derivatives and flavins) which could generate singlet oxygen and other products harmful for the organism [Ghe92] Therefore, living organisms detect and respond to blue light either by photoprotection mechanisms or by maximally exploiting this environmental input, e.g., to entrain circadian rhythms (24 hr periodic oscillation are called circadian (circa = about; dian = a day)) and optimize photosynthetic efficiency [Los08]. The existence of blue light photoreceptors in plants has been proposed since long but the receptors that are responsible for detecting the blue light have been discovered only recently.

At present there are four photoreceptor families that have been found to be responsible for the detection of blue light by plants, bacteria and other microorganisms. These are BLUF proteins [Gom02], cryptochromes [Ahm93], phototropins [Hua97] utilizing flavin as a chromophore to detect the blue light and xanthopsins [Mey85] using p-coumaric acid as chromophore for the detection of blue light. These blue light photoreceptors are discussed in detail in the following sections.

5.1 BLUF proteins

The BLUF domain was first discovered as the N-terminal part of the flavoprotein AppA from *Rhodobacter sphaeroides* [Gom02, Mas02]. AppA is a two component protein that binds FAD non-covalently at the N-terminal and can sense blue light at the N-teminal

domain and oxygen tension at its csyteine rich C-terminal domain. It was shown to control the photosynthetic gene expression in response to high intensity blue light irradiation and variation of the oxygen tension [Mas02, Gom95, Gom98]. Since the discovery of AppA, a large number of BLUF proteins have been identified but the physiological functions and spectroscopic properties have been determined for only a few of them. The characterized proteins are multidomain proteins such as, AppA from *Rb. sphaeroides* [Gom02, Bra02, Mas02], YcgF from *Escherichia coli* (functions as blue light regulated phosphodiesterase) [Gom98, Raj04, Has06], PAC from unicellular flagellate *Euglena gracilis* (blue light receptor for photophobic response) [Ise02, Nte03] as well as single domain proteins e.g. BlrB from *Rb. sphaeroides* (function not yet known) [Jun05, Zir06], Slr1694 from cyanobacterium *Synechocystis* sp. PCC6803 (responsible for negative phototaxis] [Oka05, Has04, Mas04, Gau06, Zir07a] and Tll0078 (also called TePixD) from thermophilic unicellular cyanobacterium *Thermosynechococcus elongates* [Oka06, Tak07, Fuk05, Kit05].

As stated above, BLUF domains bind a single molecule of oxidized FAD, resulting in a S_0-S_1 absorption band near 450 nm and S_0-S_2 absorption near 360 nm. Blue light excitation of the dark adapted BLUF domains (receptor state) leads to a red shift (~10-15 nm) of the S_0-S_1 band leading to the formation of a signaling state. This state recovers back to the initial absorption behaviour in dark. The fluorescence efficiency of BLUF domains in the dark adapted state is small and is even smaller in the light adapted or signaling state [Bra02, Dra05, Fuk05, Gau06, Gom02, Ise02, Kit05, Laa03, Laa06, Oka06, Tak07, Yua06, Zir05, Zir06, Zir07a, Zir07b].

5.1.1 Structural features

In BLUF domains, *in vivo* the active chromophore is FAD [Ise02, Mas02]. *In vitro,* BLUF domains don't show absolute chromophore preference for FAD. They can bind riboflavin, FMN, or FAD [Zir05, Zir06, Zir07, Mas05b]. In AppA-BLUF the chromophore

composition does not have remarkable effects on the photocycle as the light driven conformational changes are very similar in the samples containing FAD, riboflavin or FMN. A similar behaviour is shown by Slr1694 [Zir07], but the short BLUF protein BlrB shows some effect of changing the chromophore [Zir06].

In AppA, (AppA being the most studied BLUF protein) the sequence of the secondary elements (α/β folds) wraps around the chromophore. The $\beta_1\alpha_1\beta_2\beta_3\alpha_2\beta_4\beta_5$ arrangement is different in BLUF domains compared to other flavin binding proteins. The two central helices $\alpha1$ and $\alpha2$ build two walls that flank the flavin ring along its main axis, and the two important amino acids, tyrosine (Tyr21 or Y21) and glutamine (Gln63 or Q63) are localized on $\beta1$ and $\beta3$ respectively. The β-sheet is here partially organized in parallel strands, running perpendicular to the isoalloxazine ring. Hence, the BLUF domain is buried in a sort of organized coil and the chromophore is wrapped around having the majority of the interactions with the inner strands and helices (Fig 5.1) [Los07].
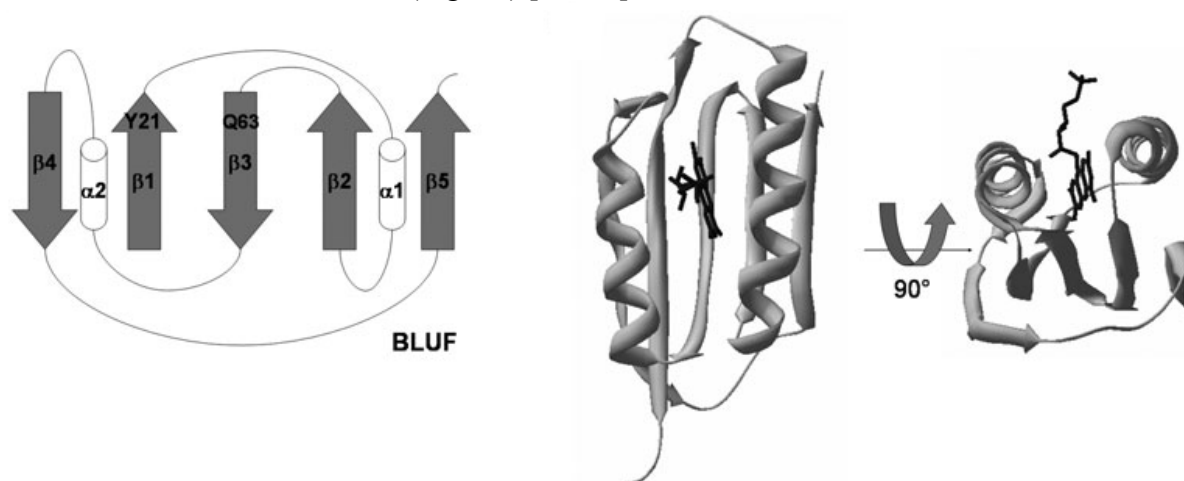

Figure 5.1   Topology of BLUF domain. The chromophore is shown in black [Los07].

Dark adapted AppA exhibits the spectral features typical of an oxidized flavin centered at 365 and 445 nm. On shining light both the absorption bands undergo a red shift becoming centered at 371 and 460 nm, respectively. These spectral changes are reversible in dark. The fluorescence quantum yield of AppA and other BLUF domains in the dark adapted

state (receptor state) is low because of the photoinduced electron transfer with protein as the electron donor and flavin being the electron acceptor. All the BLUF proteins show an AppA-like photocycle with some differences in absorption maxima, recovery time, magnitude of redshift etc. The formation of the signalling state, $BLUF_{sig}$, occurs from the excited singlet state of the FAD chromophore whereas the triplet state is formed with very low efficiency
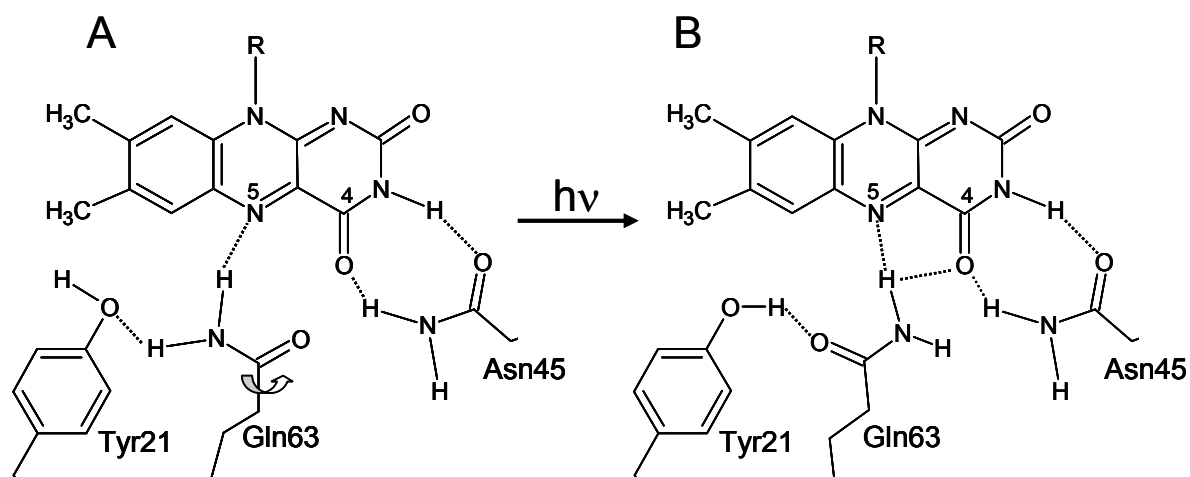

Figure 5.2 Hydrogen bond network to the flavin in AppA crystal. Hydrogen bonds are shown as dashed lines. (A) Hydrogen bond network in dark state orientation of Gln63.(B) Alternate hydrogen bond network with flipped orientation of Gln63 [And05].

[Gau05]. Two amino acids important for the BLUF photocycle are Tyr21 and Gln63 in AppA (see Fig 5.1 and Fig 5.2). Presently it is accepted, that the light induced redshifts in the absorption spectrum is caused by hydrogen bond rearrangements around the flavin chromophore (Fig 5.2) mainly strengthening the hydrogen bond at C(4)=O position and that Tyr and Gln are both required to obtain $BLUF_{sig}$.

5.1.2 The BLUF photocycle and photoactivation mechanism

Time resolved spectroscopy has been applied to BLUF domains to characterize their photocycles and to determine the intermediates on the reaction pathway towards the red shifted signaling state.

For AppA, the photocycle has been proposed as consisting of three molecular states: the FAD singlet excited state FAD^*, the FAD triplet state FAD^T and the red-shifted AppA signaling state $AppA_{sig}$ [Ken05]. The photocycle is shown in Fig 5.3. On exposure of blue light the FAD in singlet ground state goes to singlet excited state, FAD^*. FAD^* has multi-exponential decay with lifetimes of 90 ps, 590 ps and 5ns. The first two lifetimes relate to formation of signaling state $AppA_{sig}$. The singlet excited state FAD^* goes to the triplet state FAD^T via intersystem crossing with a time constant of 5 ns and with an efficiency of 9%. FAD^T returns to the singlet ground state FAD by intersystem crossing with a time constant of 3µs. The signaling state $AppA_{sig}$ returns back to the $AppA_{rec}$ with a slow time constant of 1800 s at room temperature.
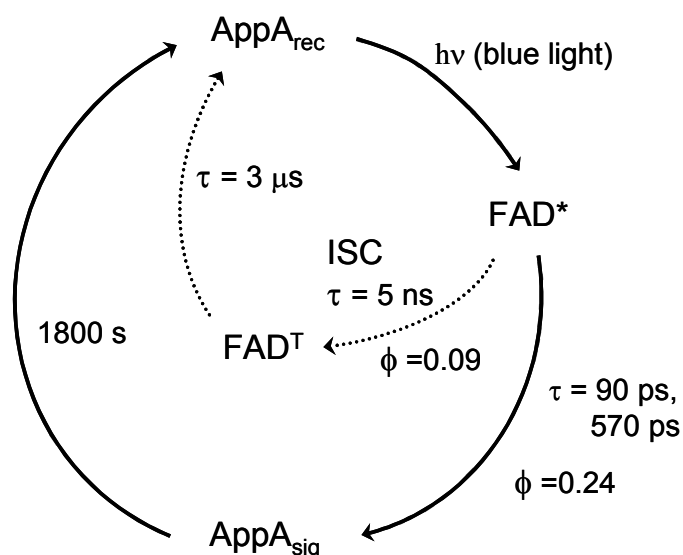

Figure 5.3 Photocycle scheme for the AppA BLUF domain [Ken05].

Thus the signaling state is formed on an ultrafast time scale and remains stable for a long time. The quantum yield of the signaling state formation was determined as 0.24 [Ken05]. For other studies on the photodynamics of AppA see [Zir05].

Spectroscopic measurements performed on Slr1694 and Tll0078 proteins at low temperatures [Fuk05, Fuk07] showed new spectral features which were interpreted as new intermediates in the BLUF photocycle by the authors. At 5 K, an intermediate called I was

assigned which is only a few nanometers shifted with respect to the parent state. By increasing the temperature, a further red shifted J intermediate was assigned, and at room temperature, the final state $BLUF_{sig}$ was formed [Fuk05, Fuk07].

5.2   Cryptochromes

Cryptochromes (CRY) are flavoproteins that exhibit high sequence and structural similarity to light dependent DNA-repair enzymes called photolyases. However cryptochromes have no photolyase activity. The photolyases and cryptochromes make up the photolyase/cryptochrome superfamily [Kan97]. According to their sequence similarities, cryptochromes from a range of organisms can be clustered into three families: plant cryptochromes, animal cryptochromes and cryptochrome-DASH proteins. The first cryptochrome to be identified was CRY1 in *Arabidopsis thaliana* (thale cress) [Ahm93]. Plant cryptochromes have been identified in *Arabidopsis thaliana*, tomato, rice, barley, fern, moss and the green alga, *Chlamydomonas reinhardtii*. Plant cryptochromes mediate inhibition of stem growth, entrainment of circadian rhythms, day light detection in photoperiodism, regulation of gene expression [Bat05]. Animal cryptochromes have been found in various animal lineages, including insects, fish, amphibians, and mammals. Animal cryptochromes act as components of the circadian clock that control daily physiological and behavioral rhythms and as photoreceptors that mediate entrainment of the circadian clock to light [Cas03]. Initially it was thought that only higher eukaryotes (cells with nucleus) have cryptochromes and that prokaryotes (cell without nucleus) have only photolyases, but later a new type of cryptochrome was found in cyanobacteria [Hit00]. This was referred to as CRY-DASH to link it to the cryptochromes found in *Drosophila* (fly*)*, *Arabidopsis* (plant*)*, *Synechocystis* (bacterium) and *Human* (mammals). CRY-DASH proteins have now been found in non-photosynthetic bacteria, fungi, plants and animals. The biological function of CRY-DASH is still not known although they have single-stranded DNA repair ability [Sel06].

Animal cryptochromes are divided into two broad groups, type 1 cryptochromes which are circadian photoreceptors (senses the light and transmits the signal) (e.g. *Drosophila* cryptochrome (dcry)) and type 2 cryptochromes which are core clock proteins (core clock proteins control circadian rhythms) (human Cry1 and Cry2 are examples) [Özt08].

5.2.1 Structural details

Plant cryptochromes have an amino N-terminal PHR (Photolyase Homology Region) of about 500 amino acids (aa) sharing the sequence homology with photolyases [San94, Ahm95, Cas99]. The length of the C-terminal extension varies strongly. In general, plant type cryptochromes contain a longer, species-specific C-terminal domain (>100 aa) than animal cryptochromes. The C terminal is absent in Cry-DASH cryptochromes which instead have a similar region on the N-terminal of the photolyase homology region [Kla07] (Fig. 5.4). Cryptochromes are 50-70 kDa proteins that contain two noncovalently bound chromophores.
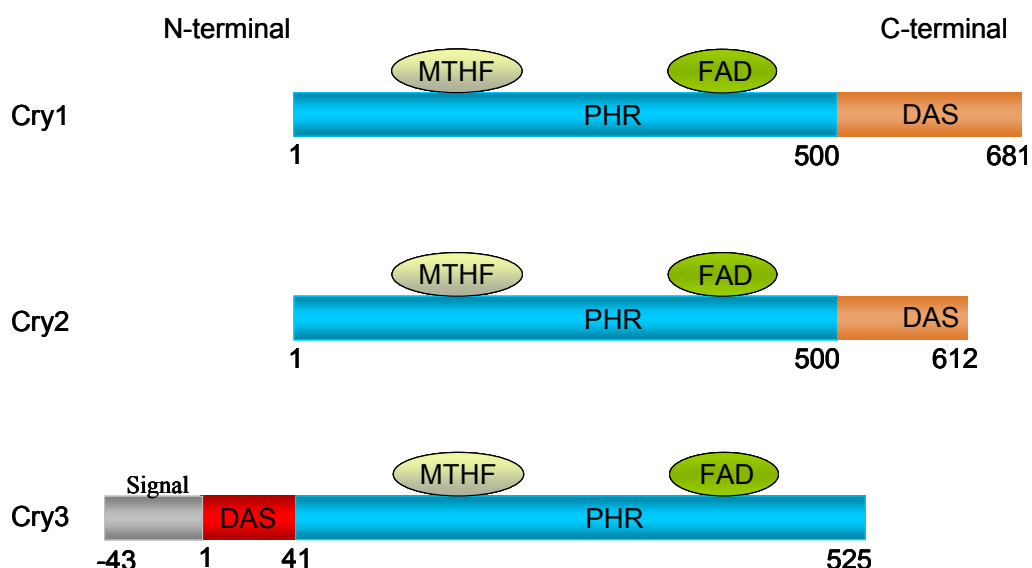

Figure 5.4   Scheme showing the N and C-terminal extensions of Cry1, Cry2 and Cry3 (or Cry-DASH) from Arabidopsis thaliana. The C-terminal contains DAS motif ('D'- conserved   aspartic acid residue, 'A'- Acidic residues, 'S'- Serine residues) which is of functional importance. Cry3 contains a DAS motif-like sequence at the N-terminal [Kla07].

One of them is FAD serving as the catalytic chromophore and the other serves as a photo-antenna and is methenyltetrahydrofolate (MTHF) [Par05, San03]. The N-terminal (α/β subdomain) binds the antenna and the C-terminal (α subdomain) binds the FAD chromophore. The catalytic FAD chromophore is deeply buried within the α-helical domain and has a U-shaped conformation with the isoalloxazine and adenine rings in close proximity [San03].

5.2.2 Photocycle

Since cryptochromes have a marked similarity with photolyases, it is expected that their primary photoreactions may be related. Photolyases can undergo two distinct light-induced electron transfer reactions upon excitation of their FAD cofactor [San03, Car01, Byr04]. The first reaction initiates DNA repair and requires the flavin in its fully reduced form which is oxidized to semi-reduced form. In the second reaction, known as photoactivation, the semi-reduced flavin is converted back to the fully reduced form by an electron ultimately provided by an extrinsic reductant. An intraprotein electron transfer pathway connecting the buried flavin to the protein surface has been derived for this photoactivation reaction in *E. coli* photolyase based on crystallographic structural information and on a combination of site-directed mutagenesis and spectroscopy [Che99, Aub00, Byr03]. This pathway comprises a chain of three tryptophan residues (Trp382-Trp359-Trp306) that are conserved throughout the photolyase/cryptochrome family. This chain of reactions may be similar to the working of Cry *in vivo*.

Recently, a photocycle scheme for Arabidopsis Cry1 has been proposed and has been found to be fundamentally different from that of photolyases [Bou07]. The *Arabidopsis* Cry1 photocycle consists of a light-dependent transition between the three interconvertible redox forms of FAD (FAD, $FADH^{\bullet}$, and $FADH^{-}$), of which the flavosemiquinone form ($FADH^{\bullet}$) is the signaling state of the receptor. In this mechanism, inactive Cry1, containing oxidized

flavin, accumulates in the dark. Blue light triggers flavin photoreduction of FAD such that the resulting photoequilibrium strongly favors the radical signaling state (FADH$^{\bullet}$). Green light reduces cryptochrome activity by reducing the concentration of the radical in favor of the inactive fully reduced form (FADH^{-}). Dark reversion occurs either from semiquinone flavin directly to oxidized flavin or from fully reduced flavin to the oxidized FAD (Fig 5.5). It was also found that the radical form of Cry1 is far more stable than that of photolyases.
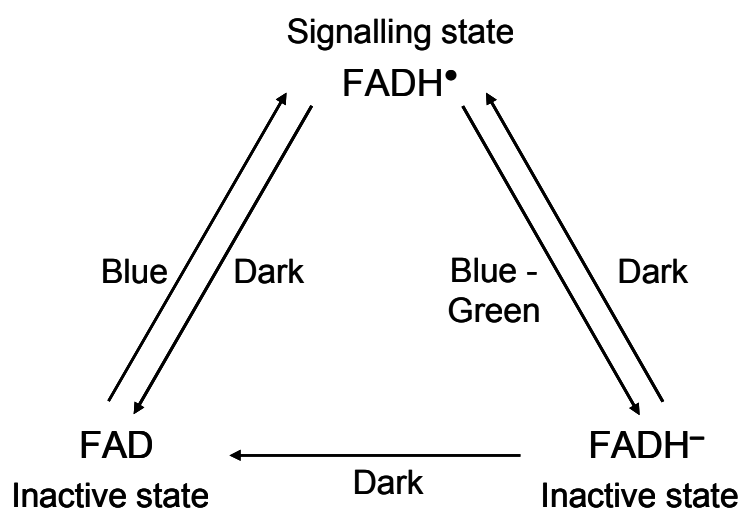
Signalling state
FADH$^{\bullet}$

Blue   Dark   Blue -   Dark
                  Green

FAD   FADH^{-}
Inactive state   Dark   Inactive state

Figure 5.5 A model of Cry1 photocycle. Cry1 exists in three interconvertible redox forms, FAD, FADH$^{\bullet}$, and FADH^{-}. The FAD form is inactive and accumulates to high levels in the dark (receptor state). Blue light triggers photoreduction of FAD to establish a photoequilibrium that favours FADH$^{\bullet}$ over FAD or FADH^{-}. The flavosemiquinone state is the signalling state of the receptor. Green light is absorbed by the radical and shifts the photoequilibrium to the fully reduced form (FADH^{-}), which is inactive. Reversion to oxidized flavin occurs in the dark, involving electron acceptors that are as yet uncharacterized. Dark reversion occurs either from semiquinone flavin directly to oxidized flavin or from fully reduced flavin to the oxidized FAD [Bou07].

The photochemistry of Cry-DASH proteins (which are nearest to the photolyases) has also been studied. Also the crystal structure of Cry-DASH protein from Arabidopsis has been obtained [Kla07]. Purified *At*-Cry3 contains MTHF antenna and a mixture of oxidized, semireduced and fully reduced FAD [Dai04, Kla07, Son06]. In *At*-Cry3, photo-excitation of FAD results in the reversible formation of the fully reduced species, FADH$_2$ (or FADH^{-}),

representing a photocycle with a very low yield (about 0.2%). When the semireduced species FADH$^\bullet$ is excited, the fully reduced FADH$_2$ (or FADH$^-$) is formed with a higher quantum efficiency of about 7%. Finally, prolonged light exposure modifies the re-oxidizable FADH$_2$ into a permanent reduced state (Fig 5.6) [Son06].
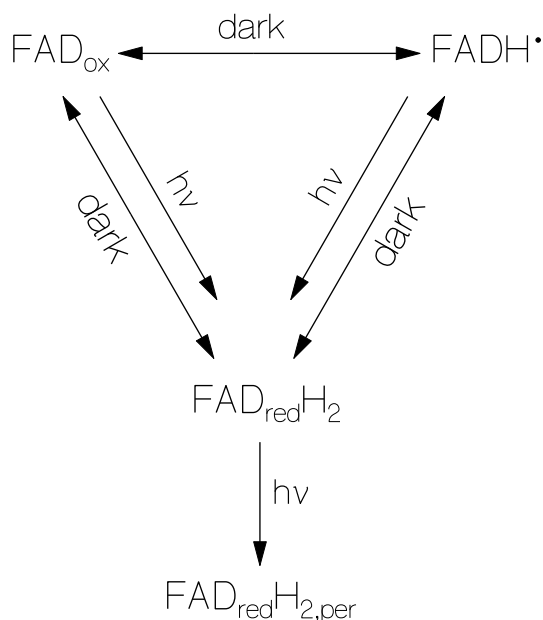

Figure 5.6 A reaction and equilibration scheme for FAD in cry3. In dark, there is an equilibrium between FAD$_{ox}$, FADH$^\bullet$, and FAD$_{red}$H2. Photo-excitation reduces FAD$_{ox}$ and FADH$^\bullet$ to FAD$_{red}$H$_2$. Prolonged light exposure modifies re-oxidable FAD$_{red}$H$_2$ to non-oxidable FAD$_{red}$H$_{2,\,per}$ [Son06]

Another Cry-DASH, VcCry1 from *Vibrio cholerae, in vitro* has the fully reduced FADH$^-$ in its dark adapted (receptor state) suggesting that this protein may indeed undergo light reactions similar to that of PHR [Wor03]. Indeed, also *in vitro, At-C*ry3 contains FADH$_2$ (or FADH$^-$) with a mole fraction of 55% but no photocycle activity of this form was found [Son06].

Animal cryptochrome from *Drosophila melanogaster* (dCry) has also been characterized [Ber07, Shi08]. The fluorescence quantum efficiency in the binding pocket of dCry was found to be low (ϕ_F= 7.4 × 10^{-5}) and the fluorescence lifetime was found to be very short ($\tau_{F,0}$=1.4 ps). Photo-excitation leads to some rise in the fluorescence efficiency due to

protein conformation changes. It has been proposed that the excitation of FAD_{ox} (which is present in dark adapted dCry) causes fast reductive intramolecular electron transfer from adenine moiety to the isoalloxazine moiety followed by external reductive electron transfer from an adjacent tryptophan residue to the positively charged adenine part forming $FAD^{\bullet-}$. The neutralized adenine part was thought to act as charge separator between the isoalloxazine anion and the tryptophan cation [Shi08]. Charge separation, protein conformational changes and charge shielding by protein polarization are thought to stabilize $FAD^{\bullet-}$ to very slow re-oxidation to FAD in the minute time range. Photo-excitation of $FAD^{\bullet-}$ causes oxidative electron transfer converting $FAD^{\bullet-}$ back to FAD and neutralizing Trp^{+} to Trp on a picosecond to nanosecond timescale. Details of the photocycle dynamics of dcry are found in [Shi08].

5.3   Phototropins/LOV domains

Phototropins are the blue light receptors controlling a range of responses that serve to optimize the photosynthetic efficiency for plant. These are phototropism, light induced stomatal opening and chloroplast movements in response to changes in light intensity [Chr01, Bri02, Kag02, Lis02, Kag03, Wad03]. The isolation of the first phototropin gene was done in 1997 [Hua97] and was found to be responsible for phototropism and hence called Phototropin [Chr99, Bri01]. It was further shown that phototropin controls other blue light activated processes as leaf expansion [Sak02] and rapid inhibition of hypocotyl elongation (plant stem growth) in dark grown seedling [Fol01] in addition to the above mentioned phenomena. The most common model plant that has been used to study the phototropin photoreceptor is *Arabidopsis thaliana* (thale cress). Phototropins are ubiquitous in higher plants and have been identified in several plant species [Chr07].

Arabidopsis thaliana contains two phototropins, phot1 and phot2 [Bri02]. Phot1 and phot2 exhibit partially overlapping roles in regulating phototropism. Both act to regulate

hypocotyl phototropism in *Arabidopsis* in response to high intensities of blue light, but under low light conditions phototropism is mediated by only phot1 [Sak01]. Also, only phot1 mediates the rapid inhibition of hypocotyl elongation by blue light [Fol01], while phot2 acts as sole photoreceptor for chloroplast high light avoidance movement [Kag01].

5.3.1 Protein structure

Protein structures of plant phototropins can be separated into two segments: a photosensory domain at the N terminal and a serine/threonine kinase domain at the C terminal (a kinase is a type of enzyme that transfers phosphate groups from high-energy donor molecules, such as ATP, to specific target molecules (substrates); the process is termed phosphorylation). Fig 5.7 shows the schematic drawing of Arabidopsis phot1 and phot2. The N-terminal photosensory domain of the phototropins contains two very similar domains of ~110 amino acids designated as LOV1 and LOV2. LOV domains are members of the large and diverse superfamily of PAS domains associated with cofactor binding and mediating protein interactions (Tay99) (PAS is an acronym formed from the names of the proteins in
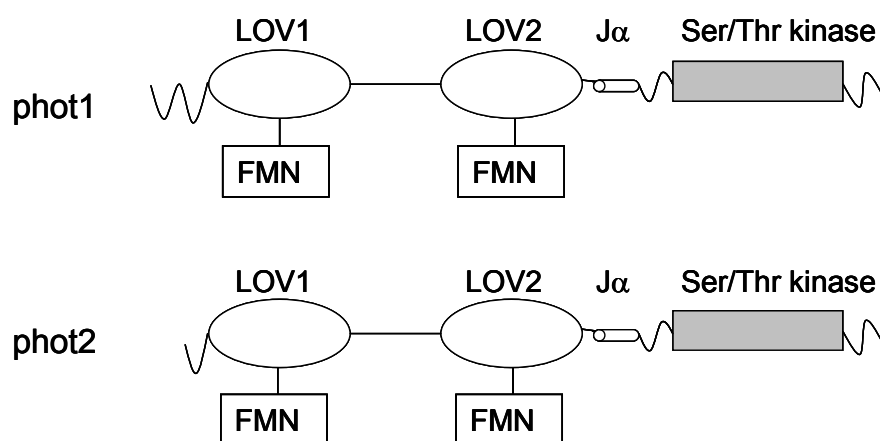

Figure 5.7   Schematic drawing of Arabidopsis phot1 and phot2 [Chr05].

which PAS motive was first recognized [Nam91]: the *Drosophilla* period clock protein (**P**ER), the vertebrate aryl hydrocarbon receptor nuclear translocator (**A**RNT) and the *Drosophilla*

66

single minded protein (<u>S</u>IM)). LOV domains are more closely related to a subset of proteins within the PAS domain superfamily that are regulated by external signals such as light, oxygen, or voltage, hence the acronym LOV [Hua97]. LOV domains bind the cofactor flavin mononucleotide (FMN) and function as bluelight sensors for the phototropin proteins [Chr99, Sal00]. At the C-terminal position of LOV2 exist a conserved α-helix (Jα). It is amphiphatic in nature, consisting of polar and apolar sides, the latter of which docks onto the β-sheet strands of the LOV2-core.

6.3.2 Phototropin activation

Phototropin activation can be viewed as a series of events beginning with the absorption of blue light by the LOV domains (Fig 5.8 A). In the dark or receptor state, the
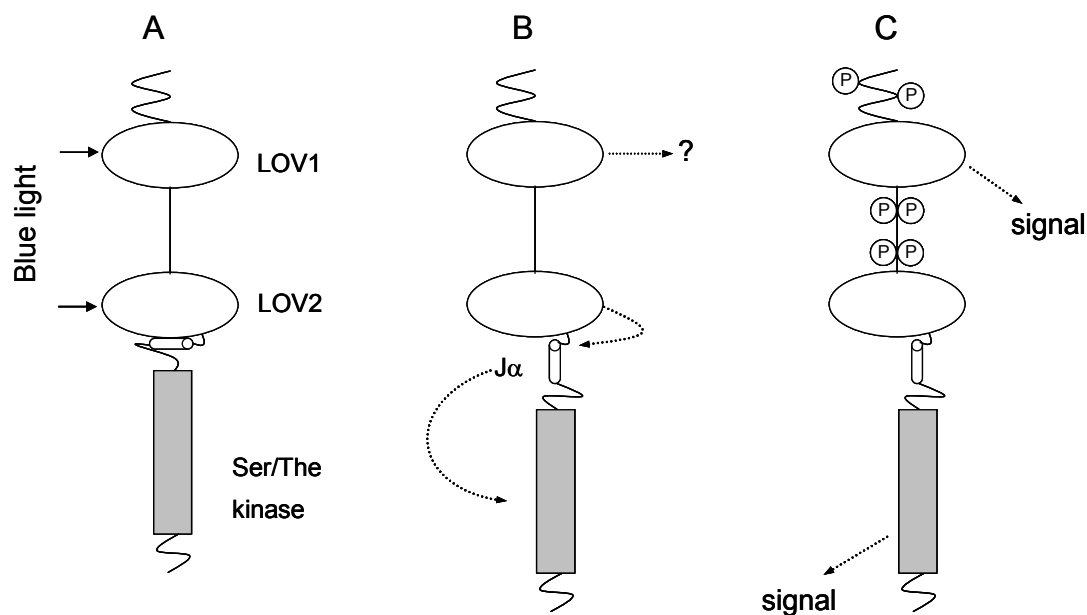

Figure 5.8   Overview of phototropin activation by blue light. (A) In the dark or ground state, the phototropin receptor is unphosphorylated and inactive. Upon irradiation, the LOV domains detect blue light. (B) Photoexcitation of LOV2 results in a protein conformational change that involves the displacement of a highly conserved α-helix from the surface of LOV2 (Jα). This protein structural change is hypothesized to lead to activation of the C-terminal kinase domain. The function of LOV1 is presently unknown. (C) Activation of the kinase domain consequently leads to autophosphorylation of the photoreceptor protein. It is unknown whether autophosphorylation is involved in receptor signaling or whether phototropin initiates signaling via substrate phosphorylation [Chr05].

67

phototropin is unphosphorylated and inactive. Upon illumination, light sensing by LOV2 is considered to result in a protein conformational change that involves the Jα helix. (Fig 5.8 B). Although the exact role of LOV1 in regulating the phototropin activity is not fully understood, the displacement of Jα in response to LOV2 photoexcitation is hypothesized to lead to activation of the C-terminal kinase domain, which in turn results in autophosphorylation of the photoreceptor protein (Fig 5.8 C) [Har03].

5.3.3 LOV-domain structure and photocycle

X-ray crystallographic studies have shown a very specific and tight non-covalent binding of FMN within a protein binding pocket [Cro01, Fed03]. In the dark state, a single molecule of FMN is held in place non-covalently through interaction with a hydrogen-bonding network on the pyrimidine side of the isoalloxazine ring and with hydrophobic residues on the dimethylbenzene moiety [Cro01]. Specifically, the FMN N3, O2, and O4 all hydrogen-bond to protein side chains; in addition, the phosphate group on the FMN ribityl chain interacts with the guanidinium groups of two arginine residues to form salt bridges. The hydroxyl groups of the FMN ribityl side chain form hydrogen bonds to the LOV-domain protein. There are two water molecules in close proximity to the chromophore. Both are within hydrogen-bonding distance of the hydroxl groups of the FMN ribityl chain.

In darkness, LOV domains bind FMN noncovalently forming a spectral species, designated as LOV_{447} or LOV_{rec}, which absorbs maximally near 447nm [Chr99, Sal00, Swa01]. Upon blue light illumination, LOV domains undergo a photocycle (Fig 5.9) that leads to the formation of a long lived species with prominent absorption band at 390 nm, referred to as LOV_{390} or LOV_{sig}. This involves the formation of a covalent adduct between the C(4a) carbon of the flavin chromophore and a conserved cysteine residue within the protein LOV domain. Mutation of the cysteine to either alanine or serine results in a loss of

photochemical reactivity [Sal00]. It is generally accepted that LOV_{390} represents the active

signalling state that leads to photoreceptor activation. For phototropin LOV domains,
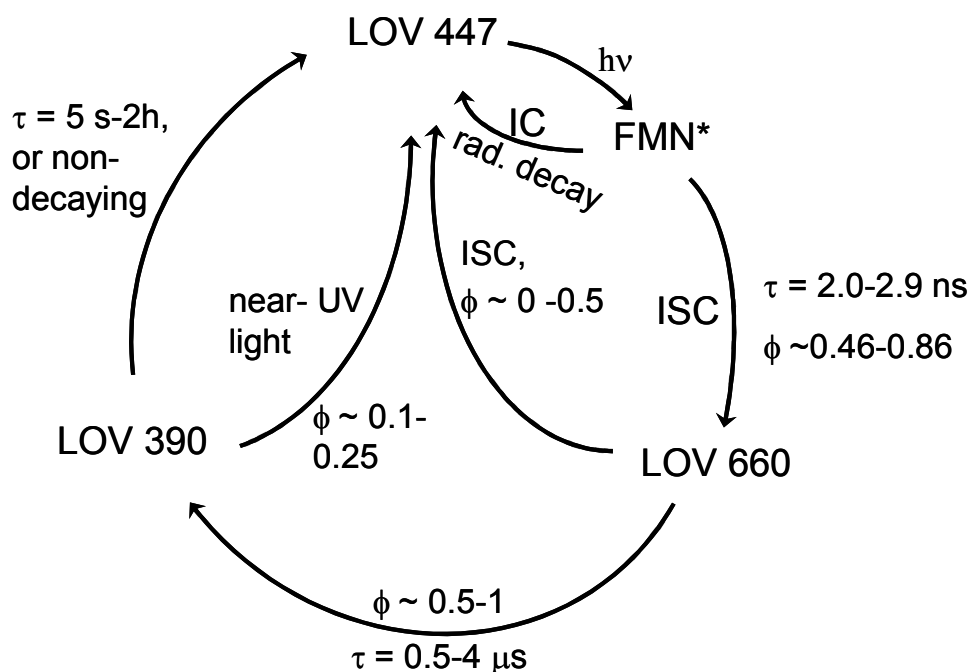

Figure 5.9   Photocycle scheme of LOV domains, based on data for plant phototropins LOV1 and
LOV2, *Chlamydomonas* phototropin LOV1 and LOV2, *Bacillus subtilis* YtvA and *Pseudomonas
putida* PpSB2-LOV. τ denotes the boundaries for measured time constants, ϕ denotes the boundaries
of reaction yields in various LOV domains [Ken05].

formation of LOV_{390} is fully reversible in darkness, returning the LOV domain back to its

initial ground state (LOV_{447}) within the order of tens to hundreds of seconds [Kas02, Sal00].

LOV domains therefore cycle between active (LOV_{390} or LOV_{sig}) and inactive (LOV_{447} or

LOV_{rec}) states depending on the light conditions. Illumination with UV-light can revert

LOV_{390} back to its initial dark state [Ken044]. However, the biological significance of this

UV-mediated reversibility with respect to the receptor function is not known.

The signalling state formation happens via the formation of an intermediate state.

Initial absorption of blue light by the FMN chromophore results in the formation of an excited

singlet state, which subsequently decays into a flavin triplet state (LOV_{660}) that absorbs

maximally in the red region of the spectrum (Ken03, Kot03, Swa01). The triplet state in turn decays to form the FMN-cysteinyl adduct. Besides the excited singlet-triplet path to the adduct form, an additional path from the excited singlet to the adduct form via photoinduced charge transfer has been described [Hol04].

5.4   Photoactive Yellow Protein, the Xanthopsin

Photoactive Yellow Protein (PYP) is a yellow coloured protein isolated for the first time from the halophilic phototropic bacterium *Halorhodospira halophila* [Mey85]. The bacterium being a phototroph can perceive the quantity and quality of the ambient radiation. It is attracted by red light but is repelled by high intensities of white light and in particular blue light. This negative phototactic response is due to the presence of PYP. Later, PYP was found in many other bacteria and the family of PYPs has been called Xanthopsins. Xanthopsins have been found so far only in proteobacteria. PYP has been nominated as the structural prototype for the complete family of the Xanthopsin of the PAS domains [Pel98].

5.4.1 Structural features

PYP is a small water soluble protein (125 amino acids, 14kD). Its chromophore is a *trans*-p-hydroxy cinnamic acid (also called p-coumaric acid) binding to the cysteine residue by a thioester bond [Bac94, Hof94]. Fig 5.10 shows a schematic representation of the photoactive site of PYP and the chemical structure of the chromophore. The phenolic oxygen of the chromophore is deprotonated and forms hydrogen bonds with the hydroxyl groups of Tyr42 and Glu46, and a hydroxyl group of Thr50 forms a hydrogen bond with Tyr42. These three residues regulate the absorption maximum of PYP. Arg52 exists near the chromophore and stabilizes the hydrogen bonding network [Bor95, Yod01, Gro02]. On photon absorption the chromophore undergoes *trans-cis* isomerization in the protein. Afterwards a proton is

transferred from Glu46 to the chromophore [Kor96, Xie96, Ima97] and a global conformation change of the protein moiety takes place which leads to formation of the signalling state [Bre95, Rub98, Hof99, Ohi01].
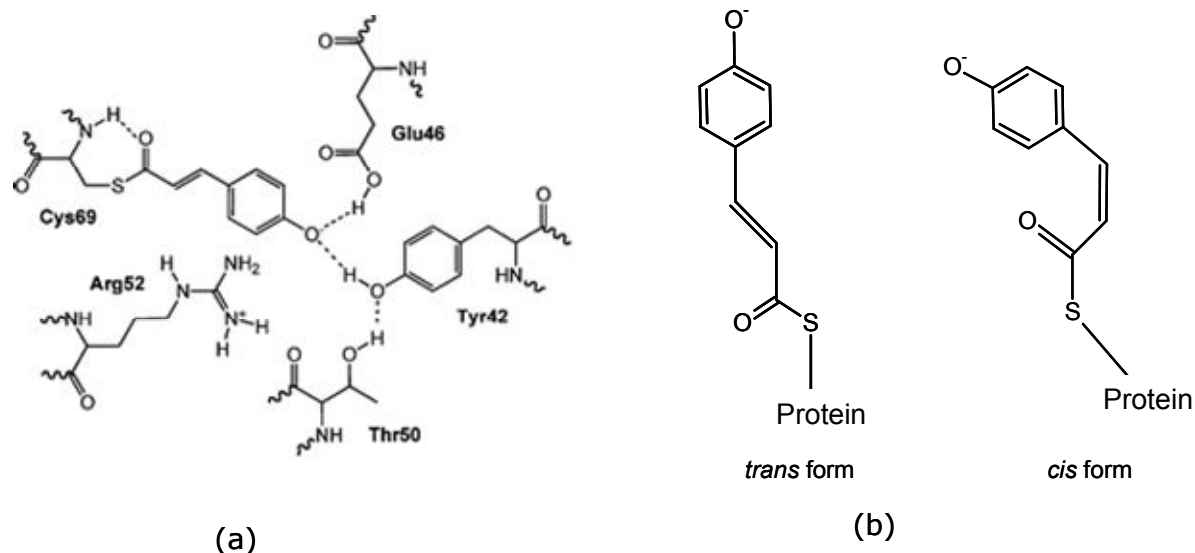

(a)   (b)

Figure 5.10 (a) A representation of the photoactive site of PYP [Esp07] and (b) the chemical structure of the PYP chromophore in *trans* and *cis* forms.

5.4.1 Photocycle of PYP

The photocycle of PYP is shown schematically in Fig 5.11 [Hor05]. The ground or dark adapted state, pG, has a deprotonated chromophore in *trans* configuration. This ground state goes to the excited state by absorption of a photon. After excitation of the ground state of PYP, its chromophore will form a twisted excited state, which subsequently results in formation of the I_0 intermediate with the chromophore in *cis* configuration, be it still twisted. Further relaxation leads to formation of pR states which are spectrally red-shifted compared to pG. These are first formed in about ~3 ns, and the chromophore is still deprotonated but has the *cis* configuration. pR actually represents two intermediates, pR_1 and pR_2. The spectra of both pR are very similar; pR_1 has a slightly higher extinction coefficient than pR_2.
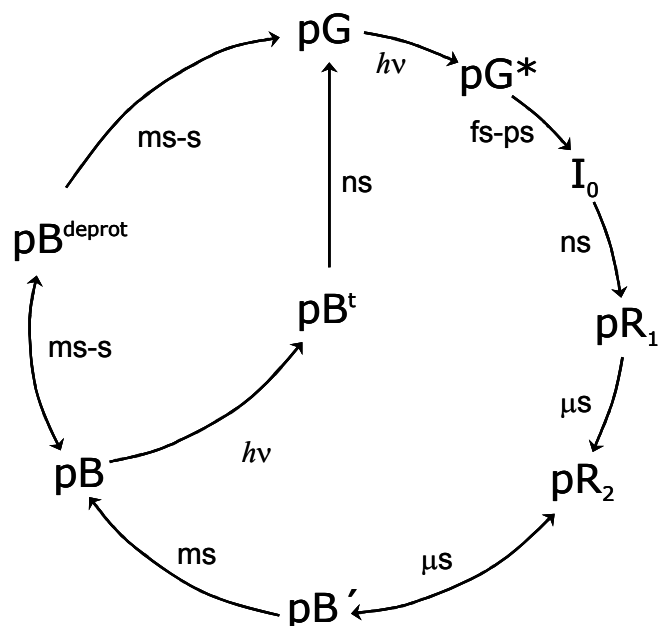
Figure 5.11 Description of photocycle of PYP at room temperature: pG and pG* refer to the ground and electronically excited state of PYP; pR and pB have a red- and a blue- shifted visible absorption maximum, respectively, as compared to the pG state. Reactions occurring upon absorption of a photon are indicated with hv; for the others the approximate lifetime is indicated. The superscript t refers to light driven *cis* to *trans* isomerization of coumaryl chromophore of PYP [Hor05].

Isomerization proceeds with a minimal amount of movement of the chromophore, through a concerted rotation around several bonds. This isomerization increases the probability of proton transfer from Glu46 to the chromophore, which results in formation of pB state via a pB′ intermediate. pR and pB′ exist in equilibrium. pB states are spectrally blue shifted states with respect to the ground state pG. They are formed on a µs/ms time scale. The pB state is presumed to be the signaling state of the PYP photoreceptor protein. The negative charge, which was stabilized via delocalization when it resided on the chromophore, via a hydrogen bonding network, and via a counter ion –now resides on Glu46 where it is very localized. This is an energetically unfavourable situation that drives subsequent structural changes, both in the N-terminal domain of the protein and around the chromophore.

After formation of the signaling state, the initial state of the photocycle recovers, which requires chromophore re-isomerization and protein re-folding. Before re-isomerization can take place, the chromophore needs to be deprotonated (leading to formation of the pB^{deprot} intermediate), and the protein needs to adopt a specific fold that allows for the re-isomerization to take place. Chromophore re-isomerization can also take place photochemically by exposure of light, which results in a rate of recovery that is three orders of magnitude faster than the dark recovery. In this branching pathway, an intermediate, pB^t (t for *trans*) is formed on a nanosecond time scale.

6 Applied experimental methods

Absorption and emission spectroscopic studies were performed to characterize a BLUF protein from the bacterium *Klebsiella pneumoniae*. It is one of the two BLUF proteins present in this bacterium. In the present chapter and the following chapters the samples are called as BlrP1 for the full length protein and BlrP1_BLUF for only the BLUF domain of this protein. Absorption measurements were carried out on the dark adapted (putative receptor state) samples. Then the samples were excited with light and brought into the light adapted state (putative signaling state). Absorption measurements on the light adapted state were also done. The fluorescence behaviour of the dark adapted and light adapted states has been studied by measuring the fluorescence quantum yields and the fluorescence lifetimes. All this information is used to develop a photocycle scheme of this BLUF domain. The following sections explain the various applied experimental methods in detail.

6.1 Absorption measurements

The absorption cross-section spectra of dark-adapted BlrP1_BLUF and BlrP1 were determined by transmission measurements with a commercial spectrophotometer (Varian Cary 50 UV-Vis Spectrophotometer). The transmission spectra, T(λ), were converted to absorption coefficient spectra, $\alpha(\lambda)$, by the relation $T(\lambda) = \exp[-\alpha(\lambda)\ell]$, where ℓ is the sample path length. The absorption cross-section spectra, $\sigma_a(\lambda)$, were calculated from the absorption coefficient spectra, $\alpha(\lambda)$, by calibration to the absorption cross-section spectrum of FAD in aqueous solution at pH 8, i.e. the absorption cross-section integrals, $\int_{\lambda > 320\,\text{nm}} \sigma_a(\tilde{\nu}) d\tilde{\nu}$, of BlrP1_BLUF, BlrP1 and FAD were set equal since the same isoalloxazine chromophore is present [Hol02] ($\sigma_a(\tilde{\nu}) = \alpha(\tilde{\nu}) \int \sigma_{a,FAD}(\tilde{\nu}) d\tilde{\nu} / \int \alpha(\tilde{\nu}) d\tilde{\nu}$, where $\sigma_{a,FAD}(\lambda)$ is the absorption

cross-section spectrum of FAD, $\tilde{\nu} = 1/\lambda$ is the wavenumber). The cofactor (FAD) number

density, N_0, is determined by $N_0 = \alpha(\lambda)/\sigma_a(\lambda)$.

The experimental setup used for measuring the absorption spectra of samples in the signalling state is shown in Fig. 6.1. The absorption cross-section spectra of the signalling state of BlrP1_BLUF and BlrP1 were determined by exciting a small-volume sample ($1.5 \times 1.5 \times 5$ mm^3) with a high-pressure mercury lamp through a broad-band interference filter (IF) (transmission range 350-440 nm), and probing the transmission with an attenuated tungsten lamp using a spectrometer − diode-array detection system (DARSS diode Array Rapid Scanning Spectrometer with TN-1710 Multichannel Analyser from Tracor Northern). The absolute absorption cross-section spectra were determined by comparing with the
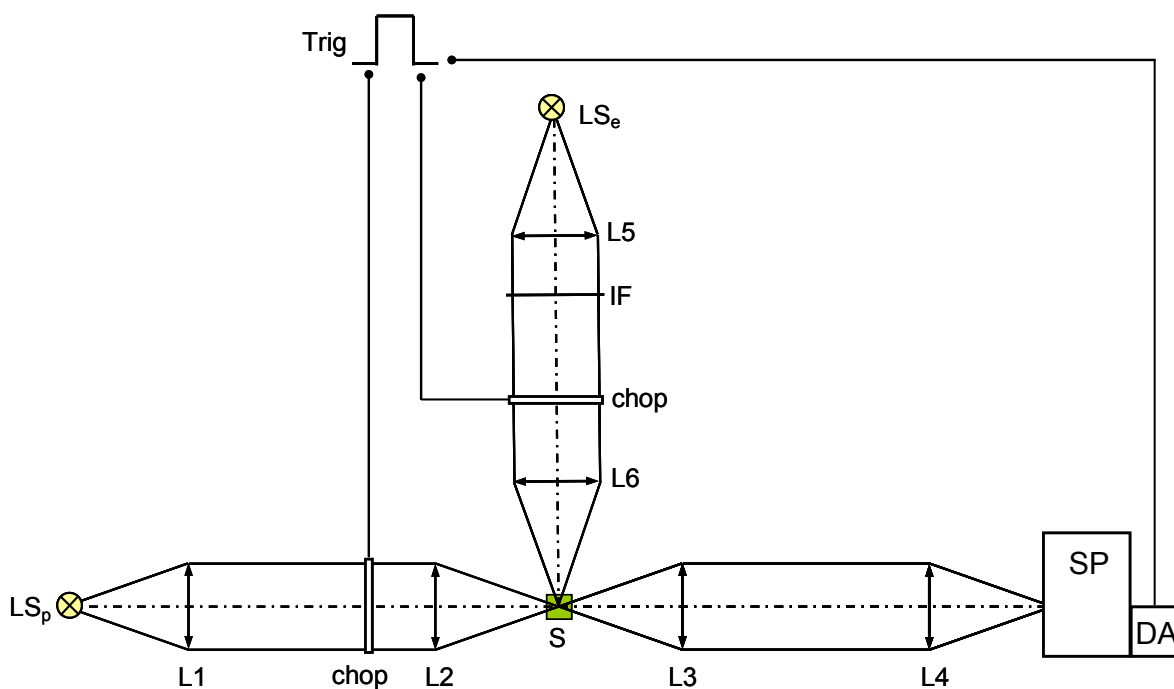

Figure 6.1   The experimental setup for studying the temporal development of absorption spectra and for photoreduction and photodegradation studies. LS$_p$: light source for probe (attenuated tungsten lamp), LS$_e$: light source for excitation (200 W mercury lamp), L1-L6: lenses, IF: interference filter, Chop: triggerable mechanical chopper, SP: spectrometer, DA: diode array, Trig: pulse generator (for triggering choppers and detector), S: sample.

transmission spectra of the samples before light exposure (isobestic point at 474.2 nm for BlrP1_BLUF, and at 462.9 nm for BlrP1). The temporal absorption changes due to the signalling-state formation by light switch-on and due to back-recovery after light switch-off have been measured by probe-light transmission measurement at a selected wavelength (interference filter) with a silicon diode detector (1 cm^2 cross-sectional area) and a digital signal recorder (time resolution 50 ms). The experimental arrangement is the same as in Fig. 6.1 except that instead of the spectrometer and diode array, an interference filter, a silicon detector and digital signal recorder are used.

The photoreduction and photodegradation of BlrP1_BLUF and BlrP1 in the signalling state was studied by long-time exposure of the samples at fixed excitation intensity and probing the transmission with a white-light tungsten lamp. The absorption changes after light switch-off (partial recovery of reduced FAD back to oxidized form) were studied by recording transmission spectra with a weak white-light tungsten lamp at certain times after pump-light switch-off. The experimental arrangement is same as in Fig. 6.1.

6.2 Spectral fluorescence measurements

The spectral fluorescence behaviour was studied with a self-assembled fluorimeter [Pen87, Hol99]. Fig. 6.2 shows the experimental setup. The samples were excited with a mercury lamp in connection with a 365 nm interference filter. The fluorescence spectra were either recorded with an intensified silicon-diode-array system (OMA system from EG&G Princeton Applied Research) or an un-intensified silicon diode-array system (DARSS diode Array). The samples were measured in a small-volume cell of $1.5 \times 1.5 \times 5$ mm^3. The absolute intrinsic fluorescence quantum distributions, $E_F(\lambda)$, (explained in chap 2) and absolute intrinsic fluorescence quantum yields, $\phi_F = \int E_F(\lambda)d\lambda$, were determined by using lumiflavin

in water buffered to pH = 8 ($\phi_{F,R}$ = 0.235) as reference because of similar fluorescence spectrum and high photostability [Hol05].
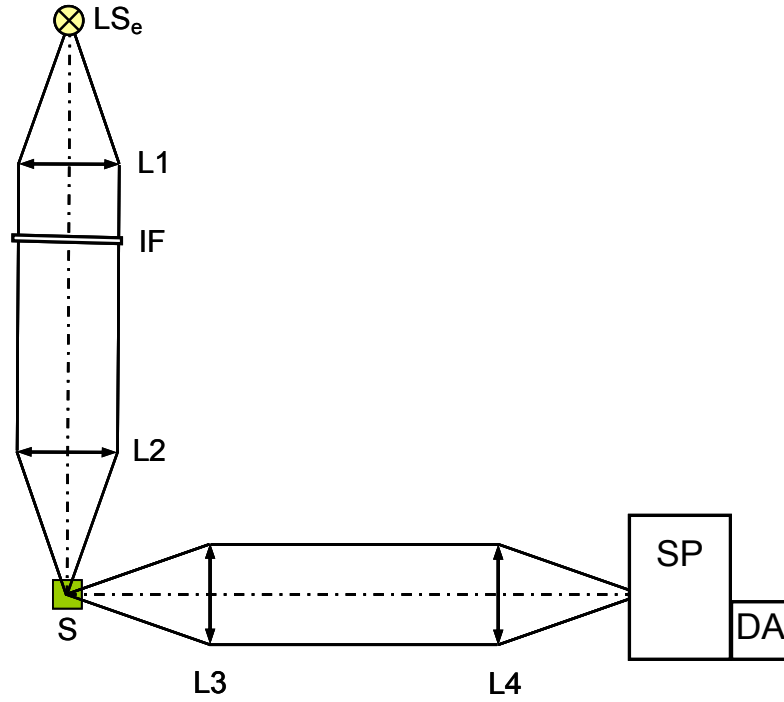

Figure 6.2   The experimental setup used for spectral fluorescence measurements. LS_e : light source for excitation, (high pressure mercury lamp), L1-L4: lenses, P1, P2: polarisers, IF interference filter, SP: spectrometer, DA: diode array, S: sample.

Dark-adapted samples and short-time high-intensity exposed samples (samples in signalling states) were studied. For dark-adapted fluorescence quantum distribution measurement the excitation intensity was reduced to I_{exc} = $1.8{\times}10^{-4}$ W cm^{-2} (excitation wavelength 365 nm) and the excitation time was set to Δt_{exp} = 5 s in order to avoid conversion to the signaling state (see chapter 7). In the case of fluorescence quantum distribution measurement of the signalling state, the BlrP1_BLUF and BlrP1 samples were excited at 365 nm with I_{exc} = 0.0126 W cm^{-2} for a duration of t_{exp} = 10 s and fluorescence was measured at the end of exposure for a period of 0.21 s (for conditions necessary to generate signaling state, see chapter 7).

The fluorescence behaviour of the samples due to long-time exposure was studied by excitation in the wavelength range from 350 - 440 nm (via a broadband interference filter) with an intensity of I_{exc} = 0.25 W cm^2 for a period of 140 min and the fluorescence spectra were recorded by intermittent changing to $\lambda_{exc,pr}$ = 365 nm with $I_{exc,pr}$ = 0.031 W cm^{-2}.

6.3 Temporal fluorescence measurements

The temporal fluorescence behaviour was studied by short laser pulse excitation at 400 nm with a Ti:sapphire femtosecond oscillator-amplifier laser system (laser system Hurricane from Spectra-Physics) and fluorescence up-conversion detection (Fig 3.3). In the frequency up-conversion technique, the fluorescence excited by the frequency doubled femtosecond laser pulses is mixed with a time delayed fundamental laser femtosecond pulse in a nonlinear optical crystal to generate the sum frequency. Since the mixing process takes place only during the presence of the fundamental laser, this technique provides a time resolution comparable to the laser pulse width [Mah75, Sha88]. For measuring the fluorescence lifetime with the up-conversion technique, the laser light at 800 nm of 120 fs duration was used as pump beam. The fundamental beam passes through a BBO crystal [Dmi91] to generate frequency doubled (400 nm) femtosecond laser pulses. A harmonic beam splitter is used to separate the fundamental and the second harmonic laser beams. The second harmonic beam excites the sample and generates a fluorescence signal. This fluorescence signal is collected by the two parabolic mirrors (PM1 and PM2) and focused on a second BBO crystal (0.2 mm thickness) where this signal is mixed with the fundamental laser pulse. Sum frequency mixing of fluorescence light with time delayed fundamental laser light happens inside the crystal. The 400 nm fluorescence excitation beam is time delayed relative to the fundamental by using a stepper motor driven linear translation stage. The up-converted signal is passed through a
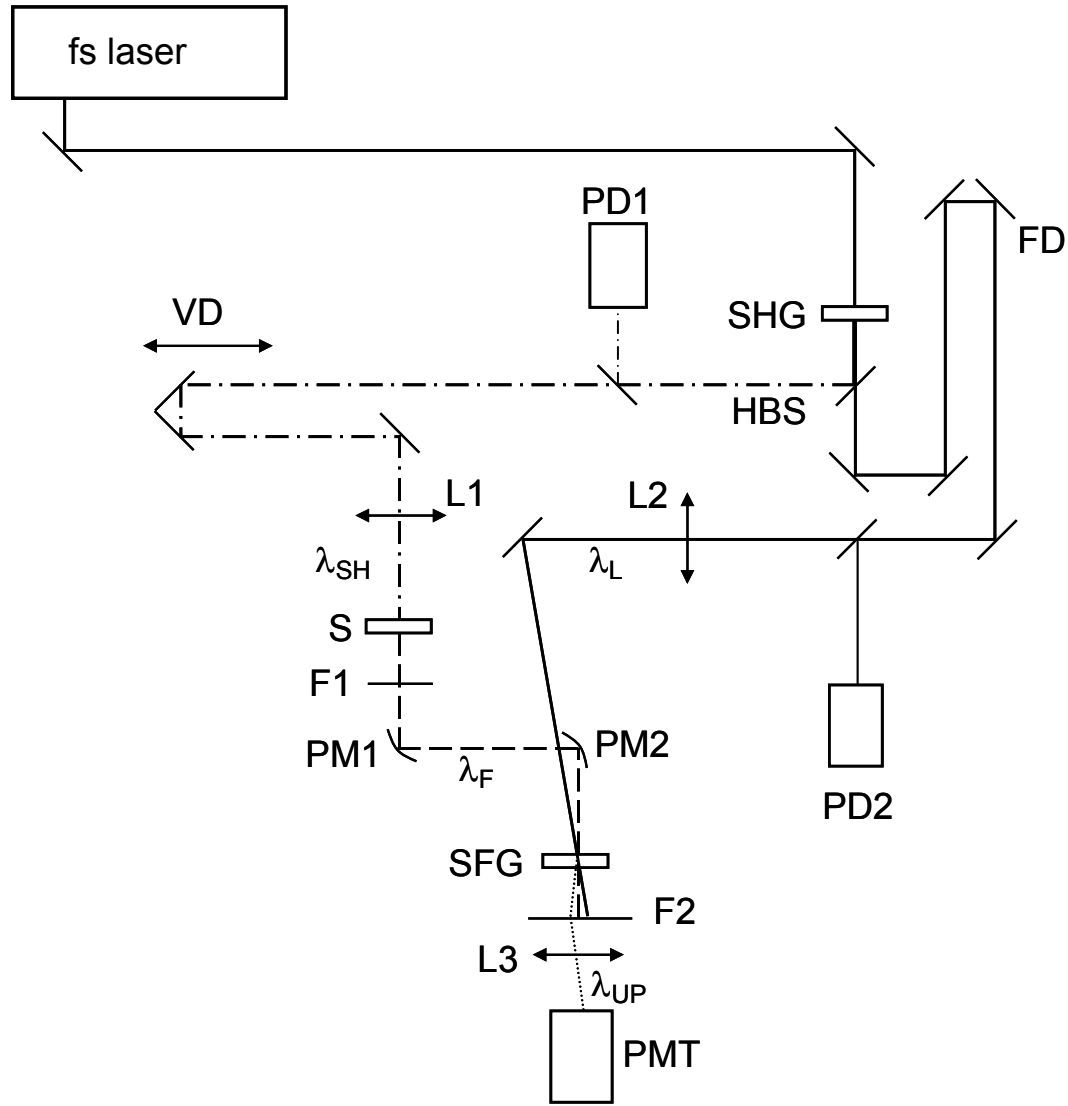
Figure 6.3 Experimental setup for fluorescence up-conversion. SHG: BBO crystal for second harmonic generation, HBS: harmonic beam splitter, FD: fixed delay line, VD: variable delay-line., L1 – L3: lenses, S: sample. PM1, PM2: parabolic mirrors. PD1, PD2: photo-detectors, F1, F2: filters, SFG: BBO crystal for sum-frequency generation. PMT: photomultiplier tube. λ_L, λ_{SH}, λ_F, λ_{UP} : fundamental laser light (800nm), second harmonic (400nm), fluorescence light from the sample, up-converted signal respectively.

broad band filter (Schott glass UG11 of 10 mm thickness, transmission range from 270 nm to 380 nm) and is detected with a photomultiplier tube (Valvo, type PM2254B) and a high speed digital oscilloscope (LeCroy, type DSO 9362). The second delay line through which the fundamental laser pulse has passed can be changed manually to increase the delay length of

the system to follow the fluorescence decay over longer times, whenever needed (varied time range without fixed delay extension is from -100 ps to 1.5 ns).

The receptor state temporal fluorescence signals were measured in a 10 mm × 4 mm cell (path length 10 mm) with a magnetic stirrer. The pulse repetition rate was set to 1 Hz and the single excitation pulse energy density was set to, $w_P \approx 2 \times 10^{-4}$ J cm^{-2}. At each delay time the up-converted signal was averaged over 30 excitation pulses. The signalling-state fluorescence signals were measured in a small-volume cell ($1.5 \times 1.5 \times 5$ mm^3). The laser was operated permanently during the whole measurement period at a repetition rate of 10 Hz with a single pulse energy density at the fluorescence cell of 1.8×10^{-3} W cm^{-2} (femtosecond pulses at 400 nm bring BLUF domains in the signalling state). At each delay time the up-converted signal was averaged over 30 excitation pulses.

7 Absorption and emission spectroscopic investigation of proteins BlrP1 and BlrP1_BLUF from *Klebsiella pneumoniae*

BLUF domains have been found in many microorganisms, *Escherichia coli* being one of them. The protein YcgF from *E.coli* has been cloned, overexpressed, purified and spectroscopically investigated. In YcgF, the N-terminal consists of a BLUF domain as in other BLUF proteins and this BLUF domain is covalently linked to an EAL domain at its C-terminal [Sch05].

The EAL (glutamic acid (E), alanine (A), leucine (L)) domain causes the enzymatic activity in hydrolysis of cyclic dimeric guanosine monophosphate (c-di-GMP). Cyclic-di-GMP is a ubiquitous second messenger in bacteria. c-di-GMP antagonistically controls motility and virulence of single, planktonic cells on one hand and cell adhesion and persistence of multicellular communities on the other. Cellular levels of c-di-GMP are controlled through the opposing activities of diguanylate cyclases (DGCs) (responsible for synthesis of c-di-GMP) and phosphodiesterases (PDEs) (responsible for degradation of c-di-GMP) [Jen06]. The GGDEF (Gly-Gly-Asp-Glu-Phe) domain is responsible for the DGC activity while EAL is responsible for the PDE activity. Thus a balanced interplay of these two activities is responsible for the c-di-GMP signaling activity. These domains are found with other domains which can receive signals. The existence of BLUF and EAL domains in YcgF is one such example. So the BLUF domain and the EAL domain together are referred to as blue light regulated phosphodiesterase (BlrP) because of this putative c-di-GMP activity though this has not yet been detected [Raj04, Tya08].

Similar BLUF-EAL proteins exist in some species of enteric bacteria, including two such proteins in *Klebsiella pneumoniae* (BlrP1 and BlrP2) and in a bacterium from the Sargasso Sea [Gom02, Raj04] (the Sargasso Sea is an elongated region in the middle of the

North Atlantic Ocean). The primary amino acid structure of the BlrP from *E.coli*, *K. pneumoniae* and *Sargasso* is shown in Fig 7.1[Raj04]. In contrast to other BLUF domains, the BLUF domains of BlrP from *E.coli*, *K.pneumoniae* and *Sargasso* contain no Tryptophan residue. Tryptophan has been discussed to be an important residue in the photocycle of previously studied BLUF proteins. But this is not the case in the BlrP proteins.

```
E.coli      1  ----------MLTTLIYRSHIRDDEPVKKIEEMVSIANRRNMQSDVTGILLFNGSHFFQL
K.pneumo    1  ----------MLTTLIYRSQVHPDRPPVDLDALVHRASSKNLPLGITGILLFNGLQFFQV
Sargasso    1  MKTKFNKRQPVLKQLVYRSQSTVKIDENELLKITNDSLPFNAKNHITGILLFDGEYFFQV

E.coli     51  LEGPEEQVKMIYRAICQDPRHYNIVELLCDYAPARRFGKAGMELFDLRLHERDDVLQAVF
K.pneumo   51  LEGTEEALESLFSEIQSDPRHRDVVELMRDYSAYRRFHGTGMRILDLRLFETDGALEEIL
Sargasso   61  LEGDCETVNALFEHHIKTDSRHSNIMKVTEMVIHKRDFG-------DWHLRTLSVAEGSRC

E.coli    111  DKGTSKFQLTYDDRALQFFRTFVLATEQSTYFEIPAEDS-WLFIADGSDKELDSCALSPT
K.pneumo  111  RFSTFGVTEPVNDRMFRLLSAFIADGGRYCLPE-PLQPSRWMMMPASGTAAPQHLPGQPC
Sargasso  114  YWLPSDINISRESRIFALLNSPASGKWRTCLSDNARKDVRANVTT--SEKAVKPFENSDI

E.coli    170  INDHFAFHPIVDPLSRRIIAFEAIVQK-NEDSPSAIAVGQRKDGE----IYTADLKSKAL
K.pneumo  170  ---QFALQAIVEPAKKRVSSFEALIRSPTGGSPVEMFAAIAAEDR-----YRFDLESKAY
Sargasso  172  ---QFAFQPIVDTYRARVSSIEALIRSNDGRYPETILEELVGPEK-----YDFDLKSKAI

E.coli    225  AFTMAHALELGDKMISINLLPMTLVNEPDAVSFLLNEIKANALVPEQIIVEFTESEVISR
K.pneumo  222  AFALAGQLPLGKHQLAINLLPGSLYHHPDAVGWLMDSLLAAGLRPDQVLIEVTETEVITC
Sargasso  224  AIKQGAALLSSDQSLSINLCPGAITSTVNVADYLHELVKRNKLKPQQLVIEVTETEIISE

E.coli    285  FDEFAEAIKSLKAAGISVAIDHFGAGFAGLLLLSRFQPDRIKISQELITNVHKSGPRQAI
K.pneumo  282  FDQFRKVLKALRVAGMKLAIDDFGAGYSGLSLLTRFQPDKIKVDAELVRDIHISGTKQAI
Sargasso  284  SDTFYQAIEQIRSQGMRVAIDDFGAGYAGLSLLADFTPDKIKLDRKITTGIHESGHRQAI

E.coli    345  IQAIIKCCTSLEIQVSAMGVATPEEWMWLESAGIEMFQGDLFAKAKLNGIPSIAWPEKK-
K.pneumo  342  VASVVRCCEDLGITVVAEGVETLEEWCWLQSVGIRLFQGFLFSRPCLNGIGEICWP----
Sargasso  344  TEAVLEFANSMGIPLVVEGVETIDEWLWLQHAGVQRFQGFLFAKPKLNGVSGIDFSFDGA
```

Figure 7.1 Alignment of the protein sequences of BlrP from Escherichia coli, *Klebsiella pneumoniae* and an unknown bacterium from the Sargasso Sea [Raj04]. Identical residues between all three proteins are boxed in black (initial blank spaces in the sequences of *E.coli* and *K.pneumoniae* is made only to bring the identical residues vertically above each other in the three sequences).

One of the two BLUF-EAL proteins from *K. pneumoniae* subsp. *pneumoniae* MGH 78578, BlrP1 (number of amino acids = 405), and its BLUF domain, BlrP1_BLUF, (encompassing the sequence corresponding to amino acids 2…93 of BlrP1) have been cloned, overexpressed and purified [Tya08]. Fig 7.2 shows the primary sequence for the BlrP1 protein

from *K. pneumoniae*. The BLUF domain (from amino acids 2….93) and the EAL domain of

BlrP1 (from 170…386 amino acids) are indicated by separate boxes.

Length: 405 amino acids
BLUF Domain : 2....93 amino acids
EAL Domain :170-386 amino acids

```
          10         20         30         40         50         60
MLTTLIYRSQ VHPDRPPVDL DALVHRASSK NLPLGITGIL LFNGLQFFQV LEGTEEALES

          70         80         90        100        110        120
LFSEIQSDPR HRDVVELMRD YSAYRRFHGT GMRILDLRLF ETDGALEEIL RFSTFGVTEP

         130        140        150        160        170        180
VNDRMFRLLS AFIADGGRYC LPEPLQPSRW MMMPASGTAA PQHLPGQPCQ FALQAIVEPA

         190        200        210        220        230        240
KKRVSSFEAL IRSPTGGSPV EMFAAIAAED RYRFDLESKA YAFALAGQLP LGKHQLAINL

         250        260        270        280        290        300
LPGSLYHHPD AVGWLMDSLL AAGLRPDQVL IEVTETEVIT CFDQFRKVLK ALRVAGMKLA

         310        320        330        340        350        360
IDDFGAGYSG LSLLTRFQPD KIKVDAELVR DIHISGTKQA IVASVVRCCE DLGITVVAEG

         370        380        390        400
VETLEEWCWL QSVGIRLFQG FLFSRPCLNG IGEICWPVAR QAMDL
```

Figure 7.2   Primary sequence of BlrP1 from *K. pneumoniae* subsp. *pneumoniae* MGH 78578. The BLUF domain and the EAL domain are marked separately [1, 2]

The cofactor in the BLUF domain is non-covalently bound FAD. The following

sections give the results that have been obtained by careful absorption and emission studies of

the full protein BlrP1 and its BLUF domain, BlrP1_BLUF.

7.1 Spectroscopic characterization in the receptor state.

7.1.1 Sample storage and sample preparation for measurement

After cloning and purifying the proteins [Tya08], the samples were divided into small aliquots (20-100 μl) into Eppendorf reaction tubes and flash frozen in liquid nitrogen (samples were dipped into the liquid nitrogen quickly) and stored at -80 °C in a freezer.

Before using a sample for measurements, it had to be thawed i.e. just given enough warmth so that it melts and no denaturation of the protein takes place (done by holding the sample in hand). Also before measurement, the thawed samples were put into a centrifuge (operated at 12000 rpm for 10 min) to sediment aggregated material. Only the supernatant (solution above the sedimented non-dissolved material) was used for measurements. Whenever a dilution of the samples was necessary this was done with aqueous Tris buffer containing 25 mM Tris (Tris is abbreviation for 2-Amino-2-hydroxymethyl-propane-1,3-diol = tris(hydroxymethyl)aminomethane, sum formula: $(HOCH_2)_3CNH_2$), 40mM NaCl, 5mM $MgCl_2$ and the pH was adjusted with HCl to 8 (1 M = 1 mol dm^{-3}). All preparations were done in the dark or under weak red light (which is not absorbed by the photoreceptor protein) to avoid bringing photoreceptor molecules out of the dark adapted (receptor) state.

7.1.2 Cofactor identification

The cofactor identification was done with HPLC (High Pressure Liquid Chromatography) by the group of Prof. Schlichting. The BlrP1_BLUF contained only FAD and was > 95 % pure. The BlrP1 protein was > 95 % pure and contained ~ 14 % FMN and ~86 % FAD.

For HPLC measurements, a concentrated protein sample is denatured (by heating) and then cooled to room temperature. The precipitate is removed via centrifugation and the supernatant is filtered out. The supernatant is applied to a reverse phase column (the column

material is hydrophobic). High pressure is used to drive the solute faster through the column. The proteins are eluted (extracted) by flowing an organic solvent such as acetonitrile through the column. The proteins elute according to their hydrophobicity i.e. polar molecules will travel with the solvent through the column faster. The time taken for a particular compound to travel through the column is called as its retention time. At the end of the column the different compounds are separated and are detected most commonly by UV absorption. The ratios of the compounds are then calculated by the corresponding absorption peak heights.

7.1.3 Absorption spectra

The transmission spectra of the dark-adapted (in receptor state) BlrP1_BLUF and BlrP1 are carried out with a commercial spectrometer. The supernatant after centrifugation was filled in a small volume quartz cell ($1.5 \times 1.5 \times 5$ mm^3). The transmission of the sample was measured against air. In an identical cell the transmission of the buffer against air was also measured and then the transmission of the sample against the buffer was calculated by dividing the transmission of sample against air by the transmission of buffer against air . The transmission spectra of the undiluted BlrP1 and BlrP1_BLUF are shown in Fig 7.3. In the undiluted samples, information on the spectra below 300 nm is not available because of the high concentration of the samples. Hence the samples were diluted with the buffer solution and measured in a 1mm $\times$ 1cm $\times$ 4.5 cm cell (optical path length = 1 mm). The dilution factors are 3.18 for BlrP1 and 4.27 for BlrP1_BLUF.
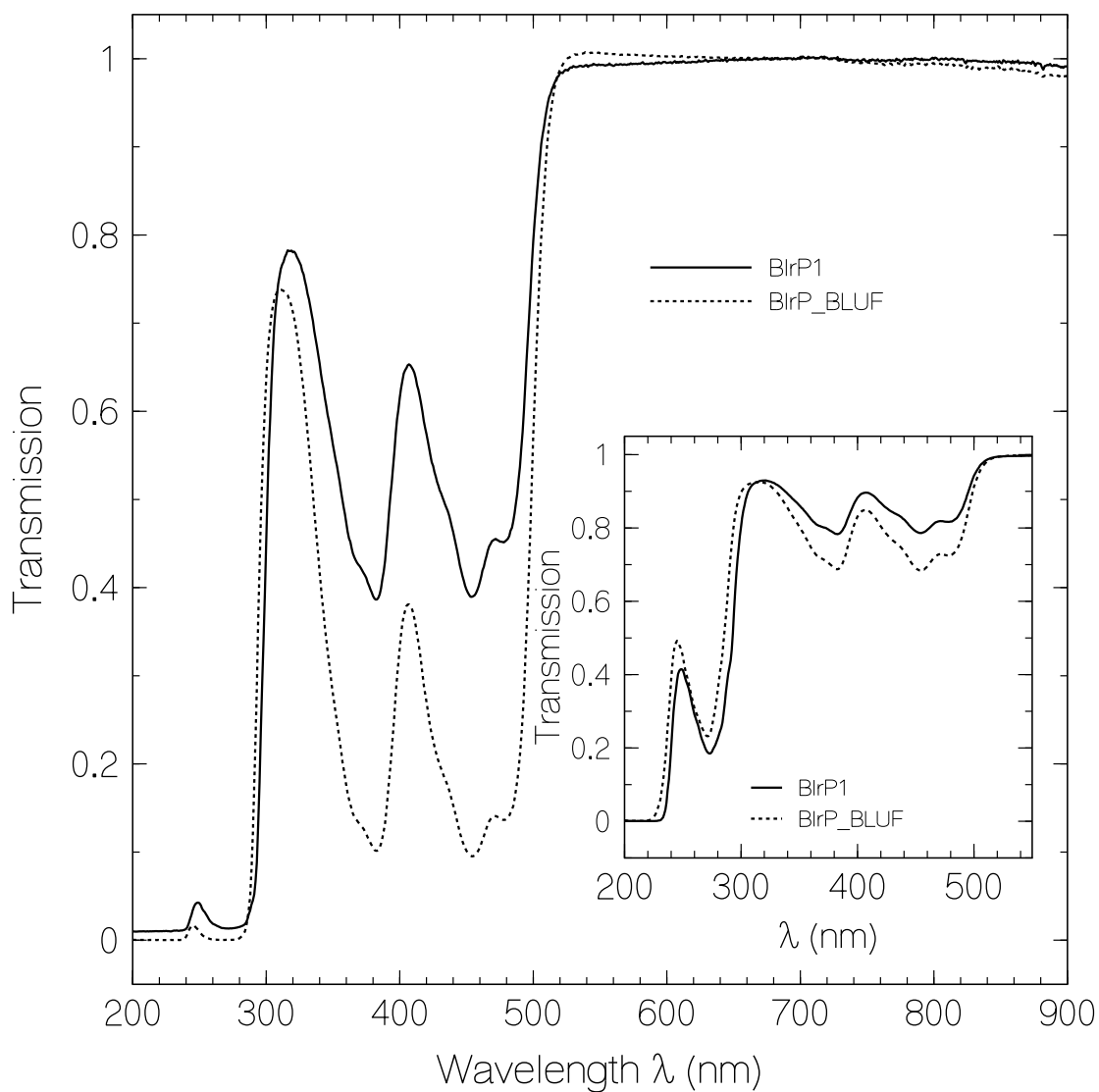
Figure 7.3 Transmission spectra of the undiluted BlrP1 (see section 7.1.4) and BlrP1_BLUF proteins against buffer. Inset shows the transmission spectra of diluted samples (with dilution factors of 3.18 for BlrP1 and 4.27 for BlrP1_BLUF).

From the transmission spectra, the absorption coefficient spectra are calculated as described in chapter 2. The absorption coefficient spectra for the undiluted and diluted BlrP1_BLUF and BlrP1 are shown in Fig 7.4.
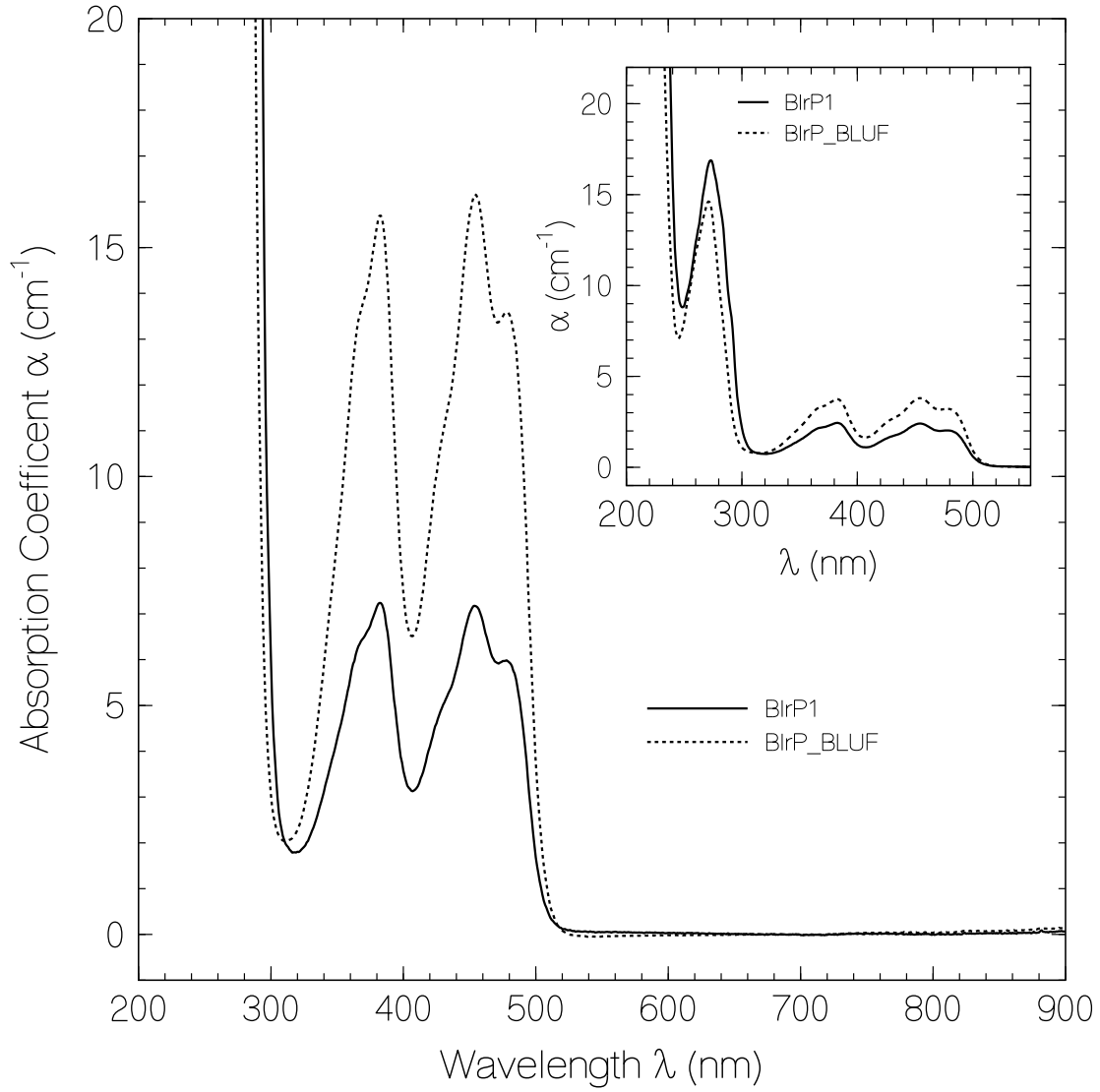
Figure 7.4 Absorption coefficient spectra of the undiluted BlrP1 and BlrP1_BLUF proteins against buffer. Inset shows the absorption coefficient spectra of diluted samples.

From the shapes of the absorption coefficient spectra, the absorption cross-section spectra, $\sigma_a(\lambda)$ of BlrP1_BLUF and BlrP1 are determined. Thereby it is assumed that the absorption cross-section integral $\int_{\lambda>320nm} \sigma_a(\tilde{\nu})d\tilde{\nu}$ of FAD in aqueous solution at pH 8 is the same as for FAD in BlrP1 and in BlrP1_BLUF. The result is shown in Fig 7.5.
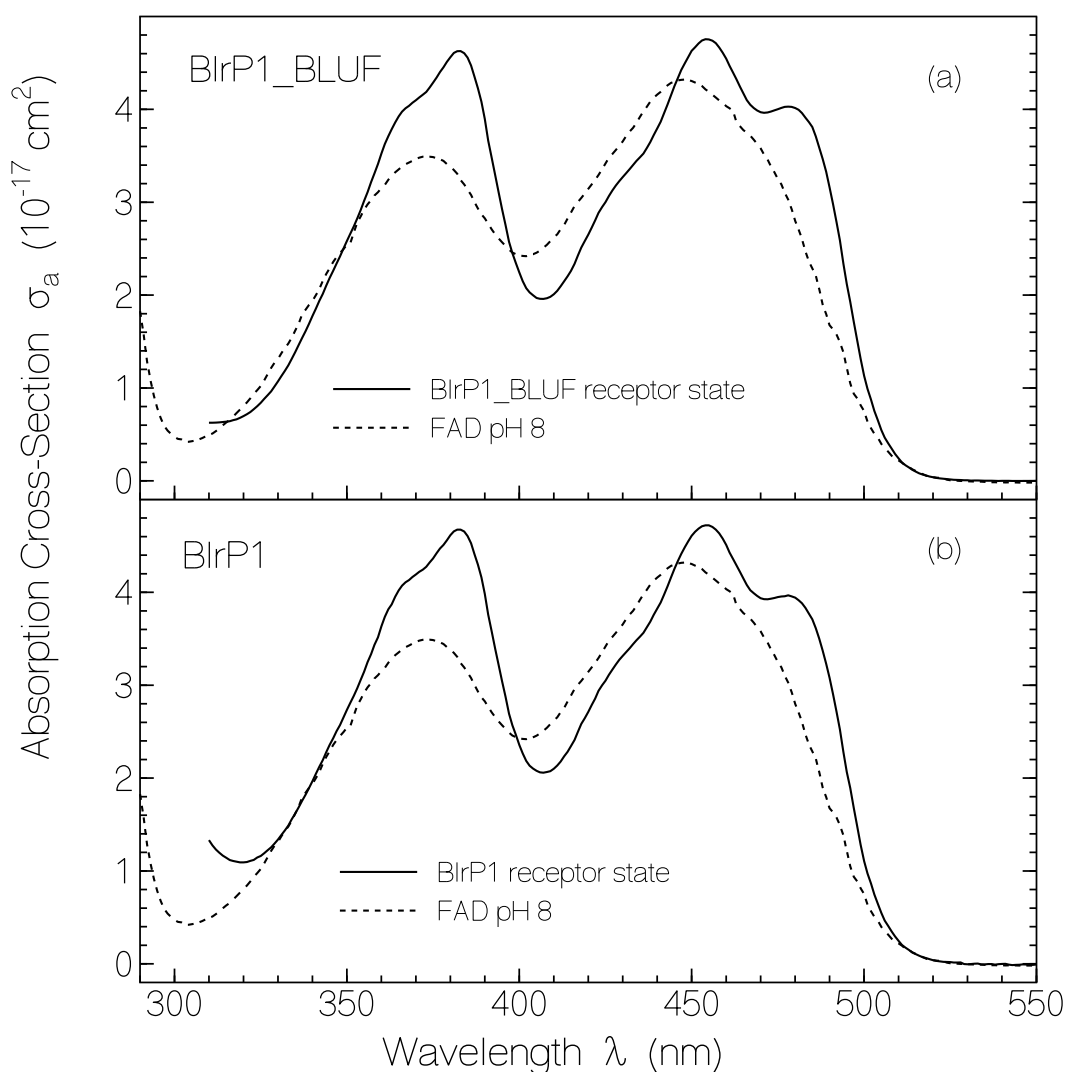
Figure 7.5 Absorption cross section for the dark adapted states of (a) BLUF domain BlrP1_BLUF (b) full length protein BlrP1 and of FAD in aqueous solution at pH 8 [Isl03b].

The chromophore FAD is responsible for the absorption peaks around 450 nm (S_0-S_1 band) and around 375 nm (S_0-S_2 band). At shorter wavelengths, $\lambda < 310$ nm, the absorption gets contribution from the amino acid residues tryptophan and tyrosine in addition to that from the FAD. Since the amino acids in the full protein are more than that in the BlrP1_BLUF, the BlrP1 absorbs more strongly in the region below 310 nm. The absorption cross section spectra of Tyr, Trp and FAD in neutral aqueous solution are shown in Fig 7.6. It clearly shows that the absorption below 310 nm gets contributions from the amino acids.
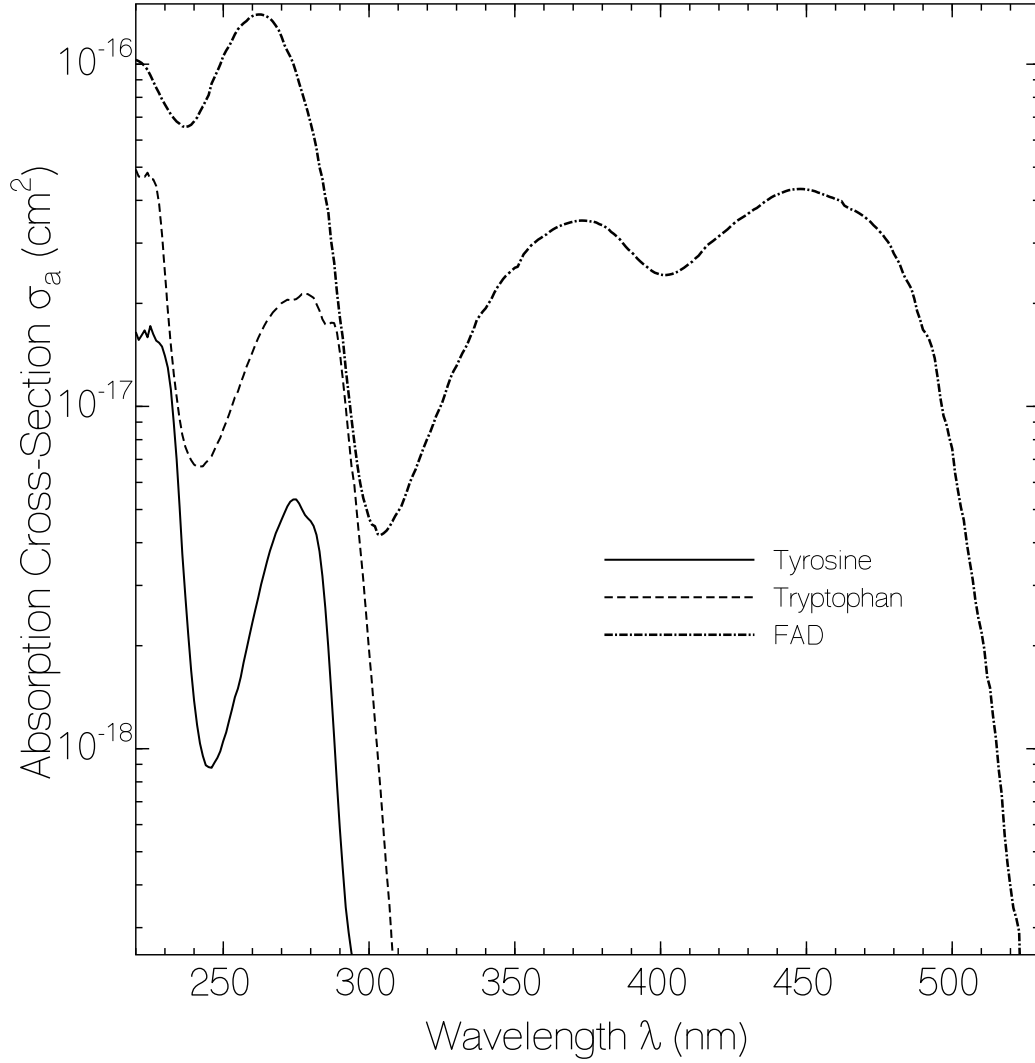
Figure 7.6   Absorption cross-section spectra of amino acids Tyrosine [3], Tryptophan [3] and FAD in aqueous solution at pH 7 [Isl03b].

7.1.4 Determination of protein concentration and cofactor concentration.

As stated in the previous section, the protein absorption in the near UV region (260 nm $< \lambda <$ 300 nm) is determined by the absorption of the amino acids tyrosine and tryptophan in addition to FAD (at lower wavelengths weaker absorbing phenylalanine and other amino acids contribute). From the absorption coefficient spectra of the samples, the protein number density N_{ap} and the chromophore number density N_{FAD} are accessible via the absorption cross-

section spectra of the constituents. Knowing the chromophore concentration and the protein concentration, the chromophore loading of the proteins is obtained by the concentration ratio. The chromophore loading factor κ_{FAD} is given by

$$\kappa_{FAD} = \frac{N_{FAD}}{N_{ap}} \tag{7-1}$$

The total absorption coefficient spectrum is the sum of the absorption coefficient spectra of the various components i.e.

$$\alpha(\lambda) = \sum_i \alpha_i(\lambda) = \sum_i N_i \sigma_i(\lambda) = N_{ap}\sigma_{ap}(\lambda) + N_{FAD}\sigma_{FAD}(\lambda) \tag{7-2}$$

where N_{ap} is the number density of the protein molecules (apo-protein), and σ_{ap} is the absorption cross-section of the apo-protein (apo-protein = protein without chromophore). N_{FAD} is the number density of FAD and σ_{FAD} is the absorption cross section of FAD.

N_{ap} will be determined by the absorption at 280 nm (see Fig 7.6). At this wavelength, the absorption cross-sections are σ_a (Tyr) $\approx 4.63 \times 10^{-18}$ cm^2, σ_a (Trp) $\approx 2.02 \times 10^{-17}$ cm^2 and $\sigma_{FAD} \approx 6.7 \times 10^{-17}$ cm^2 [Shi08]. The absorption cross-section of the apo-protein, σ_{ap}, is given by

$$\sigma_{ap} = n_{Tyr}\sigma_a(Tyr) + n_{Trp}\sigma_a(Trp) \tag{7-3}$$

where n_{Tyr} and n_{Trp} are the number of Tyr and Trp residues per apo-protein. These numbers are $n_{Tyr} = 8$ and $n_{Trp} = 5$ for BlrP1, and $n_{Tyr} = 3$ and $n_{Trp} = 0$ for BlrP1_BLUF (see Fig 7.2). Inserting these numbers into eqn. 7-3 gives, σ_{ap} (280 nm) $= 1.39 \times 10^{-17}$ cm^2 (for BlrP1_BLUF) and σ_{ap} (280 nm) $= 1.38 \times 10^{-16}$ cm^2 (for BlrP1).

N_{FAD} is determined by the absorption coefficient of BlrP1 and BlrP1_BLUF at 450 nm (see Fig. 7.5). At 450 nm absorption coefficients of the diluted samples are α(BlrP1_BLUF) = 3.7 cm^{-1} and α(BlrP1) = 2.3 cm^{-1}. Using σ_a(FAD, 450 nm) = 4.3×10^{-17} cm^2, the number densities of the diluted samples are found to be N_{FAD} (BlrP1_BLUF) = α/σ_a = 8.6 × 10^{16} cm^{-3} and N_{FAD} (BlrP1) = α/σ_a = 5.4 × 10^{16} cm^{-3}. At 280 nm, absorption coefficients of the diluted samples are α(BlrP1_BLUF) = 10.3 cm^{-1} and α(BlrP1) = 14.9 cm^{-1}.

The apo-protein concentration is determined according to eqn. 7-2

$$N_{ap} = \frac{\alpha(280nm) - N_{FAD}\sigma_{FAD}(280nm)}{\sigma_{ap}(280nm)}$$
7-4

Insertion of the parameters into eqn. 7-4 gives

for diluted BlrP1_BLUF,

$$N_{ap} = 3.2 \times 10^{17} cm^{-3}$$

and for BlrP1

$$N_{ap} = 8.2 \times 10^{16} cm^{-3}$$

The chromophore loading factors according to eqn. 7-1 are found to be

$$\kappa_{FAD}(\text{BlrP1\_BLUF}) = \frac{N_{FAD}}{N_{ap}} = \frac{8.6 \times 10^{16}}{3.2 \times 10^{17}} \approx 0.27,$$

7-5

$$\kappa_{FAD}(\text{BlrP1}) = \frac{N_{FAD}}{N_{ap}} = \frac{5.4 \times 10^{16}}{8.2 \times 10^{16}} \approx 0.66$$

7.1.5 Fluorescence studies

7.1.5.1 Spectral fluorescence measurements

The spectral fluorescence measurements were carried out with the help of the experimental setup described in the section 6.2. The samples were used after centrifugation. They were measured in $1.5 \times 1.5 \times 5$ mm^3 volume fused silica cells. The samples were excited with a high pressure mercury lamp and the excitation wavelength was selected with a 365 nm interference filter (FWHM = 9.5 nm). For dark adapted samples the excitation intensity was reduced to $I_{exc} = 1.8 \times 10^{-4}$ W cm^{-2} and the excitation time was set to $\Delta t_{exp} = 5$ s
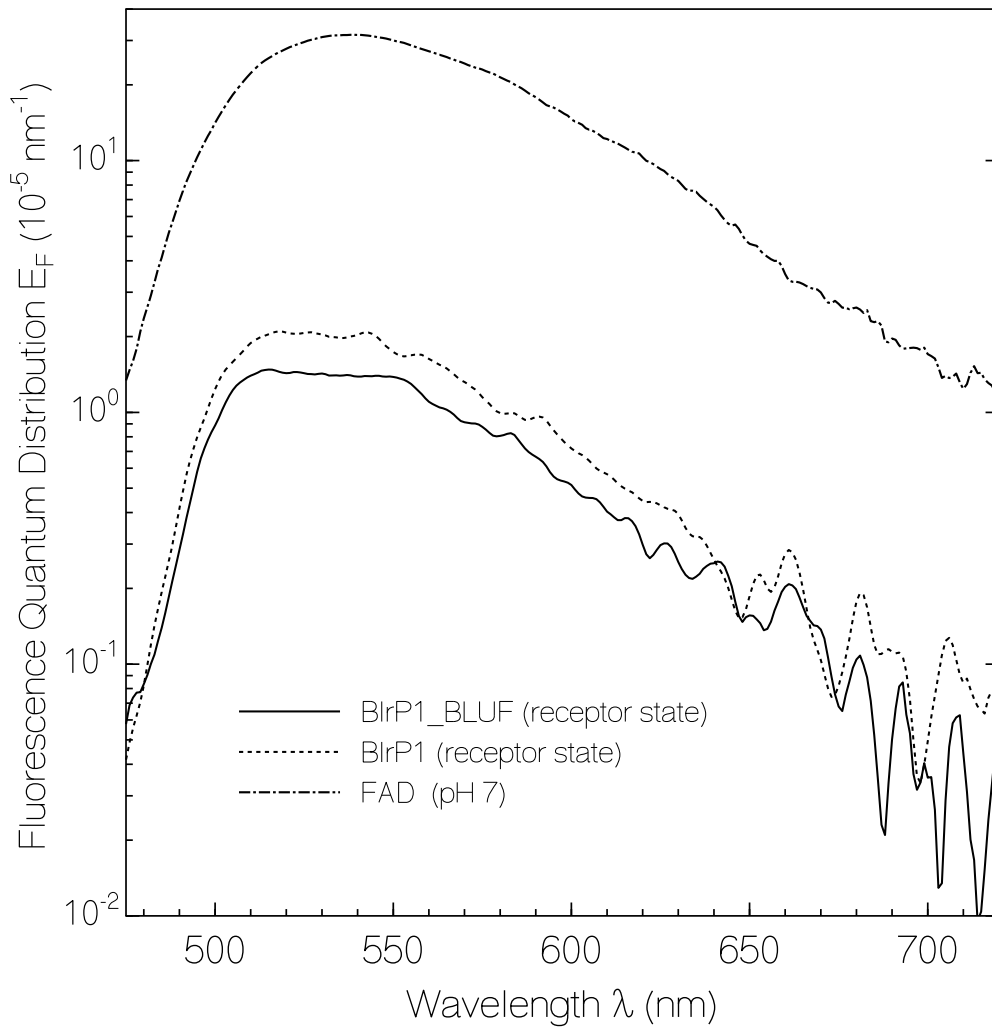
Figure 7.7 Fluorescence quantum distributions, $E_F(\lambda)$, of BlrP1_BLUF and BlrP1 in the receptor state and of FAD in aqueous solution at pH 7 (from [Isl03b]).

92

so that the proteins remain in the dark adapted state.. The absolute intrinsic fluorescence quantum distributions, $E_F(\lambda)$, (explained in chapter 2) and absolute intrinsic fluorescence quantum yields, $\phi_F = \int E_F(\lambda)d\lambda$, were determined by using lumiflavin in water buffered to pH = 8 ($\phi_{F,R}$ = 0.235) as reference because of similar fluorescence spectrum and high photostability [Hol05]. Fig 7.7 shows the absolute intrinsic fluorescence quantum distributions, $E_F(\lambda)$, of BlrP1_BLUF and of BlrP1 in the receptor states. Included is the fluorescence quantum distribution of free FAD in aqueous solution at pH 7 [Isl03b].

The areas under the curves give the quantum yields. The obtained fluorescence quantum yields, ϕ_F, of the proteins in the receptor state are ϕ_F(BlrP1_BLUF) = $(1.4\pm0.1)\times10^{-3}$ and ϕ_F(BlrP1) = $(2.0\pm0.1)\times10^{-3}$. The fluorescence quantum yield of FAD at pH 7 is $\phi_F \approx 0.032$ [Isl03b].

7.1.5.2 Temporal fluorescence measurements

Along with the spectral fluorescence measurements, temporal fluorescence measurements were carried out . For the lifetime measurements of the proteins in the receptor state, the samples were diluted by adding some buffer. The samples were measured in a 10 mm × 4 mm cell (path length 10 mm). The cell content was continuously mixed by magnetic stirring (a teflon studded magnetic rod was put in the cell and a rotating magnetic field was applied). The samples were studied by femtosecond laser pulse excitation at 400 nm with a Ti:sapphire femtosecond oscillator-amplifier laser system and fluorescence up-conversion detection as described in chapter 6. The laser pulse repetition rate was set to 1 Hz and the single excitation pulse energy density was set to, $w_P \approx 2\times10^{-4}$ J cm^{-2}. At each delay time the up-converted signal was averaged over 30 excitation pulses. The measured temporal fluorescence traces for BlrP1_BLUF and BlrP1 in the receptor state are displayed in Fig 7.8.
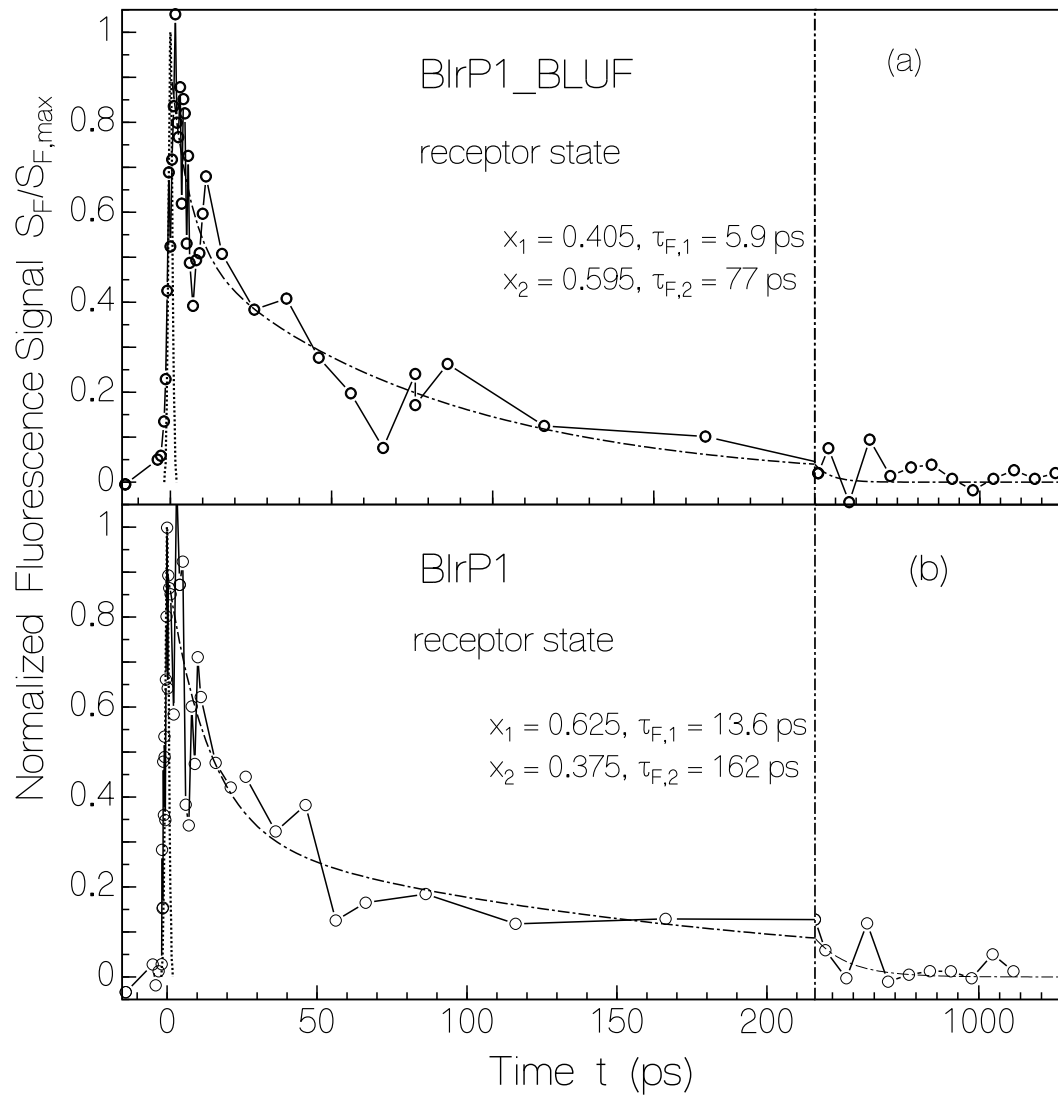
Figure 7.8 Temporal fluorescence behaviour determined by femtosecond laser fluorescence up-conversion of dark - adapted state BlrP1_BLUF (a) and BlrP1 (b) in aqueous solution at pH 8 at room temperature. Line connected circles are the normalised fluorescence up-conversion signals. Dotted lines show the system response function. Dash-dotted curves are the non linear regression fits according to eq. 7-6. The fitted parameters are shown in the figure.

The fluorescence traces of the proteins in the dark-adapted state are fitted to a bi-exponential decay. The applied function is

$$S_F(t) = S_{F,max} \sum_{i=1}^{2} x_i \exp(-t / \tau_{F,i}),$$ (7-6)

and $\sum_{i=1}^{n} x_i = 1$

The obtained lifetimes are $\tau_{F,1}$ = 5.9 ps and $\tau_{F,2}$ = 77 ps for the BlrP1_BLUF, and $\tau_{F,1}$ = 13.6 ps and $\tau_{F,2}$ = 162 ps for the full protein, BlrP1. The fitted parameters x_1, x_2 and $\tau_{F,1}$, $\tau_{F,2}$ are listed in Fig. 7.8 and in the table 7.1.

The presented fluorescence decay curves and parameters, for the receptor state, in Fig. 7.8 give apparent fluorescence quantum yields of ϕ'_F(BlrP1_BLUF) $\approx 2.5 \times 10^{-3}$, and ϕ'_F(BlrP1) $\approx 3.6 \times 10^{-3}$, by using the relation

$$\phi'_F = \frac{1}{\tau_{rad}} \frac{\sum_{i=1}^{2} x_i \tau_{F,i}}{\sum_{i=1}^{2} x_i}, \qquad \qquad 7\text{-}7$$

with the radiative lifetime of FAD being $\tau_{rad} \approx 19$ ns [Zir07a]. These apparent fluorescence quantum yields are significantly larger than the measured fluorescence quantum yields (see above and table 7.1) indicating a partial fluorescence decay (fraction x_0) with fluorescence decay time, $\tau_{F,0}$, shorter than the experimental time resolution of our detection system which is $\tau_{res} \approx 300$ fs. The real fluorescence decay traces are given by the relation

$$S_F(t) = S_{F,0}\left[x_0 \exp(-t/\tau_{F,0}) + (1-x_0) \frac{\sum_{i=1}^{2} x_i \exp(-t/\tau_{F,i})}{\sum_{i=1}^{2} x_i} \right]. \qquad 7\text{-}8$$

The fraction of the fluorescence signal with decay time $\tau_{F,0}$ may be determined from the fluorescence quantum yield relation

$$\phi_F = \frac{1}{\tau_{rad}} \left[x_0 \tau_{F,0} + (1 - x_0) \frac{\sum\limits_{i=1}^{2} x_i \tau_{F,i}}{\sum\limits_{i=1}^{2} x_i} \right].$$

7-9

Solving Eq.7-9 for x_0 gives

$$x_0 = \frac{\dfrac{\sum\limits_{i=1}^{2} x_i \tau_i}{\sum\limits_{i=1}^{2} x_i} - \phi_F \tau_{rad}}{\dfrac{\sum\limits_{i=1}^{2} x_i \tau_i}{\sum\limits_{i=1}^{2} x_i} - \tau_{F,0}} \approx \frac{\sum\limits_{i=1}^{2} x_i \tau_i - \phi_F \tau_{rad} \sum\limits_{i=1}^{2} x_i}{\sum\limits_{i=1}^{2} x_i \tau_i}.$$

7-10

The obtained fractions, x_0, are 0.43 for BlrP1_BLUF and 0.45 for BlrP1.

7.2 Dynamics of signalling state formation

7.2.1 Intensity dependence of signalling state formation

As discussed earlier, excitation of BLUF proteins with blue light leads to the formation of a signalling or light adapted state. In order to determine the minimum amount of blue light intensity that is needed to bring the samples dominantly into the signalling state, the samples were excited with different light intensities. The experimental setup used for these measurements is the same as that shown in Fig 6.1 of chapter 6. The excitation was done with a high pressure mercury lamp and using a broad-band interference filter transmitting in the range 350-440 nm. The exposure time was set to 60 s. At the end of exposure the transmission was probed with the help of an attenuated tungsten lamp with the probe intensity of $I_{probe} \approx 10^{-5}$ W cm^{-2}. Between two exposures a dark pause of 3 minutes was made in order to bring all the molecules that have been excited into signalling state back to the dark adapted state. Fig 7.9

shows the results for BlrP1_BLUF. Upper panel of the figure shows the absorption coefficient spectra of the protein after being excited with different intensities. A clear formation of the signalling state is seen for the higher intensities. Lower intensities could not bring all the molecules into the signalling state. In the lower panel of Fig 7.9, absorption coefficient difference spectra are plotted. The maximum absorption changes are observed near $\lambda \approx 502$ nm for BlrP1_BLUF. Similar curves and results were obtained for the BlrP1 (curves are not shown here). The maximum absorption changes for BlrP1 were observed near $\lambda \approx 501$ nm.
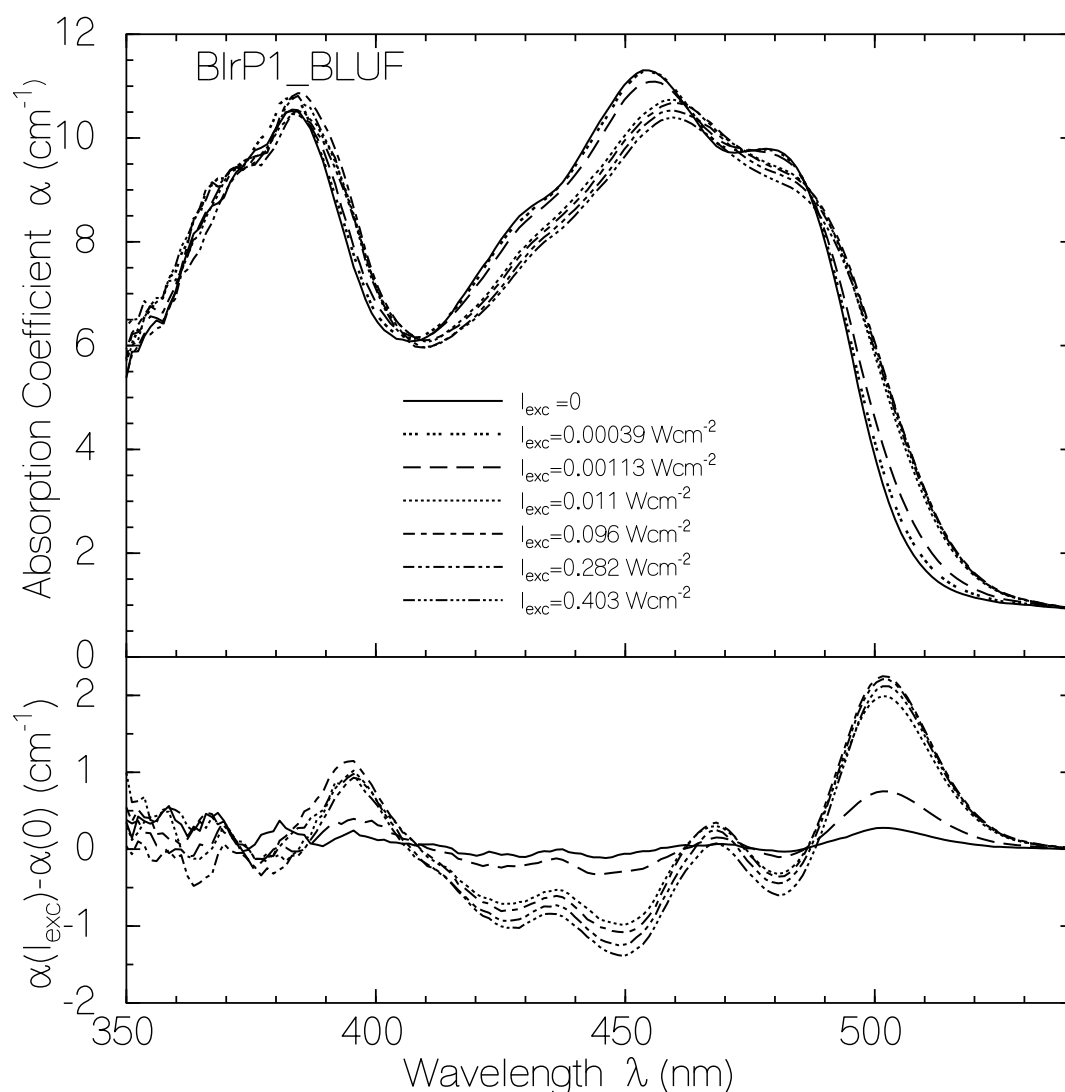
Figure 7.9 Intensity dependent signalling state formation of BlrP1_BLUF. Exposure time, $t_{exp} = 60$ s, Excitation intensities, I_{exc}, are shown in the graph. Excitation wavelength, $\lambda_{exc} = 350$-440 nm, Time interval between two exposure, $t_{int} = 3$ min, Intensity for probing, $I_{probe} = 10^{-5}$ Wcm^{-2}.

The changes $\alpha(I_{exc}) - \alpha(0)$ at the wavelength of maximum absorption change against the excitation intensity are shown in Fig 7.10. The upper panel belongs to BlrP1_BLUF and the lower panel belongs to BlrP1. From these curves the intensity necessary to bring the molecules into the signalling state is seen ($I_{exc, min} \approx 2 \times 10^{-2}$ Wcm^{-2} in both the cases). The data might be used to determine the quantum yield of signalling state formation [see e.g. [Zir06] (here another technique is used below in section 7.2.2.1)
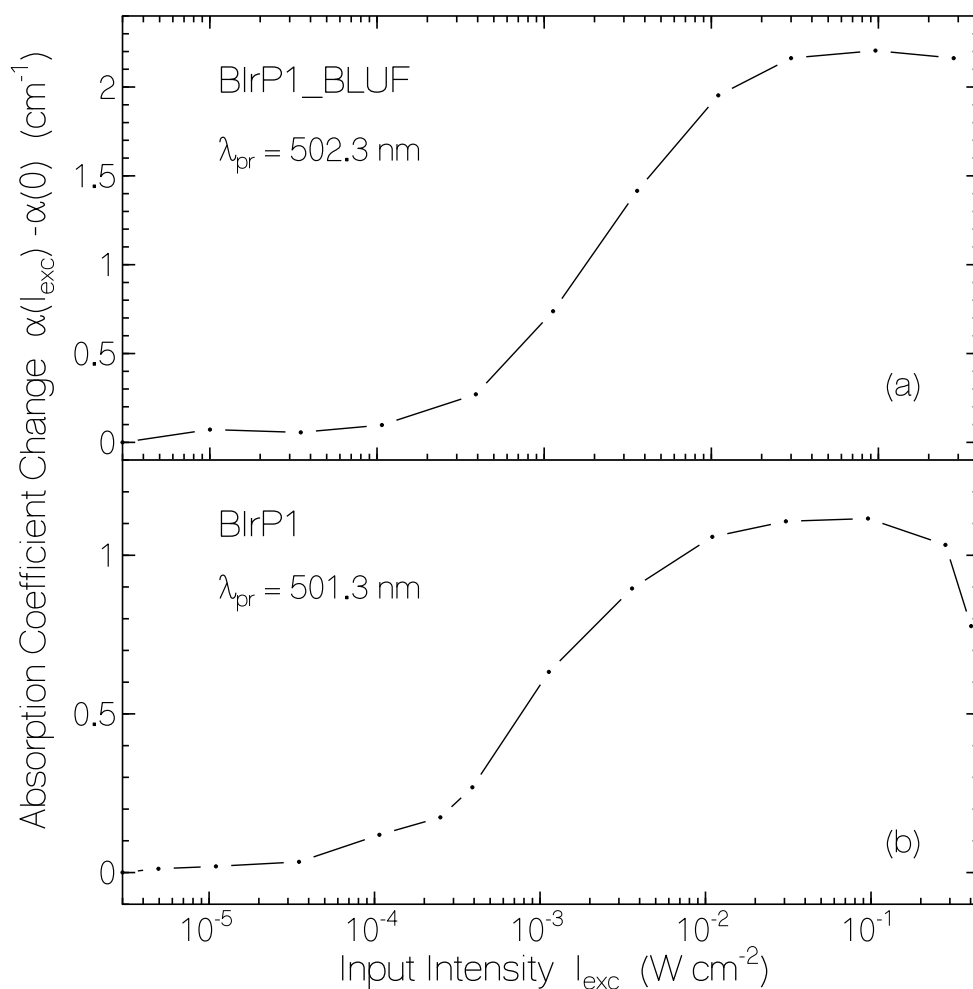
Figure 7.10 Intensity dependent signalling state formation. (a) BlrP1_BLUF at λ = 502.3 and (b) BlrP1 at λ = 501.3. Exposure time, t_{exp} = 60 s.

7.2.2 Receptor state-signalling state photodynamics

The photoinduced signalling state formation and recovery in the dark of BlrP1_BLUF and BlrP1 were followed via the absorption coefficient changes at probe wavelength λ_{pr} = 500 nm (wavelength selected near to the wavelength of maximum absorption changes). The measurements were carried out at four different temperatures in the range between 5 °C and 27.8 °C The samples were excited for 1 min in the wavelength range from 350 - 440 nm with an excitation intensity, I_{exc} = 0.0286 W cm^{-2} for three temperatures and with I_{exc} = 0.012 W cm^{-2} at temperature ϑ = 5 °C. The temporal change of absorption during exposure and after exposure was followed. The obtained data are shown in Fig 7.11. The absorption rises steeply to a plateau after light switch-on which indicates a steady state light adapted system formation. Comparison with Fig. 7.10 makes clear that for the applied intensity the obtained steady state belongs to complete conversion of the system to the signalling state. This absorption saturation is exploited below (next section) to determine the quantum efficiency of signalling state formation. After light switch-off the absorption recovers completely back to the original dark-adapted situation. The absorption recovery follows a single-exponential dependence. The absorption recovery time is temperature dependent. It reduces from τ_{rec} = (227±10) s at 5 °C to τ_{rec} = (18.4±2) s at 27.8 °C for BlrP1_BLUF, and from τ_{rec} = (300±15) s at 5 °C to τ_{rec} = (32.6±2) s at 27.5 °C for BlrP1. The temperature dependence of τ_{rec} (signalling state recovery time to receptor state) is shown by the insets in Fig. 7.11. An Arrhenius type activation barrier for signalling state recovery will be estimated below (over next section) from the temperature dependence of the absorption recovery time.
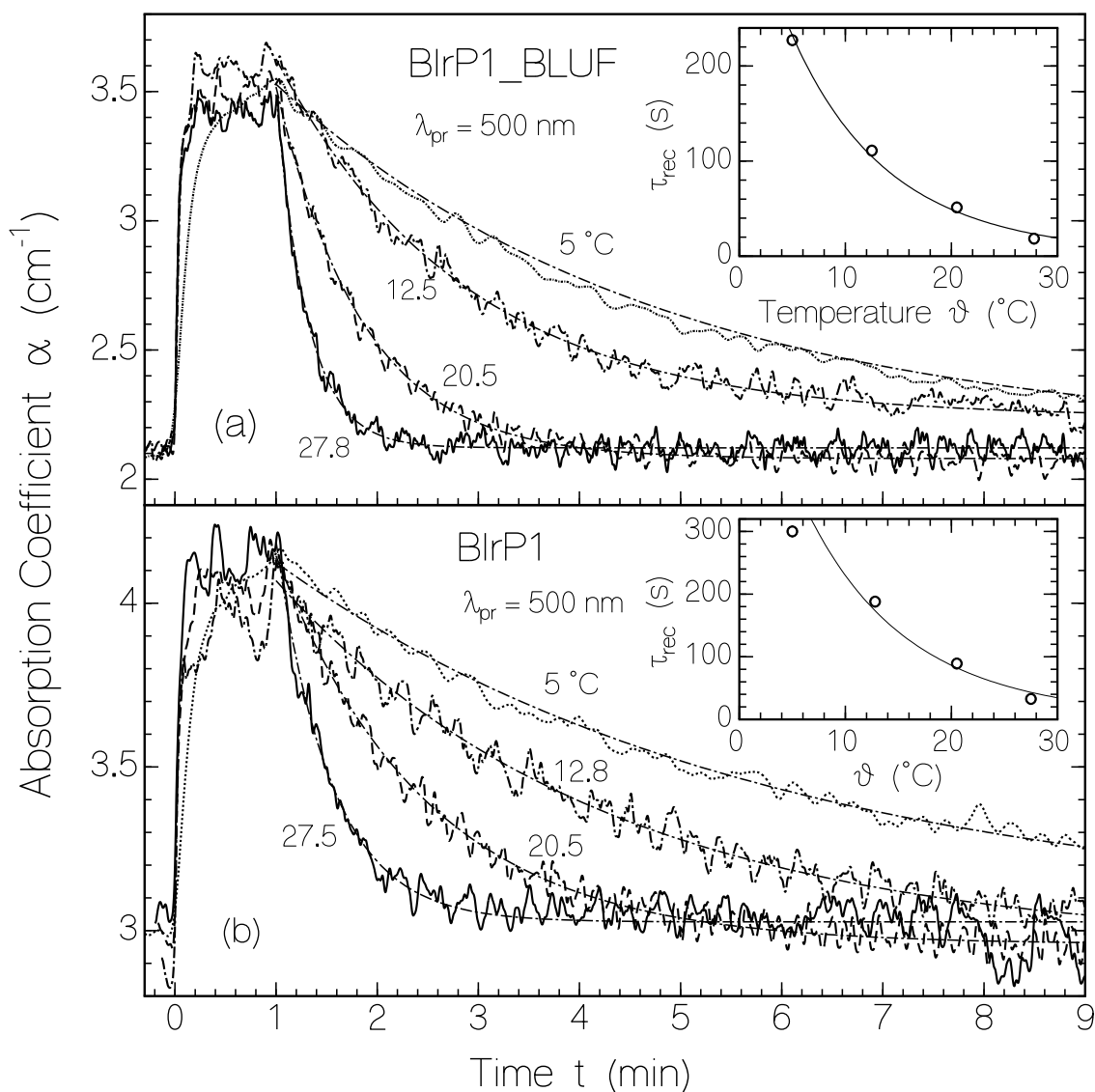
Figure 7.11 Photo-induced signalling-state formation and recovery to the initial dark state after light switch-off for four different temperatures for (a) BlrP1_BLUF and (b) BlrP1 in aqueous solution at pH 8. The absorption recovery fits to single-exponential curves as seen by the dash-dotted curves. The determined recovery times versus temperature are shown by circles in the insets. The solid curves in the insets are fitted by Eq. 7-14 (BlrP1_BLUF: $\tau_{rec,0}$ = 15.5 ps, W_b = 1.165×10^{-19} J, BlrP1: $\tau_{rec,0}$ = 80 ps, W_b = 1.1214×10^{-19} J).

7.2.2.1 Quantum efficiency of signaling state formation

The quantum efficiency of signalling state formation, ϕ_s, by blue light exposure is extracted from the rise of the absorption coefficient α_{pr} at wavelength λ_{pr} = 500 nm shown in

Fig. 7.11. The quantum efficiency is given by the ratio of length integrated number density of converted molecules, ΔN_s, to the number density of absorbed molecules, $\Delta n_{ph,abs}$, according to

$$\phi_s = \frac{\Delta N_s}{\Delta n_{ph,abs}} \,.$$

7-11

The length-integrated number density of generated signalling state molecules due to blue-light exposure for a period of t_{exp} is given by

$$\Delta N_s = \frac{\alpha_{pr}(0) - \alpha_{pr}(t_{exp})}{\sigma_{a,r}(\lambda_{pr}) - \sigma_{a,s}(\lambda_{pr})} \ell \,.$$

7-12

$\lambda_{pr} = 500$ nm was selected as probe wavelength. $\alpha_{pr}(0)$ is the absorption coefficient of the sample before light exposure. $\alpha_{pr}(t_{exp})$ is the absorption coefficient of the sample after a short time, t_{exp}, of light exposure. t_{exp} has to be short compared to the signalling state recovery time τ_{rec}, and the fraction of molecules transferred to the signalling state should be small compared to the total number of molecules to avoid saturation effects. ℓ is the sample length. $\sigma_{a,r}(\lambda_{pr})$ and $\sigma_{a,s}(\lambda_{pr})$ are the absorption cross-sections of the flavin cofactor in the receptor state and in the signalling state at the probe wavelength λ_{pr}, respectively.

The number density of absorbed excitation photons is given by

$$\Delta n_{ph,abs} \approx \frac{I_{exc}t_{exp}}{h\nu_{exc}}\left(1 - \frac{T(\lambda_{exc},0) + T(\lambda_{exc},t_{exp})}{2}\right) = \frac{I_{exc}t_{exp}}{h\nu_{exc}}\left(1 - \frac{\exp[-\alpha_{exc}(0)\ell] + \exp[-\alpha_{exc}(t_{exp})\ell]}{2}\right)$$

7-13

From Fig. 7.11a ($\vartheta = 20.5$ °C curve) for BlrP1_BLUF, a quantum yield of signalling state formation of ϕ_s(BlrP1_BLUF) ≈ 0.165 is calculated ($t_{exp} = 0.3$ s, $I_{exc} = 0.0286$ W cm^{-2}, $\sigma_{a,r}(\lambda_{pr}=500$ nm$) = 1.04\times10^{-17}$ cm^2, $\sigma_{a,s}(\lambda_{pr}=500$ nm$) = 2.82\times10^{-17}$ cm^2, $\sigma_{a,r}(\lambda_{exc}) \approx 2.9\times10^{-17}$ cm^2, $\ell = 0.15$ cm). For BlrP1, ($\vartheta = 20.5$ °C), at a value of ϕ_s(BlrP1) ≈ 0.084 is extracted from

the data of Fig. 7.11 b (t_{exp} = 0.3 s, I_{exc} = 0.0286 W cm^{-2}, $\sigma_{a,r}(\lambda_{pr}$=500 nm) = 9.85×10^{-18} cm^2, $\sigma_{a,s}(\lambda_{pr}$=500 nm) = 2.77×10^{-17} cm^2, $\sigma_{a,r}(\lambda_{exc}) \approx$ 2.8×10^{-17} cm^2, ℓ = 0.15 cm).

7.2.2.2 Thermal recovery in the dark

The signalling state is found to recover back to the original receptor state single-exponentially with a temperature dependent recovery time. At ϑ = 20.5 ºC the recovery times are τ_{rec}(BlrP1_BLUF) = 51.2 s and τ_{rec}(BlrP1) = 89.3 s. The recovery time is thought to be determined by a barrier height, W_b, between the signalling state and the receptor state. Using the Arrhenius-type equation [Fle86, Sch89]

$$\tau_{rec}(\vartheta) = \tau_{rec,0} \exp\left(\frac{W_b}{k_B \vartheta}\right)$$

7-14

and applying it to two temperatures, ϑ_1 and ϑ_2, gives

$$W_b = \frac{k_B \vartheta_1 \vartheta_2 \ln[\tau_{rec}(\vartheta_2)/\tau_{rec}(\vartheta_1)]}{\vartheta_1 - \vartheta_2},$$

7-15

where k_B is the Boltzmann constant, and $\tau_{rec,0} = k_{rec,0}^{-1}$ is the inverse attempt frequency of barrier crossing.

In the insets of Fig 7.11 the experimental recovery times are fitted by application of Eq. 7.14 and Eq. 7.15 (solid curves). The obtained attempt frequencies of barrier crossing are $k_{rec,0}$(BlrP1_BLUF) = (6.5±0.4)×10^{10} s^{-1} and $k_{rec,0}$(BlrP1) = (1.25±0.05)×10^{10} s^{-1}. The obtained barrier heights are W_b(BlrP1_BLUF) = (1.165±0.01)×10^{-19} J and W_b(BlrP1) = (1.121±0.01)×10^{-19} J. The parameters in wavenumbers, i.e. $W_b/(hc_0)$ where h is Planck's constant and c_0 is the speed of light in vacuum, are 5865 cm^{-1} for BlrP1_BLUF and 5645 cm^{-1} for BlrP1 (data listed in table 7.1).

7.2.3 Illustration of receptor state-signalling state photodynamics

The above experimental results for the receptor –signalling state dynamics are summarised schematically as shown Fig 7.12.
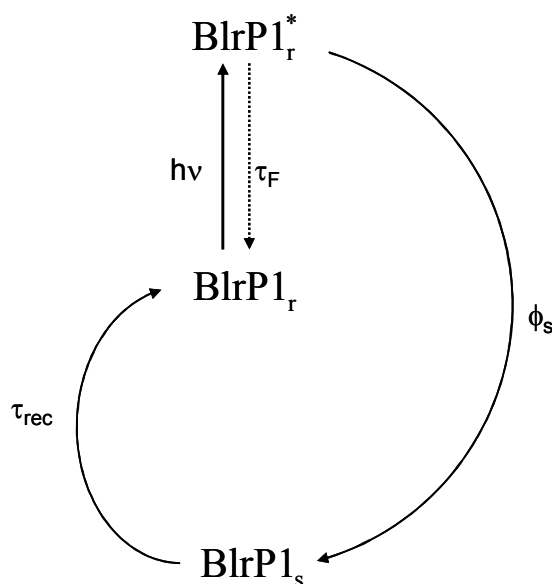

Figure 7.12 Schematic representation of the receptor –signalling state dynamics. τ_F : radiative and non radiative excited receptor state relaxation, ϕ_s : quantum efficiency of signalling state formation from excited receptor state, τ_{rec} : time constant of signalling state recovery to the receptor state in the dark.

7.3 Spectroscopic characterisation of proteins in the signalling state

7.3.1 Absorption spectra

After measuring the various spectroscopic parameters of BlrP1_BLUF and BlrP1 in the dark adapted or receptor state, the proteins were studied in the light adapted or the

signalling state. Fig 7.13 shows the absorption cross-section spectra of the proteins in the signalling state along with the corresponding receptor state spectra to visualise the red shift
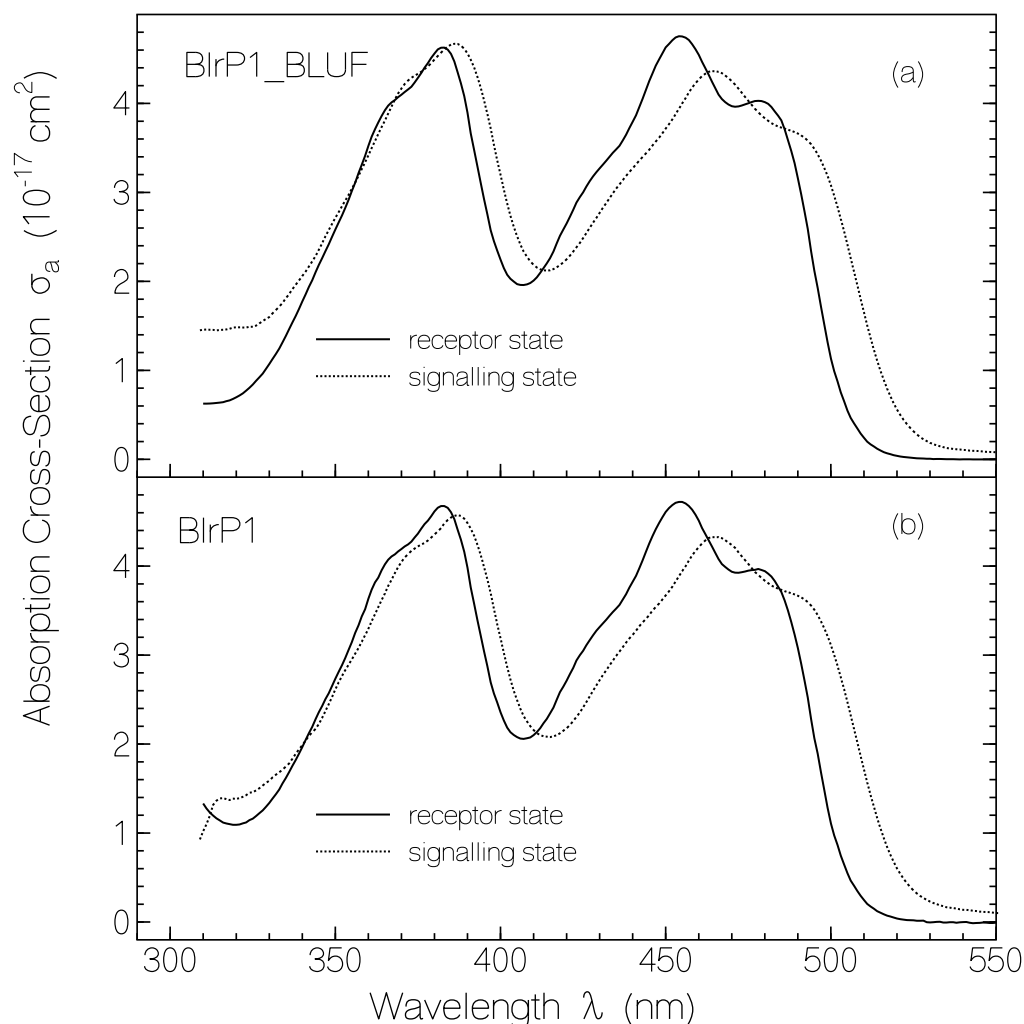
Figure 7.13 Absorption cross section spectra of (a) BLUF domain BlrP1_BLUF, and (b) full length protein BlrP1. Solid curves belong to receptor state and dashed curves belong to signalling state.

due to the signalling state formation. These spectra have been calculated from transmission spectra as described in chapter 2. The signalling state spectra are taken after exciting the samples at $\lambda_{exc} = 350\text{-}440$ nm with an intensity of $I_{exc} = 0.386$ Wcm^{-2} for a duration of 43 s. The absorption cross-section spectra of the BLUF domain and of the full-length protein in the signalling state are approximately 10 nm red-shifted compared to the receptor state.

7.3.2 Fluorescence results

7.3.2.1 Spectral dependencies

The spectral fluorescence measurements on the proteins in the signalling state were done with the help of the experimental setup described in section 6.2. The samples were measured in a $1.5 \times 1.5 \times 5$ mm^3 volume cell. The BlrP1_BLUF and BlrP1 samples were excited at $\lambda_{exc} = 365$ nm with $I_{exc} = 0.0126$ W cm^{-2} for a duration of $t_{exp} = 10$ s and fluorescence recording was done at the end of exposure for a period of 0.21 s. The absolute intrinsic fluorescence quantum distributions, $E_F(\lambda)$, of BlrP1_BLUF and BlrP1 in the receptor-state and in the signalling state are shown in Fig. 7.14 a and b.
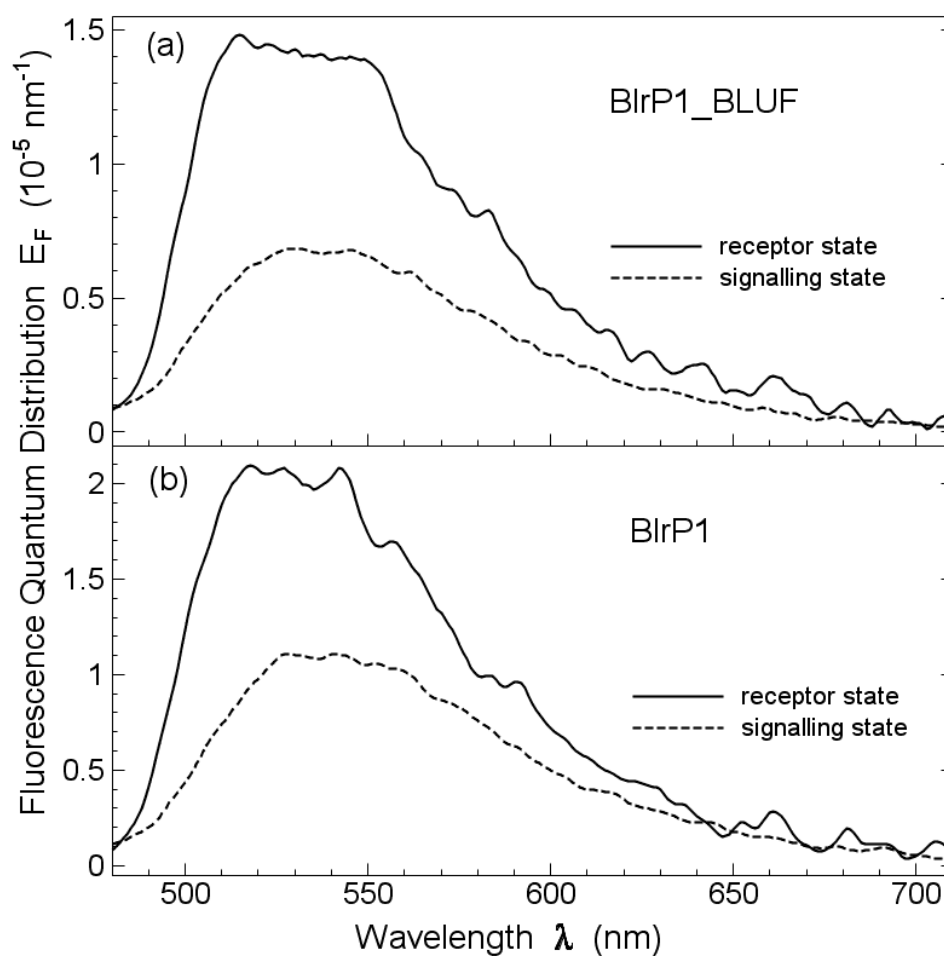
Figure 7.14 Fluorescence quantum distributions, $E_F(\lambda)$, of (a) BlrP1_BLUF and (b) BlrP1. Solid curves belong to receptor state and dashed curves belong to signalling state.

The absolute intrinsic fluorescence quantum yields have been calculated from $E_F(\lambda)$ using the relation $\phi_F = \int E_F(\lambda)d\lambda$. Lumiflavin in water buffered to pH 8 ($\phi_{F,R} = 0.235$ [Hol05]) was used as the reference.

Fig 7.14 shows that the fluorescence efficiency in the signalling state is smaller than in the receptor state. The fluorescence quantum yields, ϕ_F, for the proteins in the signalling state are $\phi_F(\text{BlrP1\_BLUF}) = (5.3\pm0.5) \times 10^{-4}$ and $\phi_F(\text{BlrP1}) = (1.2\pm0.1) \times 10^{-3}$.

7.3.1.2 Temporal dependencies

The signalling-state temporal fluorescence signals were measured in a small-volume cell ($1.5\times1.5\times5$ mm^3). The samples were used after centrifugation. The Ti:sapphire femtosecond laser was used to excite the samples. The laser was operated permanently during the whole measurement period at a repetition rate of 10 Hz with a single pulse energy density at the fluorescence cell of 1.8×10^{-3} J cm^{-2} (femtosecond pulses at 400 nm bring BLUF domains into the signalling state). At each delay time the up-converted signal was averaged over 30 excitation pulses. The fluorescence traces of BlrP1_BLUF and BlrP1 in signalling state are shown in Fig 7.15. The fluorescence decays of the proteins in the signalling state are fitted to a tri-exponential decay. The applied function is

$$S_F(t) = S_{F,max} \sum_{i=1}^{3} x_i \exp\left(-t/\tau_{F,i}\right),\qquad\qquad 7\text{-}16$$

with $\sum_{i=1}^{n} x_i = 1$.

The lifetime measurements in the signalling states, for the BlrP1-BLUF, reveal three components with $\tau_{F,1} = 10.4$ ps , $\tau_{F,2} = 101$ ps, and $\tau_{F,3} = 3$ ns. Similarly, for the full protein BlrP1, three components with $\tau_{F,1} = 6.83$ ps , $\tau_{F,2} = 74.6$ ps, and $\tau_{F,3} = 3$ ns are obtained. The fluorescence component with time constant $\tau_{F,3} \approx 3$ ns (fluorescence lifetime of free FAD in

aqueous solution [Isl03b] is thought to be due to FAD release from the protein in the signalling state during the measuring time (laser excitation over a period of about 30 min for the measurement of a decay curve over a time span of 1.5 ns). It is not a fluorescence time constant of flavin in the signalling state. The fit parameters x_i and $\tau_{F,i}$ are listed in Fig. 7.15 and in table 7.1.
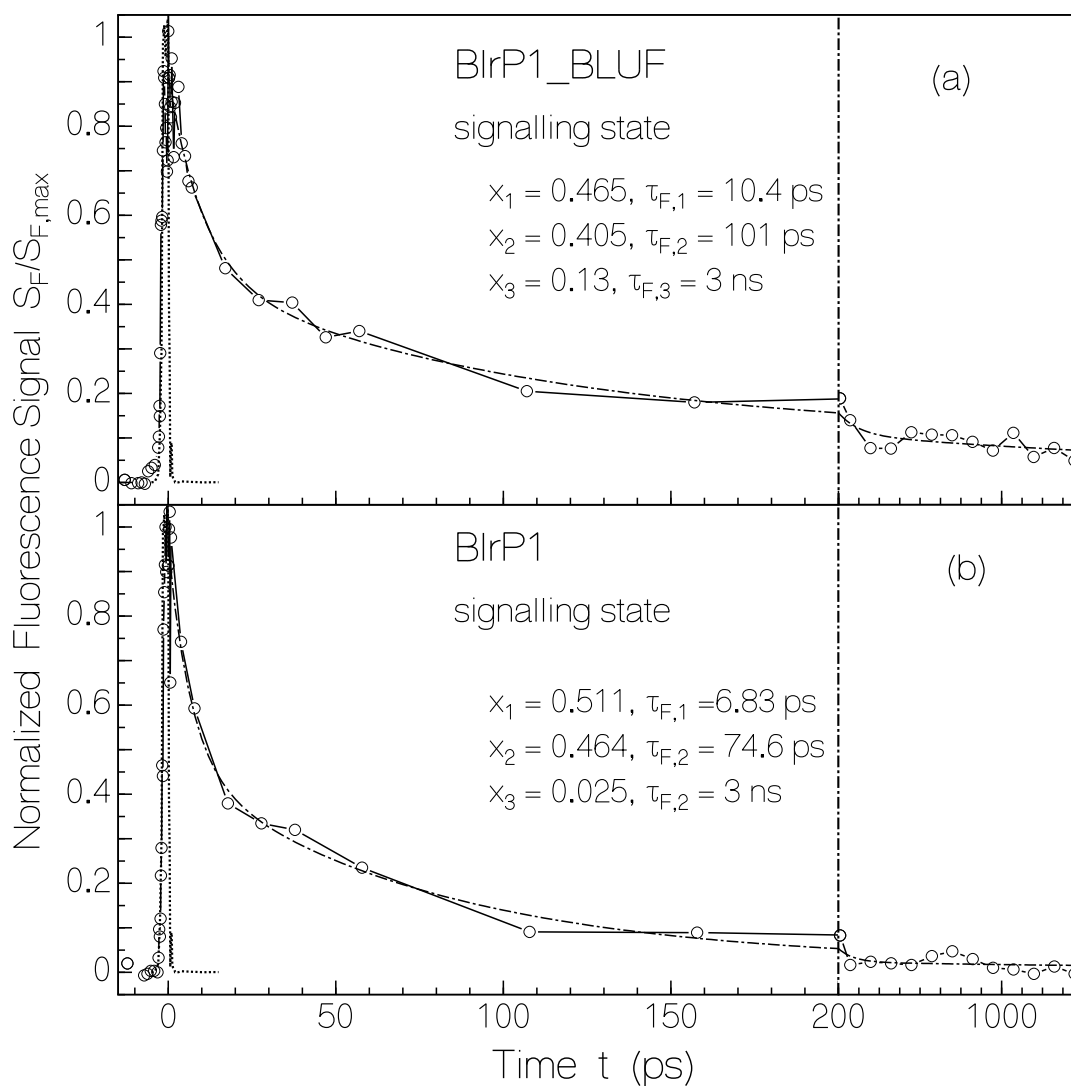

Figure 7.15 Temporal fluorescence behaviour determined by femtosecond laser fluorescence up-conversion for signalling state (a) BlrP1_BLUF and (b) BlrP1 in aqueous solution at pH 8 at room temperature. Line connected circles are the normalised fluorescence up-conversion signals. Dotted lines show the system response function. Dash-dotted curves are the non linear regression fits according to eq. 7-16. The fitted parameters are shown in the figure.

The presented fluorescence decay curves and parameters in Fig. 7.15 give apparent fluorescence quantum yields of $\phi'_F(BlrP1\_BLUF) = 2.8\times10^{-3}$ and $\phi'_F(BlrP1) = 2.1\times10^{-3}$ in the signalling state by using the relation

$$\phi'_F = \frac{1}{\tau_{rad}}\frac{\displaystyle\sum_{i=1}^{2}x_i\tau_{F,i}}{\displaystyle\sum_{i=1}^{2}x_i}, \qquad\qquad\qquad 7\text{-}17$$

with the radiative lifetime of $\tau_{rad} \approx 19$ ns for FAD [Zir07a]. These apparent fluorescence quantum yields are also significantly larger than the measured fluorescence quantum yields as in the case of quantum yields in the receptor state, indicating a partial fluorescence decay (fraction x_0) with fluorescence decay time, $\tau_{F,0}$, shorter than the experimental time resolution of $\tau_{res} \approx 300$ fs of our detection system. The real fluorescence decay is given by eqn. 7-8

The fraction of the fluorescence signal with decay time $\tau_{F,0}$ may be again determined from the fluorescence quantum yield relation of eqn. 7-9. The fraction of fast decaying molecules, x_0, is again given by eqn. 7-10.

The obtained fractions x_0 for the signalling state are 0.81 for BlrP1_BLUF and 0.42 for BlrP1

The two fast fluorescence decays (time constants $\tau_{F,0}$ and $\tau_{F,1}$) will be interpreted in section 7.5 to be due to photo-induced charge-separated state formation (reductive electron transfer from an adjacent electron donating amino acid to the electron accepting photo-excited FAD), and the slower fluorescence decay (time constant $\tau_{F,2}$) will be interpreted to be due to relaxation to the initial signalling ground-state by charge recombination (electron transfer back from FAD semiquinone radical anion to amino acid radical cation, a thermodynamic equilibrium between FAD^{-} and $FAD_{ox,r}^*$ is assumed, fluorescence emission from $FAD_{ox,r}^*$ and possible contribution from charge-separated state [FAD^{-}...aa].

7.4 Signalling state photo-excitation dynamics

7.4.1 Absorption behaviour

The photodynamics in the signalling state is determined by photo-reduction and photo-degradation of BlrP1_BLUF and BlrP1 in the signalling state. These processes were studied by long-time exposure of the samples at fixed excitation intensity and probing the transmission with a white-light tungsten lamp. The absorption changes after light switch-off (partial recovery of reduced FAD back to oxidized form) were studied by recording transmission spectra with a weak white-light tungsten lamp at certain times after pump-light switch-off.

The samples were excited at λ_{exc} = 350-440 nm with an excitation intensity of I_{exc} = 0.386 Wcm^{-2}. For the results shown in Fig. 7.16a, BlrP1_BLUF was exposed for t_{exp} = 43 s, 3.7 min, 7.7 min, 14.7 min, 27.7 min, 40.7 min, 53.7 min and 80.7 min.. Fig 7.16 b shows some absorption spectra of BlrP1_BLUF after the sample had been exposed for 9 min and then the excitation light was turned off. The intensity of the probe light was kept well below the intensity required to bring the samples into the signalling state. For BlrP1,the excitation results are shown in Fig 7.17a. The presented curves belong to exposure time of t_{exp} = 43 s, 2.7 min, 7.7 min, 18.7 min, 29.7 min, 40.7 min, 51.7 min, 83.7 min. Fig 7.17 b shows the recovery in dark for the BlrP1 sample that has been exposed for 5 min.

As seen in the Fig 7.16 (a) and 7.17 (a), the absorption bands centred at 465 nm (S_0-S_1 transition) and 380 nm (S_0-S_2 transition) decrease, and a rise in absorption occurs below 340 nm is seen. The absorption spectra at the end of long-time exposure resemble the absorption spectrum of fully reduced FAD (neutral form $FAD_{red}H_2$ or anionic form $FAD_{red}H^-$, at pH 8 the anionic form is dominant [Son07]).
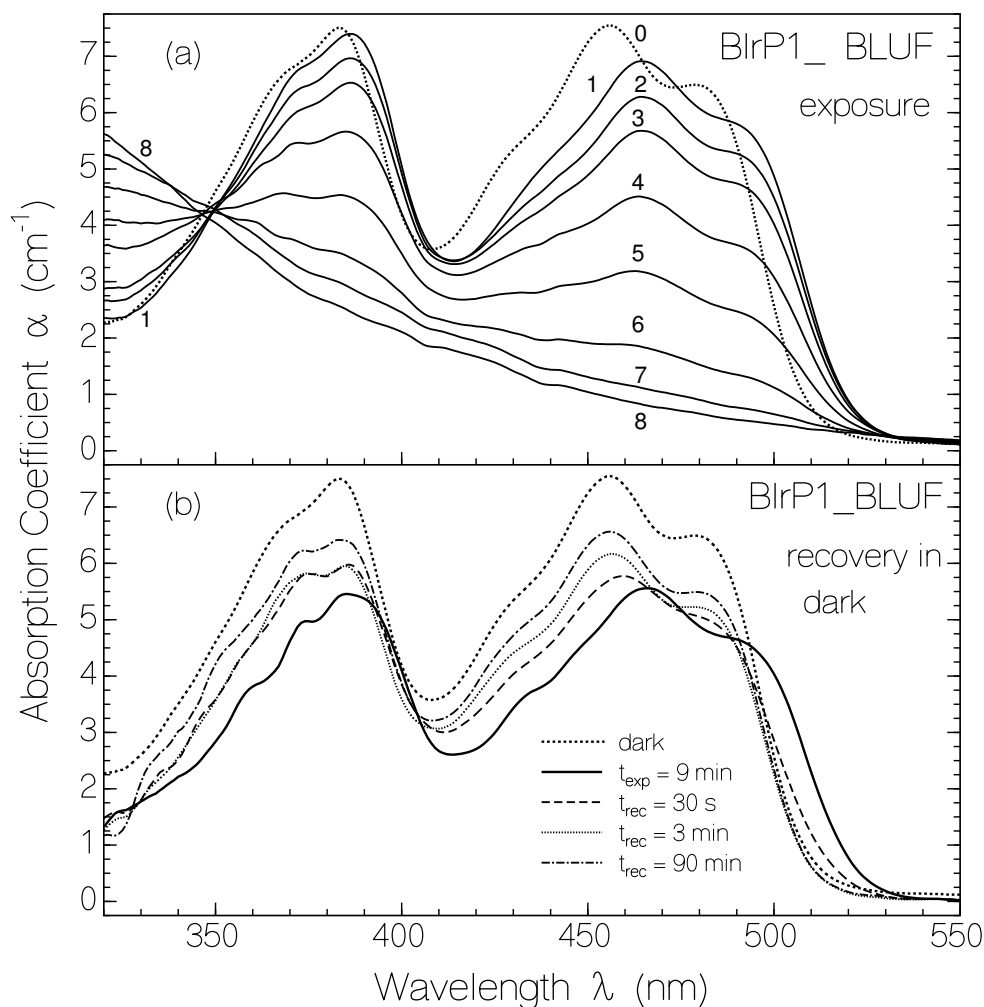
Figure 7.16 Dynamics of FAD photoconversion and dark recovery for BlrP1_BLUF in aqueous solution at pH 8. Light exposure at λ_{exc} = 350-440 nm with I_{exc} = 0.386 W cm^{-2}.
(a) Exposure of BlrP1_BLUF. Exposure times: t_{exp} = 0 (0), 43 s (1), 3.7 min (2), 7.7 min (3), 14.7 min (4), 27.7 min (5), 40.7 min (6), 53.7 min (7), and 80.7 min (8).
(b) Recovery of BlrP1_BLUF in the dark after 9 min of exposure.

The absorption recovery displayed in Fig. 7.16b (BlrP1_BLUF, 9 min of exposure) and in Fig. 7.17b (BlrP1, 5 min exposure) reveals a fast return of the absorption of the oxidized FAD in the signalling state to the receptor state absorption. Then in the case of BlrP1_BLUF a partial re-oxidation of the reduced FAD form ($FAD_{red}H^-$) to the oxidized form (FAD_{ox}) follows, while FAD in BlrP1 remains irreversibly reduced.
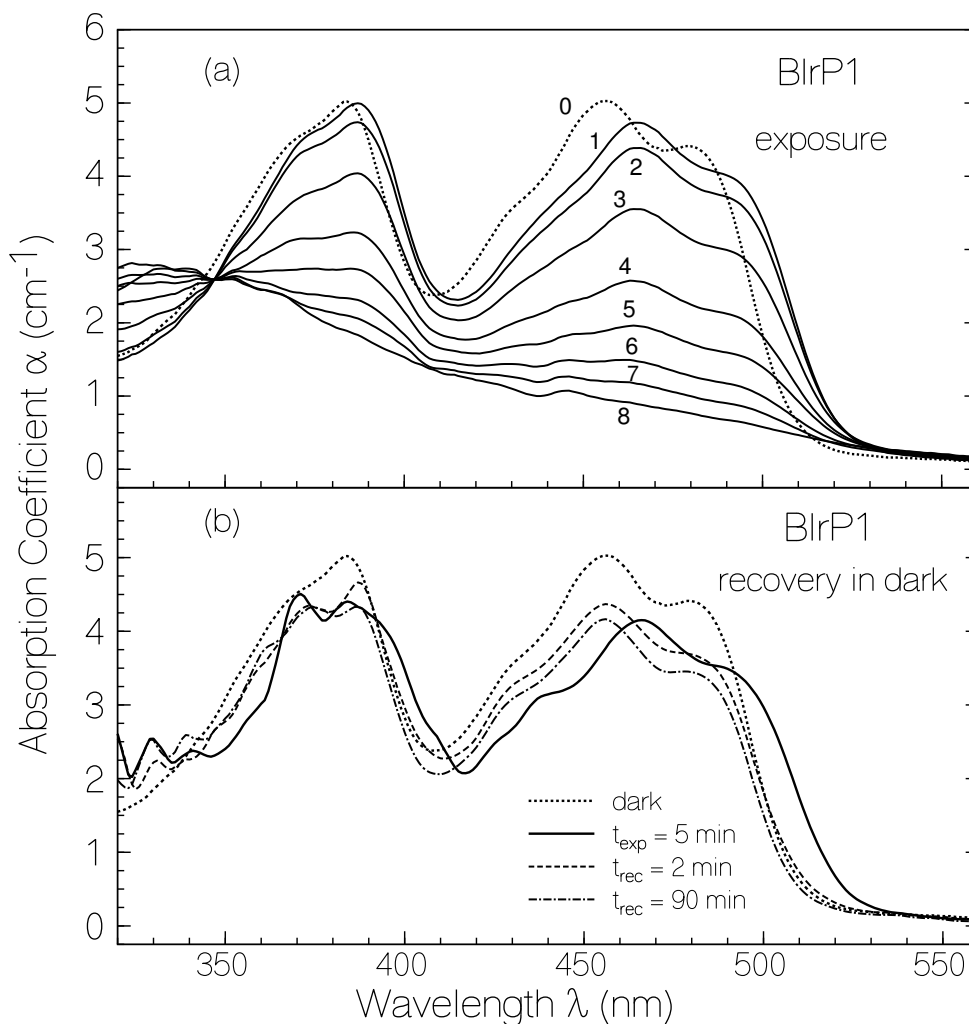
Figure 7.17 Dynamics of FAD photoconversion and dark recovery for BlrP1 in aqueous solution at pH 8. Light exposure at λ_{exc} = 350-440 nm with I_{exc} = 0.386 W cm^{-2}.
(a) Exposure of BlrP1. Exposure times: t_{exp} = 0 (0), 43 s (1), 2.7 min (2), 7.7 min (3), 18.7 min (4), 29.7 min (5), 40.7 min (6), 51.7 min (7), and 83.7 min (8).
(b) Recovery of BlrP1 in the dark after 5 min of exposure.

During light exposure the light scattering of the samples increased. For the spectra shown in Fig. 7.16 and Fig. 7.17 the light scattering contribution is approximately subtracted and therefore not seen. The rise of scattering continued after ending of light exposure. The

scattering effect turned out to be stronger for the full-length protein BlrP1 than for the BLUF domain BlrP1_BLUF. The scattering is due to protein aggregation [Pen08] which may be caused by protein unfolding (denaturation).

The temporal dependence of the absorption at λ_{pr} = 456 nm during exposure and after exposure is shown in Fig. 7.18a (BlrP1_BLUF) and Fig. 7.18b (BlrP1). In the figure the dots show absorption coefficients during light exposure, and the open circles show the absorption coefficient development after light switch-off. The excitation causes a sharp decrease in absorption due to signalling state formation (smaller absorption cross-section at 456 nm). It follows a continued decrease in absorption during the light exposure due to FAD reduction
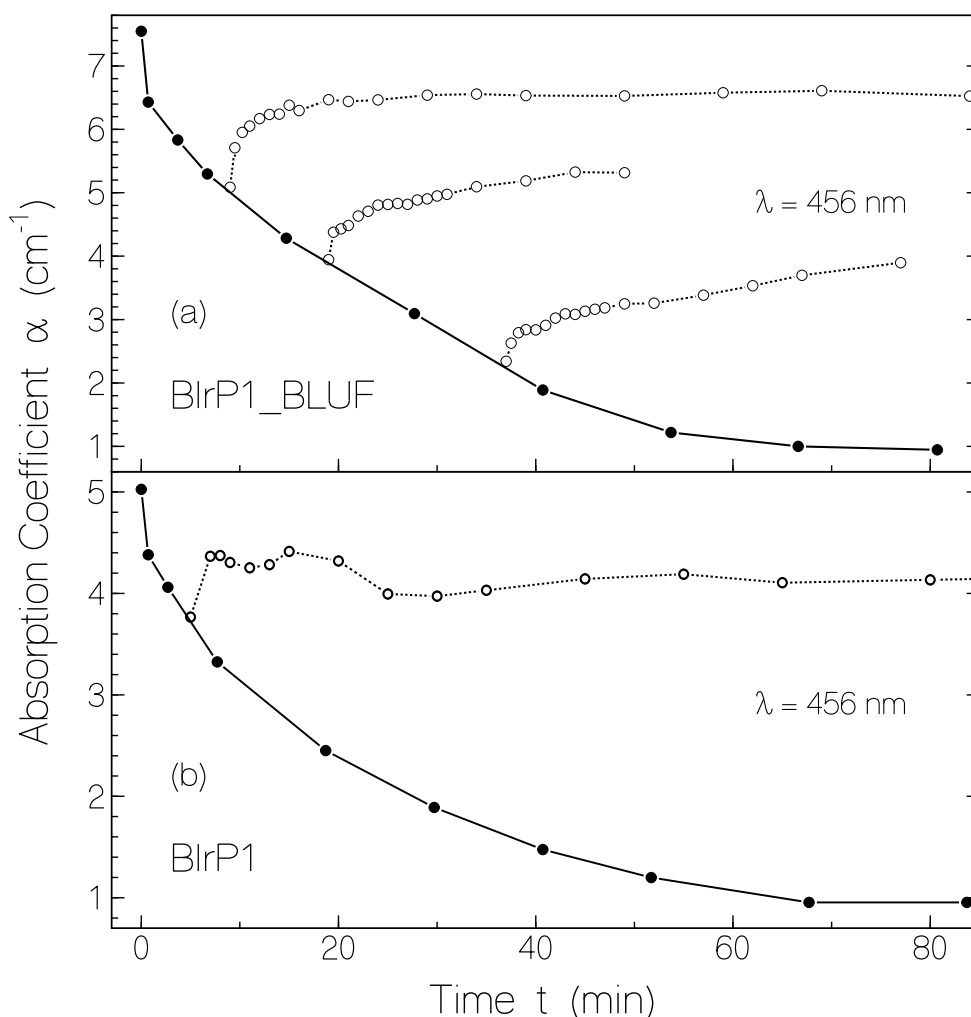

Figure 7.18 Temporal absorption behaviour, $\alpha(t)$, at λ = 456 nm of (a) BlrP1_BLUF and of (b) BlrP1 in aqueous solution at pH 8 during (dots) and after light exposure (open circles) at λ_{exc} = 350-440 nm with I_{exc} = 0.386 W cm^{-2}.

and photodegradation. After light switch-off a sudden rise in absorption occurs because of the signalling state recovery to the receptor state. In the case of BlrP1_BLUF a slow absorption rise follows due to FAD re-oxidation. A mole-fraction of $\chi_{reox} \approx 0.35$ of the fully reduced FAD gets re-oxidized. The rest remains reduced. In the case of BlrP1 no re-oxidation of reduced FAD is observed.

7.4.2 Fluorescence behaviour

The fluorescence spectra development of BlrP1_BLUF and BlrP1 during light exposure is shown in Fig. 7.19. The excitation occurred at λ_{exc} = 350-440 nm with an intensity of 0.25 W cm^{-2}. The fluorescence spectra were recorded by intermittent changing to $\lambda_{exc,pr}$ = 365 nm with $I_{exc,pr}$ = 0.031 W cm^{-2}. The presented spectra are normalized to the dark-adapted fluorescence peak. The fluorescence spectra above 500 nm first decrease because of signalling state formation. With prolonged exposure the fluorescence in the FAD$_{ox}$ spectral region increases, then levels off and decreases. This behaviour is thought to be due to FAD$_{ox}$ release (with low efficiency, see below) from the protein with subsequent FAD$_{ox}$ photodegradation [Hol05]. In the wavelength range between 400 nm and 500 nm fluorescence builds up, then levels off (consumption of released FAD), and for BlrP1 begins to decrease (photodegradation of primary photoproducts). A fluorescence structure peaking at 478 nm is attributed to lumichrome emission in the rising emission tail of FAD$_{ox}$ [Hol05].

The free FAD$_{ox}$ has higher fluorescence quantum efficiency ($\phi_{F,FAD,free} \approx 0.033$) than the bound FAD$_{ox}$ (in the receptor state: $\phi_{F,r}$(BlrP1_BLUF) ≈ 0.00144, $\phi_{F,r}$(BlrP1) ≈ 0.002; in the signalling state: $\phi_{F,s}$(BlrP1_BLUF) $\approx 5.3 \times 10^{-4}$, $\phi_{F,s}$(BlrP1) ≈ 0.0012). In the case of long-time exposure of BlrP1_BLUF, the FAD fluorescence contribution rises to $\phi_{F,FAD,max} \approx 0.003$ corresponding to fraction of released FAD of $\chi_{release} \approx (\phi_{F,FAD,max} - \phi_{F,s})/(\phi_{F,FAD,free} - \phi_{F,s}) \approx$ 0.077. In the case of long-time exposure of BlrP1 the FAD fluorescence contribution rises to
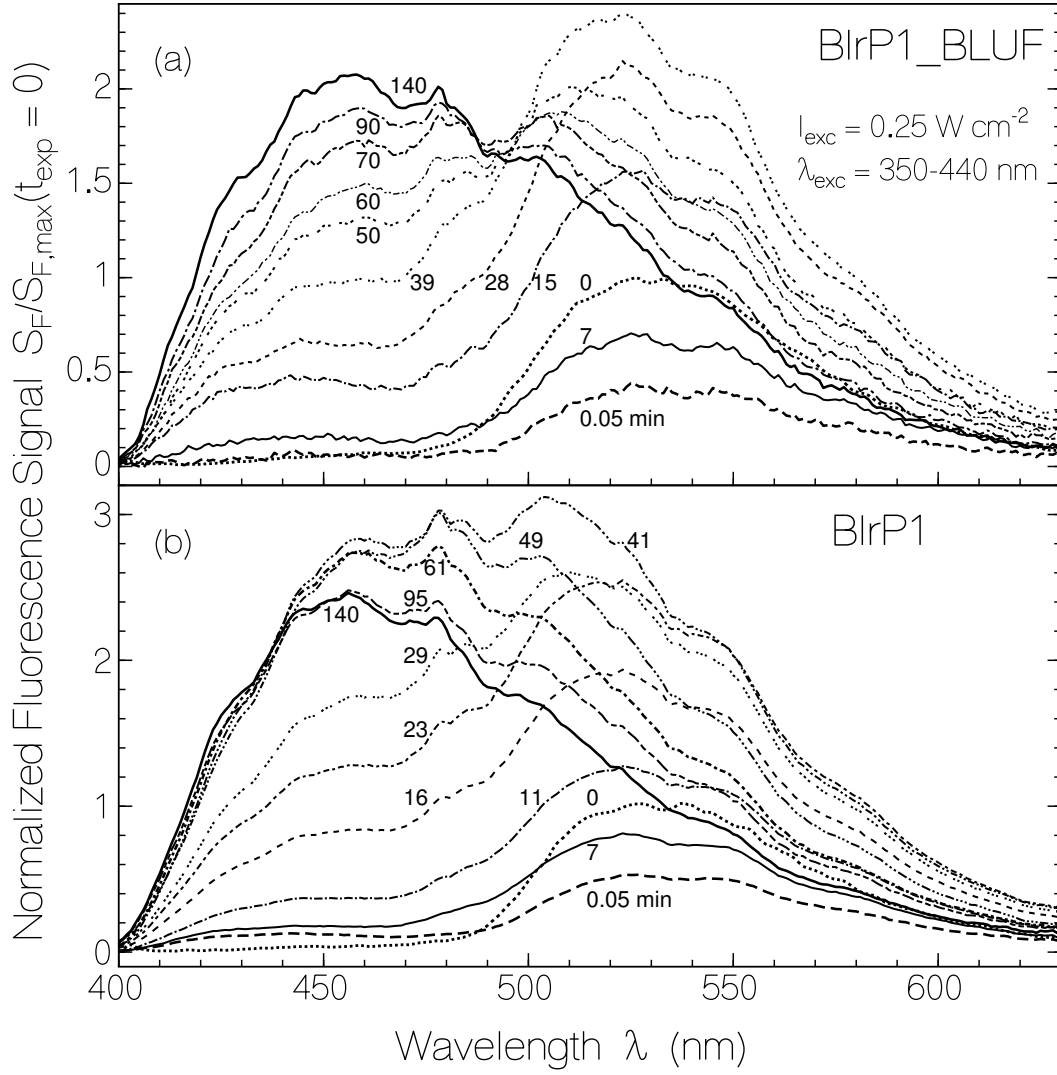
Figure 7.19 Temporal development of fluorescence with exposure time, t_{exp}, of (a) BlrP1_BLUF and (b) BlrP1 in aqueous solution at pH 8. Light exposure at λ_{exc} = 350-440 nm with I_{exc} = 0.25 W cm^{-2}. Fluorescence probing by excitation at $\lambda_{exc.pr}$ = 365 nm with intensity I_{excpr} = 0.031 W cm^{-2} using short-wavelength cut-off filters of Schott KV399 and KV408 in the fluorescence detection path. Exposure times in min are indicated at the curves.

$\phi_{F,FAD,max} \approx 0.0051$ corresponding to fraction of released FAD of $\chi_{release} \approx (\phi_{F,FAD,max} - \phi_{F,s})/(\phi_{F,FAD,free} - \phi_{F,s}) \approx 0.13$. The release of FAD is limited by the conversion of FAD$_{ox}$ in the signalling state to FAD$_{red}$H^{-}. The photoinduced release of the FAD cofactor is thought to occur together with partial protein unfolding (denaturation) showing up in increased light scattering due to protein aggregation which is facilitated by unfolding [Pen08].

7.4.3 Quantum efficiency of photoinduced FAD release in the signalling state

The quantum efficiency of photoreleased FAD is given by the ratio of length integrated number density of photoreleased molecules, ΔN_{rel}, to the number density of absorbed molecules, $\Delta n_{ph,abs}$, according to

$$\phi_{rel} = \frac{\Delta N_{rel}}{\Delta n_{ph,abs}} .$$
7-18

The length-integrated number density, ΔN_{rel}, of photoreleased FAD molecules in the signalling state generated in a time interval $t_{exp} = t_2 - t_1$ may be extracted from Fig. 7.19 by the relation

$$\Delta N_{rel} = \frac{S_F(\lambda_F, t_2) - S_F(\lambda_F, t_1)}{S_{F,r}(\lambda_F)} \frac{\phi_{F,r}}{\phi_{F,free}} N_0 \ell .$$
7-19

$S_F(\lambda_F, t_i)$ is the fluorescence signal at wavelength λ_F at time t_i. $\lambda_F = 530$ nm is used in the analysis (about wavelength position of maximum FAD emission). $S_{F,r}(\lambda_F)$ is the fluorescence signal at λ_F of the sample in the receptor state (dark-adapted state). $\phi_{F,r}$ is the fluorescence quantum yield of FAD in the receptor state, and $\phi_{F,free}$ is the fluorescence quantum yield of released FAD ($\phi_{F,free} = 0.033$ [Isl03b]). N_0 is the total number density of FAD molecules in the samples, and ℓ is the sample length. The number density of absorbed photons is again given by Eq.7-13. Using the fluorescence signal curves for $t_1 = 0.05$ min and $t_2 = 7$ min from Fig. 7.19, values of $\phi_{rel}(BlrP1\_BLUF) = (5.0\pm0.2)\times10^{-6}$ and $\phi_{rel}(BlrP1) = (4.6\pm0.2)\times10^{-6}$ are calculated.

7.4.4 Illustration of signalling state photodynamics

The above experimental results for the signalling state photo-excitation dynamics are summarised schematically in Fig. 7.20. More details are given in the discussion part.
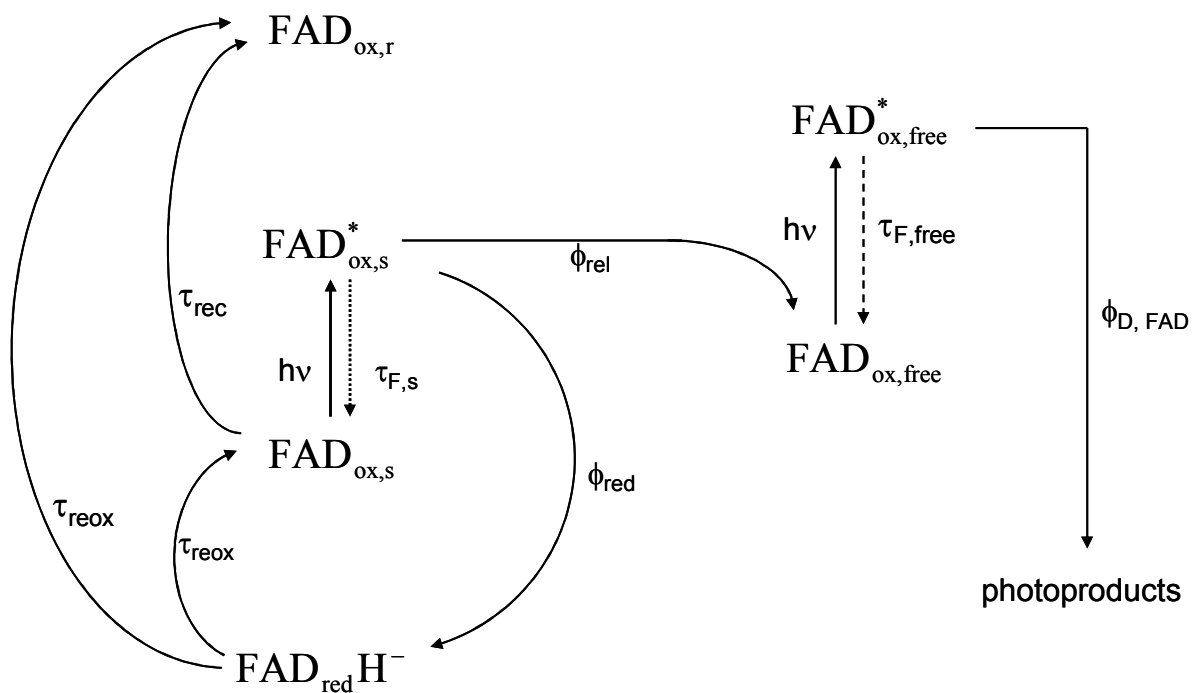

Figure 7.20 Schematic representation of the signalling state photo-excitation dynamics. The start point in this scheme is $FAD_{ox,s}$.

Table 7.1: Parameters of BLUF domain BlrP1_BLUF and of full-length protein BlrP1 from *K. pneumoniae*

	BlrP1_BLUF Receptor state	BlrP1_BLUF Signalling state	BlrP1 Receptor state	BlrP1 Signalling state
$\lambda_{a,max}$ (nm)	454.3	464.7	454.3	464.7
$\sigma_{a,max}$ (cm^2)	4.75×10^{-17}	4.37×10^{-17}	4.72×10^{-17}	4.33×10^{-17}
ϕ_F	$(1.44 \pm 0.1) \times 10^{-3}$	$(5.3 \pm 0.5) \times 10^{-4}$	$(2.0 \pm 0.1) \times 10^{-3}$	$(1.2 \pm 0.1) \times 10^{-3}$
x_0	0.43	0.81	0.45	0.42
τ_{rec}(20.5 °C) (s)		51.2 ± 1		89.3 ± 2
$k_{rec,0}$ (s^{-1})		$(7.5 \pm 04) \times 10^{10}$		$(1.25 \pm 0.05) \times 10^{10}$
$W_b/(hc_0)$ (cm^{-1})		5865 ± 50		5645 ± 50
ϕ_s	0.165 ± 0.01		0.084 ± 0.01	
ϕ_{red}		$(3.4 \pm 0.2) \times 10^{-5}$		$(3.9 \pm 0.2) \times 10^{-5}$
ϕ_{rel}		$(5.0 \pm 0.2) \times 10^{-6}$		$(4.6 \pm 0.2) \times 10^{-6}$
χ_{reox}		≈ 0.35		≈ 0
τ_{reox} (min)		≈ 17		

Abbreviations: $\lambda_{a,max}$: wavelength of maximum of first absorption band. $\sigma_{a,max}$: maximum absorption cross-section in first absorption band. ϕ_F: fluorescence quantum yield. x_0: fraction of cofactor molecules with fluorescence decay time $\tau_{F,0}$. τ_{rec}: time constant of signalling state recovery to the receptor state in the dark. $k_{rec,0}$: attempt frequency of barrier crossing between signalling state and recovery state. W_b: barrier height. ϕ_s: quantum efficiency of signalling state formation, ϕ_{red}: quantum efficiency of photoinduced reduction oxidized flavin cofactor to fully reduced anionic flavin hydroquinone in the signalling state. ϕ_{rel}: quantum yield of photoinduced flavin cofactor release in the signalling state. χ_{reox}: mole fraction of fully reduced anionic flavin hydroquinones which get re-oxidized in the dark. τ_{reox}: time constant of re-oxidation.

7.5 Discussion

Using all the information that has been obtained from the spectroscopic studies, an overall photodynamics scheme is presented and separate schemes for the receptor state and signalling state photodynamics are given.

An overall photodynamics scheme is shown in Fig. 7.21. In the top part the receptor state – signalling state photocycle is illustrated. FAD_{ox} in the receptor state ($FAD_{ox,r}$) is photoconverted to the signalling state ($FAD_{ox,s}$) with a quantum yield of ϕ_s. In the dark $FAD_{ox,s}$ recovers to $FAD_{ox,r}$ with a time constant τ_{rec}. The lower left part shows the photoreduction of $FAD_{ox,s}$ with quantum yield ϕ_{red}.
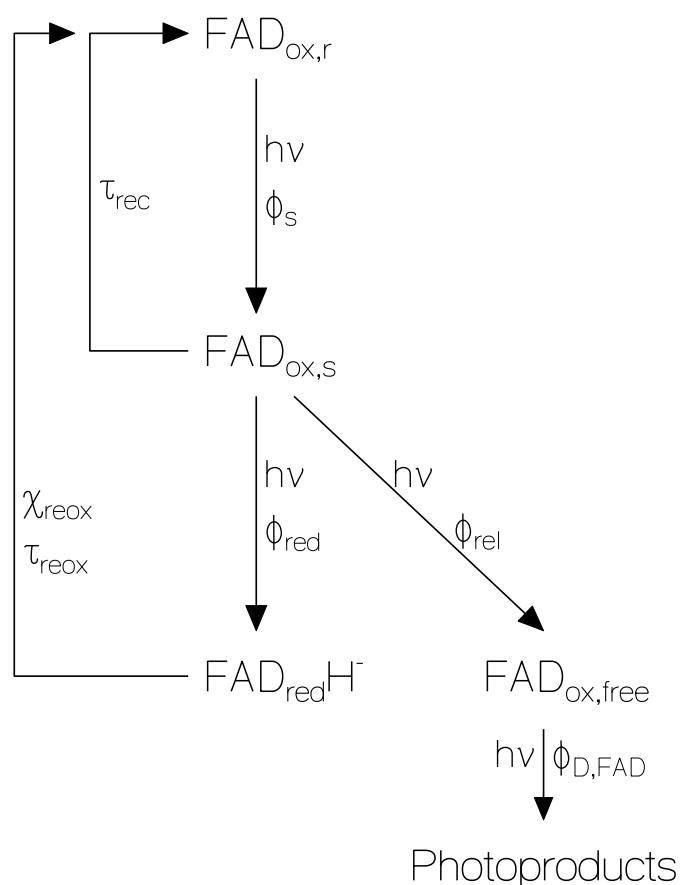
Figure 7.21 Overall photodynamic scheme for FAD in BlrP1_BLUF and BlrP1.

A mole-fraction χ_{reox} recovers back to $FAD_{ox,r}$ in the dark with a time constant τ_{reox}. The other fraction $(1-\chi_{reox})$ remains permanently reduced. The reduction of FAD_{ox} to the anionic form $FAD_{red}H^-$ is assumed since at pH 8 $FAD_{red}H^-$ is the stable reduced form of FAD [Son07]. The lower right part shows the photoinduced release of $FAD_{ox,s}$ to $FAD_{ox,free}$ with a quantum yield of ϕ_{rel}. The photodegradation of $FAD_{ox,free}$ to photoproducts with efficiency $\phi_{D,FAD}$ is included.

7.5.1 Receptor state - signalling state photodynamics

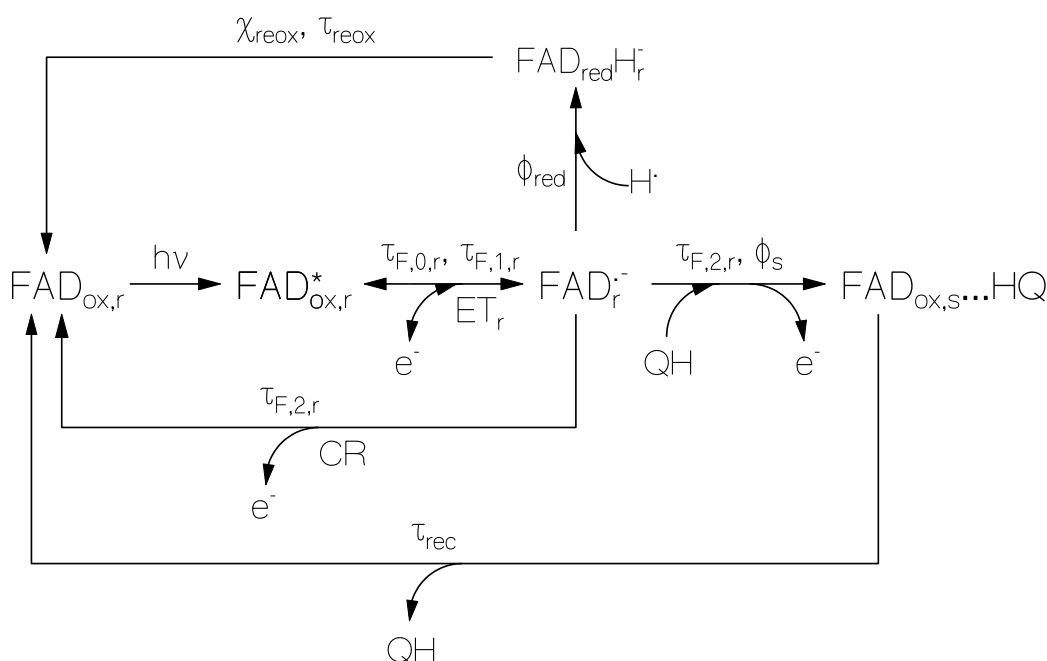The reaction scheme of the receptor state - signalling state photocycle dynamics is shown in Fig. 7.22.

Figure 7.22 Reaction scheme of receptor state to signalling state conversion by blue-light or violet light excitation, and back-recovery in the dark.

In the presented scheme, $FAD_{ox,r}$ is photo-excited to $FAD^*_{ox,r}$. In thermodynamic equilibrium with an aminio acid residue, which is likely to be tyrosine, a reductive electron

transfer is expected to occur from the amino acid donor, aa, to the photoexcited FAD acceptor [Zir07b] forming FAD_r^- with the time constants $\tau_{F,0,r}$ and $\tau_{F,1,r}$. The two time constants hint to two conformations with slightly different donor-acceptor distance, the electron transfer being exponentially distance dependent [Orr03]). The anionic FAD semiquinone is thought to recover back to the quinone form $FAD_{ox,r}$ by charge recombination between FAD_r^- and aa^+ with the time constant $\tau_{F,2,r}$ according to FAD_r^- ...$aa^+ \rightarrow FAD_{ox,r}$...aa, (a more complex reaction path via $FADH^-$ formation cannot be excluded [Gau06]) During the lifetime $\tau_{F,2,r}$, fluorescence emission from photo-excited $FAD_{ox,r}^*$ and some fluorescence contribution from the charge-separated state $[FAD_r^-...aa^+]$ are thought to occur [Shi08]. During the anionic FAD semiquinone lifetime $\tau_{F,2,r}$, a protein conformational change is thought to be induced leading to a hydrogen bonding change which brings FAD to the signalling state $FAD_{ox,s}$ with a quantum efficiency of ϕ_s. The relevant reaction is FAD_r^-...$QH \rightarrow FAD_{ox,s}$...$HQ + e^-$. QH presents the amino acid and $FAD_{ox,s}$...HQ presents the hydrogen-bond complex in the signalling state. The e^- is given to aa^+ (Tyr^+) by charge recombination. Finally, in the dark $FAD_{ox,s}$ recovers back to $FAD_{ox,r}$ with a time constant τ_{rec} by hydrogen bond re-formation. In Fig. 7.22 the very weak reduction of FAD_r^- to $FAD_{red}H^-$ by H^- uptake and subsequent partial re-oxidation to $FAD_{ox,r}$ is included.

The FAD^- intermediate has a similar S_0-S_1 absorption spectrum as FAD_{ox} with a factor of two lower absorption strength [Shi08]. The absorption cross-section spectra of FAD^- together with absorption cross-section spectrum of FAD_{ox} is shown in Fig 7.23. It does not show up in the continuous absorption studies performed in this work (Fig. 7.16 and Fig 7.17) because of its short lifetime (FAD^- lifetime given by $\tau_{F,2,r}$).

In the presented experiments the photo-induced electron transfer is monitored by fast fluorescence decay (time constants, $\tau_{F,0,r}$, $\tau_{F,1,r}$), and the charge recombination is monitored by the slower fluorescence decay (time constant $\tau_{F,2,r}$) in femtosecond laser fluorescence up-

conversion measurements. The occurrence of hydrogen-bond changes within the charge-separated state lifetime is plausible by Coulombic forces present in the charge separated situation.
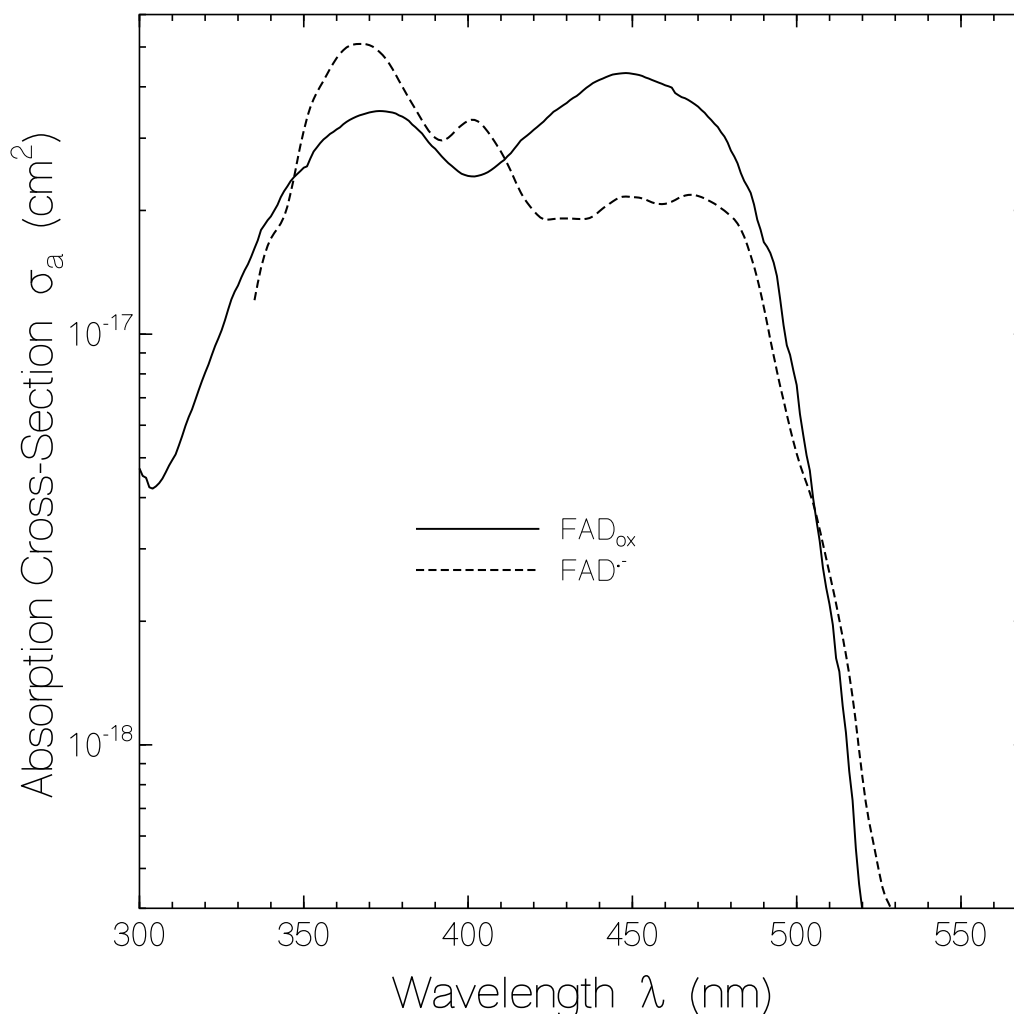

Figure 7.23 Absorption cross section spectra of FAD_{ox} in aqueous solution at pH 7 and of $FAD^{\cdot-}$ [Shi08].

7.5.2 Photo-excitation dynamics in the signalling state

Fig 7.24 shows the reaction scheme of the photo-induced electron transfer with subsequent charge recombination, and of the photoreduction of $FAD_{ox,s}$ to the fully reduced $FAD_{red}H^-$ hydroquinone anion in the signalling state conformation of BlrP1 and BlrP1_BLUF. In this scheme, $FAD_{ox,s}$ is photo-excited to $FAD^{\bullet}_{ox,s}$. In thermodynamic equilibrium with an

aminio acid residue, a reductive electron transfer is expected to occur from the amino acid donor, aa, to the photoexcited FAD acceptor [Zir07b] forming $FAD_s^{\cdot-}$ with the time constants $\tau_{F,0,s}$ and $\tau_{F,1,s}$. These two time constants again hint to two conformations with slightly different donor-acceptor distance (see last section). The anionic FAD semiquinone $FAD_s^{\cdot-}$ is
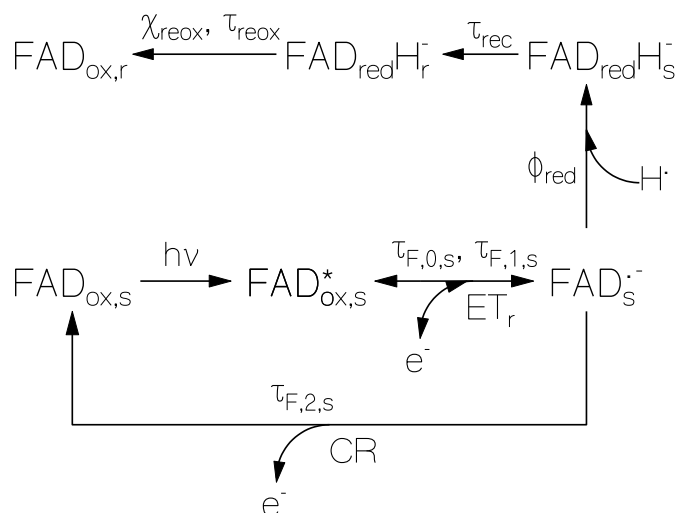

Figure 7.24 Reaction scheme of signalling state photo-excitation, reductive electron transfer, charge-recombination, FAD reduction, and re-oxidation. ET_r: reductive electron transfer. CR: charge recombination.

thought to recover back to the quinone form $FAD_{ox,s}$ by charge recombination between $FAD_s^{\cdot-}$ and aa^+ with the time constant $\tau_{F,2,s}$ according to $FAD_s^{\cdot-}\ldots aa^+ \rightarrow FAD_{ox,s}\ldots aa$. During the lifetime $\tau_{F,2,s}$, fluorescence emission from photo-excited $FAD_{ox,s}^*$ and some fluorescence contribution from the charge-separated state $[FAD_s^{\cdot-}\ldots aa^+]$ are thought to occur. There also happens a reduction of $FAD_s^{\cdot-}$ into $FAD_{red}H_s^-$ during this time. $FAD_{red}H_s^-$ further recovers to $FAD_{red}H_r^-$, a fraction χ_{reox} of which subsequently recovers back to $FAD_{ox,r}$. The hydrogen-bond rearrangement is thought to remain unchanged in the signalling state photo-cycle,

$$FAD_{ox,s} \xrightarrow{\;h\nu\;} FAD_{ox,s}^* \longleftrightarrow FAD_s^{\bullet-} \longrightarrow FAD_{ox,s}$$
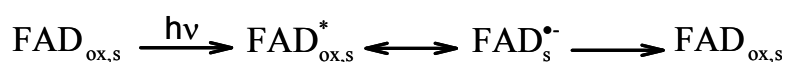
7.5.3 Photoinduced FAD release and free FAD photodegradation

Fig 7.25 shows schematically the photoinduced release of $FAD_{ox,s}$ to $FAD_{ox,free}$ and the photo degradation of this free FAD into photoproducts during prolonged exposure.

$$FAD^{*}_{ox,s} \qquad\qquad FAD^{*}_{ox,free}$$

$$\phi_{red} \qquad h\nu \qquad\qquad h\nu \qquad \phi_{D}$$

$$FAD_{red}H^{-} \qquad FAD_{ox,s} \qquad FAD_{ox,free} \qquad \text{Photoproducts}$$

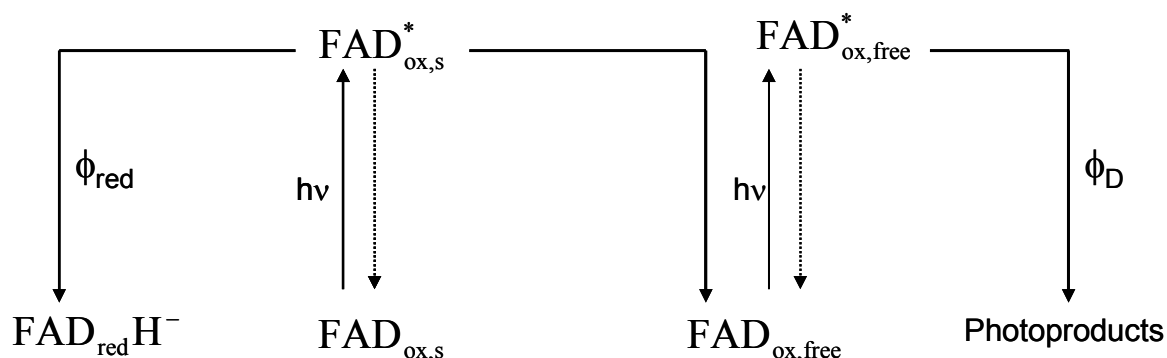**Figure 7.25** Scheme for photoinduced FAD release and free FAD photodegradation.

According to the scheme of Fig 7.25, $FAD_{ox,s}$ is photo excited to $FAD^{*}_{ox,s}$. A part of $FAD^{*}_{ox,s}$ is reduced to $FAD_{red}H^{-}$. This is clearly seen from the absorption spectra of BlrP1_BLUF and BlrP1 obtained after prolonged light exposure as shown in Fig 7.16 and Fig 7.17. The spectra resemble that of the fully reduced FAD. Along with that there occurs also some release of the FAD from the protein denoted as $FAD_{ox,free}$. This results in an increased fluorescence in the spectral region above 500nm, clearly seen in Fig. 7.19. The $FAD_{ox,free}$ is photoexcited to $FAD^{*}_{ox,free}$ which subsequently photodegrades into primary photoproducts like lumichrome with a quantum efficiency ϕ_{D}.

8 Comparison of BlrP1 protein with other BLUF proteins

The few BLUF proteins which so far have been cloned, overexpressed, purified, and spectroscopically investigated are AppA and BlrB from *R. sphaeroides* [Gom98, Bra02, Mas02, Jun05, Zir06], Tll0078 (also called TePixD) from *Thermosynechococcus elongatus* [Oka06, Tak07, Fuk05, Kit05] Slr1694 (also called PixD) from *Synechocystis* sp. PCC6803 [Has04, Has05, Mas04, Mas04, Oka05, Gau06, Zir07a], photoactivated adenylyl cyclase PAC from the unicellular flagellate *Euglena gracilis* [Ise02] and protein YcgF (BlrP) from *Escherichia coli* [Gom98, Raj04, Mas05, Has06].

Table 8.1 compares some parameters that have been obtained by various workers on these BLUF-proteins. The given parameters are $\lambda_{a,max,r}$ (S_0-S_1 absorption maximum in the receptor state), $\lambda_{a,max,s}$ (S_0-S_1 absorption maximum in the signalling state), $\delta\lambda$ (wavelength red-shift of signalling state), τ_{rec} (recovery time of signalling state to receptor state) and ϕ_s (quantum yield of signalling state formation.)

The receptor state absorption maximum, $\lambda_{a,max,r}$, varies between $\lambda_{a,max,r} = 438$ nm for Tll0078 for *T. elongatus* [Fuk05] and $\lambda_{a,max,r} = 459$ nm for YcgF (BlrP) from *E.coli* (wavelength span of 21 nm) [Has06]. This spreading indicates an influence of the protein environment on the FAD absorption peak. Non-conserved amino acids in the binding pocket with different hydrogen bonding action towards FAD are thought to be responsible for this behaviour. It is found that the presence of a serine residue in the FAD binding pocket causes a spectral absorption red shift (AppA wild type is 15 nm red-shifted compared to AppA S41A mutant) [Mat07].

The wavelength red-shift of the signalling state relative to the receptor state varies between $\delta\lambda = 10$ nm for Tll0078, YcgF, BlrP1 and $\delta\lambda = 15$ nm for AppA. This is thought to

Table 8.1: Absorption peaks, recovery times, and quantum yields of signalling state formation of wild-type BLUF proteins at room temperature

	$\lambda_{a,max,r}$ (nm)	$\lambda_{a,max,s}$ (nm)	$\delta\lambda$ (nm)	τ_{rec} (s)	ϕ_s	Reference
BlrP1_BLUF	454.3	464.7	10.4	51.2	0.165	[Tya08]
BlrP1	454.3	464.7	10.4	89.3	0.084	[Tya08]
YcgF-BLUF	459	469	10	196		[Has06]
YcgF	459	469	10	196		[Has06]
BlrB	445.7	457.6	11.9	2	0.40	[Zir06]
AppA	445	460	15	1000	0.24	[Zir05]
Slr1694	444.3	457.3	13	17	0.63	[Zir07a]
Tll0078	438	448	10	16		[Fuk05]

Abbreviations: $\lambda_{a,max,r}$: S_0-S_1 absorption maximum in the receptor state. $\lambda_{a,max,s}$: S_0-S_1 absorption maximum in the signalling state. $\delta\lambda$: wavelength red-shift of signalling state. τ_{rec}: recovery time of signalling state to receptor state. ϕ_s: quantum yield of signalling state formation.

due to the differences in the hydrogen bonding network between the BLUF protein binding pockets and FAD in the receptor state and the signalling state. At low temperatures the wavelength red-shift of the signalling-state was found to be reduced in Tll0078 [Fuk05, Fuk08, Fuk07] indicating that conformational changes take place during the picosecond to sub-nanosecond lifetime of the photo-induced charge-separation that are frozen out at low temperature.

BlrP1 and YcgF(BlrP), both being BLUF-EAL proteins, give the same spectral red shift on photoexcitation. TheYcgF ground state absorption peak position, $\lambda_{a,max,r}$, is about 5 nm red-shifted compared to BlrP1. This shift can be understood since the amino acid identity

is only 41 % [Raj04]. A red-shift of only $\delta\lambda = 4$ nm was reported for light-exposed YcgF(BlrP) by [Raj04], but in this case the excitation intensity was too low and the duration of exposure too short to transfer all BLUF domains to the signalling state.

The time constants of signalling state recovery to the receptor state in the dark at room temperature vary between $\tau_{rec} = 2$ s for BlrB [Zir06] and $\tau_{rec} = 1000$ s for AppA [Zir05]. This difference is large (factor of 500), but the activation barrier between the signalling state and the receptor state, which is thought to be responsible for the rate of recovery, does not vary strongly (exponential energy dependence for Arrhenius-type barrier crossing). Barrier heights of $W_b/(hc_0) \approx 7560$ cm^{-1} for AppA [Zir05] and $W_b(hc_0) \approx 4340$ cm^{-1} for BlrB [Zir05] have been estimated (factor of 1.74).

The determined quantum yields of signalling-state formation vary between 0.084 (BlrP1) [Tya08] and 0.63 (Slr1694) [Zir07a]. The efficiency of signalling state formation is thought to be determined by the lifetime of the intermediate anionic FAD semiquinone [Laa06] and the driving force of hydrogen-bond conformation change during the anionic FAD semiquinone lifetime.

The presented basic photo-cycle scheme that has been shown in Fig 7.23 is thought to be followed by all BLUF domains studied thus far [Zir06, Gau06, Zir07a, Zir05 Dra05, Zir07b]. The photo-induced reductive electron-transfer is generally accepted to occur from an adjacent Tyr residue to the isoalloxazine part of FAD [Zir06, Gau06, Zir07a, Zir05 Dra05, Ste07, And05, Jun06, Mas07, Gri06a, Zir07b, Shi08, Gau05, Gri06b, Mat07, Fuk07, Fuk08]. It is also generally accepted that an adjacent conserved Gln residue is involved in the H-bonding change (first described in [And05, Jun06]). But the orientation of Gln [Jun05, Kit05, And05, Unn06] is unclear and also whether Gln makes a 180° flip to change from the receptor-state to the signalling state (flip first proposed in [And05, Jun06], no flip stated in [Sad08]) is not clear. It has also not yet been clarified whether Gln remains in its keto form in both the dark and light adapted state [Gau06, And05, Jun06] or whether the keto form of the

dark state changes to the enol form in the signalling state. The keto form ($—CO—NH_2$) and the enol form ($—COH=NH$) of Gln are shown in Fig. 8.1. The keto-enol tautomerisation
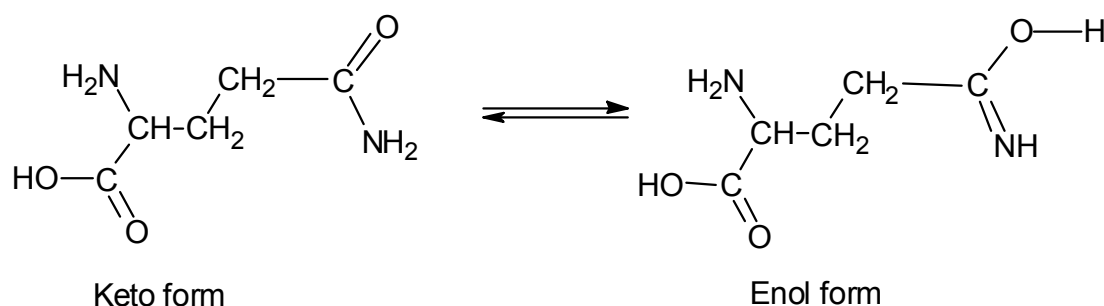

Figure 8.1 Keto and enol forms of glutamine.

was proposed by [Ste07] and it was determined as best reaction path in quantum mechanics/molecular mechanics calculations [Dom08, Sad08]. Also not uniquely clear is the location of a Trp (W) residue and a Met (M) residue (position change of Trp and Met) in the dark state and in the signalling state. If Trp is adjacent to Gln and FAD it is called as W_{in} arrangement; if Trp is at the protein surface exposed to the solvent it is known as W_{out} arrangement. Crystal structure studies on the wild-type AppA BLUF domain in the dark state showed the W_{in} arrangement [And05], and on the AppA-C20S BLUF domain in the dark showed the W_{out} arrangement [Jun06]. NMR measurement analysis [Gri06a, Gri06b] and Raman spectroscopy [Unn06] suggested a W_{in} arrangement. In the dark state, the active site, Gln, is assumed to be oriented by W_{in} such that it forms a hydrogen bond between its hydroxyl group and that of active site Tyr [Gau06, And05, Gri06a, Toh08, Gri06b]. A Gln rotation is assumed to occur in the signalling state formation process. In contrast, this conformation has been ascribed to the signalling state and linked to the light induced Gln rotation to a $W_{out} \rightarrow W_{in}$ switch by some other workers [Jun06, Dom08, Sad08, Oba08].

The photo-cycle similarities of BlrP1_BLUF with the AppA, BlrB, Slr1694, and Tll0078 BLUF domains (similar spectral red-shift, strong fluorescence quenching) show that

the involvement of Trp is not a necessary condition for the BLUF domain photo-cycle activity since BlrP1_BLUF contains no Trp. The investigation of the AppA-W104F BLUF domain also showed the maintenance of BLUF photo-activity [Laa06, Gau07] (only one Trp is left which is not adjacent to Gln and FAD).

The signalling state photo-excitation again causes a fast reductive electron transfer and charge recombination on a picosecond timescale [Zir06, Zir07a, Zir05, Toh08, Zir07b, Tya08]. Prolonged intense light exposure showed different photo-stability for the investigated BLUF proteins in [Zir06, Zir05, Zir07a, Tya08] (photoreduction, cofactor release, photodegradation, denaturation).

For comparison of the findings on the photo-cycle dynamics of BlrP1-BLUF and BlrP1 with the findings on other BLUF domains [Gau065, Gau06, Laa06, Gau07, Ste07, Toh08] which also involved experiments giving access to the observation of hydrogen-bond changes, protonation effects, and neutral radical pair involvement, in Fig. 8.2 dynamics schemes of receptor to signalling state formation are re-drawn. From the fluorescence results, a thermodynamic equilibrium between FAD_{ox}^{*} and FAD^{-} both in the receptor state and in the signalling state has been concluded from our studies. The two time constants of photo-induced reductive electron transfer, $\tau_{F,0}$ and $\tau_{F,1}$, with different values in the receptor state and the signalling state indicate the strong distance dependence and the conformation dependence of the electron transfer [Orr03, Mar85, Mos88, Shi07] and may be different for different BLUF domains. The photo-reduction of FAD^{-} to $FAD_{red}H^{-}$ with low efficiency ϕ_{red} is shown for both FAD_{r}^{-} and FAD_{s}^{-} in Fig. 8.2 but it cannot be resolved experimentally for the receptor state since ϕ_{red} is orders of magnitude smaller than ϕ_{s}. A re-oxidation of $FAD_{red}H^{-}$ to FAD_{ox} in the dark is possible but is not shown in Figure 8.2 in order not to overload the scheme. A photo-reduction may not necessarily be present in other BLUF photocyles. In the path from FAD^{-} to $FAD_{ox,s}$, both for the receptor state cycle and for the signalling state cycle, $FADH^{\bullet}$ may be involved [Gau06, Toh08]. It is not accessible by our applied fluorescence up-

conversion method. It is expected that a dominant charge recombination from FAD^- to aa^+ (Tyr^+) in the back transfer from FAD^- to FAD_{ox} [Mar85, Shi07] both for the receptor state (efficiency of signalling state formation is only $\phi_s(BlrP1\_BLUF) \approx 0.17$ and $\phi_S(BlrP1) \approx 0.08$) and the signalling state might occur, but a return of FAD^- and aa^+ to FAD_{ox} and aa via neutral radicals [Dom08, Sad08, Toh08] cannot be excluded. In the recovery from $FAD_{ox,s}$ to $FAD_{ox,r}$ intermediates may be involved.
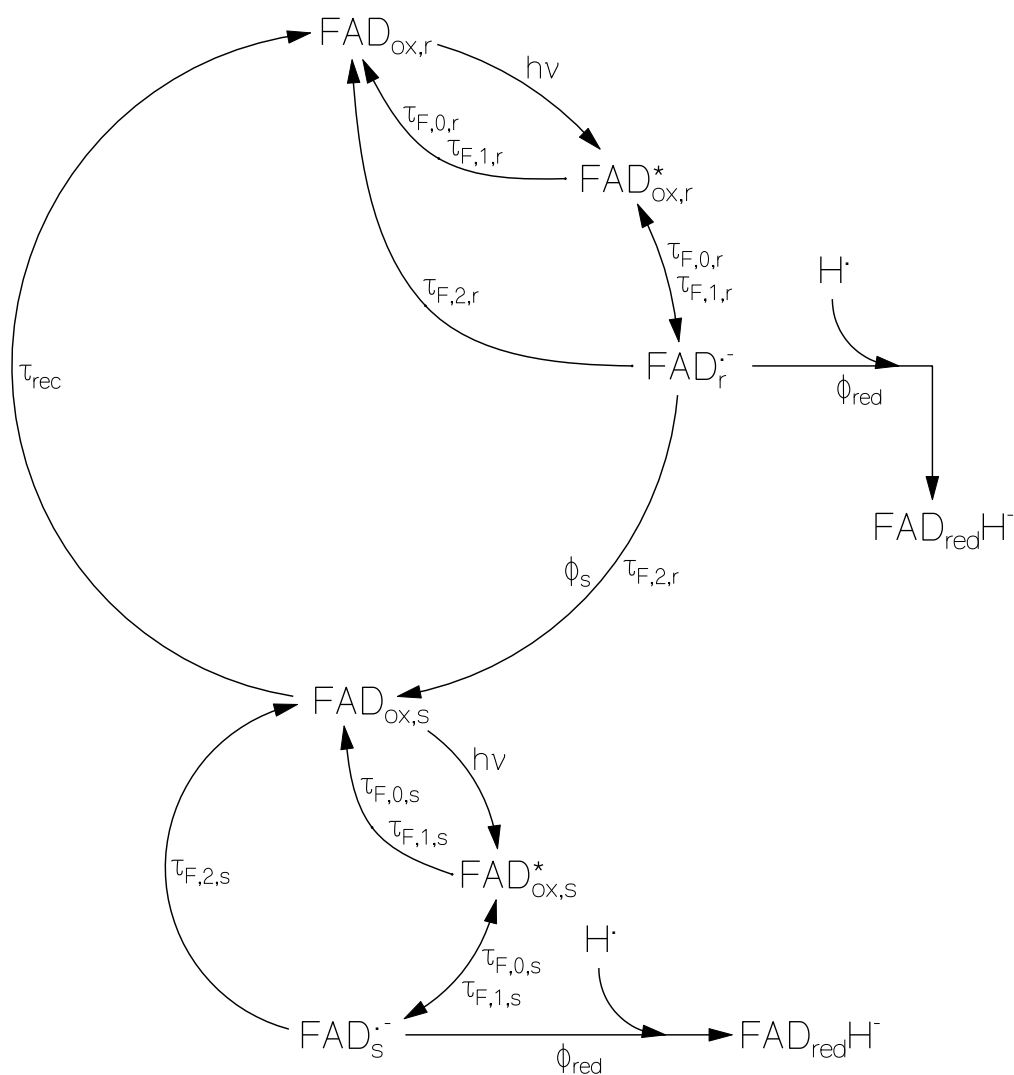

Figure 8.2 Illustrative photo-cycle scheme for dark-state photo-excitation and light-state photo-excitation of BlrP1_BLUF and BlrP1. Possibly present intermediates between FAD_r^- and $FAD_{ox,r}$, FAD_r^- and $FAD_{ox,s}$ (FADH intermediate), FAD_s^- and $FAD_{ox,s}$, $FAD_{ox,s}$ and $FAD_{ox,r}$ are not included.

The basic scheme presented in Fig.8.2 is in agreement with the photo-cycle studies on AppA [Zir05] , AppA-H44R [Zir07b], BlrB [Zir06] and Slr1694 [Zir07a]. The time-resolved pump-probe absorption measurements on AppA [Gau05] are compatible with the receptor-state signalling-state photo-cycle scheme of Fig. 8.2. The presence of FAD^* in different protein conformations was found in these studies but no intermediate between FAD^* and FAD_s was observed [Gau05]. The dark-state photocycle of AppA given in [Gau05] has been re-interpreted in terms of new measurements on the light-state photo-cycle of AppA [Toh08]. The reported findings agree with the scheme of Fig. 8.2 (in the path from FAD^- to FAD_s, $FADH^\bullet$ is involved). The photo-cycle of Slr1694 has been studied by time-resolved pump-probe absorption measurements in [Gau06]. The resolved photo-cycle agrees with the scheme of Fig. 8.2. $FADH^\bullet$ was resolved as an intermediate between FAD^- and FAD_s. Temperature dependent photo-cycle studies on Tll0078 revealed a 5 nm red shifted signalling state at 10 K and a 10 nm red-shifted signalling state for temperatures above 50 K [Oka06, Fuk05, Fuk07] indicating protein conformational restrictions at low temperature on the hydrogen-bond changing dynamics.

9   Conclusions

The photodynamics of the BLUF domain BlrP1_BLUF and of the full-length protein BlrP1 from the enteric bacterium *K. pneumoniae* has been studied by absorption and fluorescence spectroscopy under dark-adapted, light-adapted, and prolonged light exposure conditions. These studies have been embedded in a general photodynamic description of BLUF proteins.

The full protein BlrP1 and BLUF domain BlrP1_BLUF show similar behaviour upon excitation by light. A signalling state is formed by blue light absorption which is red shifted by about 10 nm with respect to the dark state. This spectral red shift is caused by light induced conformational changes in the protein binding pocket causing a modification of the hydrogen bonding upon light absorption. The signalling state is formed with an efficiency of $\approx 16\%$ in BlrP1_BLUF and of $\approx 8\%$ in BlrP1.

The recovery of the signalling state back to the receptor state (dark state) in the absence of light is temperature dependent. For the BlrP1-BLUF the recovery time reduces from about 230 s at 5 °C to about 19 s at 27.8 °C. Similarly for the full protein, BlrP1, the recovery time reduces from about 300 s at 5 °C to about 33 s at 27.5 °C. At $\vartheta = 20.5$ ºC, the recovery times are τ_{rec}(BlrP1_BLUF) = 51.2 s and τ_{rec}(BlrP1) = 89.3 s. The recovery time is thought to be determined by a barrier height, W_b, between the signalling state and the receptor state.

The fluorescence lifetime measurements have yielded three fluorescence decays. The two fast fluorescence decays have been attributed to photo-induced charge-separated state formations (reductive electron transfer from an adjacent electron donating amino acid to the electron accepting photo-excited FAD). The most likely amino acid for the electron transfer to the FAD is the highly conserved tyrosine (Tyr63 in APPA [And05], Tyr8 in Slr1694 [Yua06], Tyr9 in BlrB [Jun05]). In BlrP1_BLUF there are 3 Tyr, but which one is adjacent to FAD is

not yet known since the crystal structure of BlrP1_BLUF is not yet available. The slower fluorescence decay has been attributed to relaxation to the initial ground-state by charge recombination (electron transfer back from FAD semiquinone radical anion $FAD^{\bullet-}$ to amino acid radical cation likely Tyr^+).

The photoexcitation of BlrP1_BLUF and BlrP1 in the light-adapted signalling state caused reductive electron transfer from $FAD^*_{ox,s}$ to anionic FAD semiquinone $FAD^{\bullet-}_s$. Some reduction of $FAD^{\bullet-}_s$ to $FAD_{red}H^-$ with low quantum efficiency was observed. On a minute time scale, a partial re-oxidation of $FAD_{red}H^-$ to FAD_{ox} occurs by hydrogen radical and electron release for BlrP1_BLUF, while no re-oxidation occurs in the case of the full-length protein.

In BlrP1-BLUF the hydrogen-bond re-arrangement in the photo-excited receptor-state towards the signalling state formation occurs without the involvement of a tryptophan since no tryptophan is present in the domain. Nevertheless the photo-cycle dynamics is rather similar to other BLUF domains containing one (BlrB, Slr1694, Tll0078) or two (AppA) Trp residues.
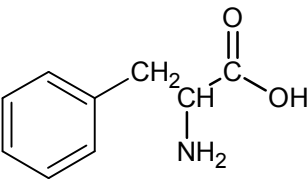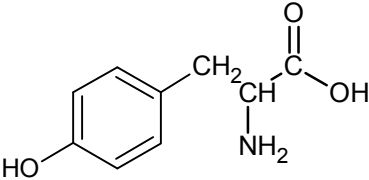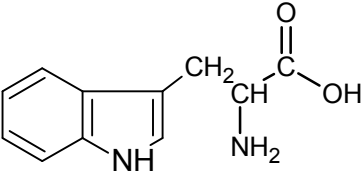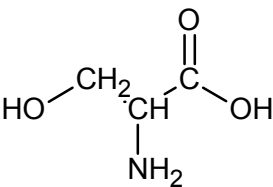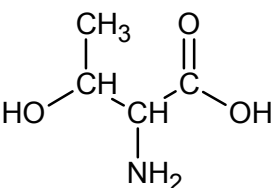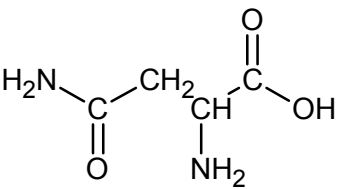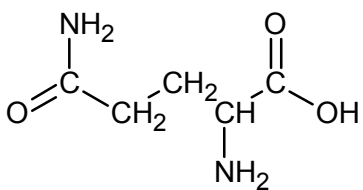
Since the crystal structures of BlrP1 and BlrP1_BLUF are not yet known, it is not possible to identify the amino acids involved in the photodynamics and the hydrogen bond rearrangement and hence it is not possible to give a more detailed description of the protein photodynamics of BlrP1 and BlrP1_BLUF from *K. pneumoniae.*

The research on flavin based blue-light photoreceptors is expected to remain active in the coming years. There is expected a progress in an understanding of the atomistic mechanistic processes by X-ray and NMR crystal structure studies, infrared spectroscopy, EPR spectroscopy, time resolved fluorescence and absorption pump-probe spectroscopy. Also, further quantum-chemical simulations will contribute to an understanding of the photoreceptor action. Then it has to follow an understanding of the signal transduction from the receptor via mediators to the organism response.

A.1 Appendix

The table lists the three-letter code, the one-letter code, the molar masses and some properties of the 20 standard amino acids. The masses listed are based on weighted averages of the elemental isotopes at their natural abundances. During the formation of a peptide bond there is elimination of a molecule of water, so the mass of an amino acid unit within a protein chain is reduced by 18.01524 Da (1 Da = 1 Dalton = 1 g mol^{-1}).

Amino Acid	3 Letter Code	1 Letter Code	Structure	Molar Mass (Da)	Properties
Aliphatic Amino Acids					
Glycine	Gly	G		75.07	Smallest amino acid, no charge, not hydrophilic
Alanine	Ala	A		89.09	No charge, hydrophobic
Valine	Val	V		117.15	No charge, hydrophobic
Leucine	Leu	L		131.17	No charge, hydrophobic, isomer of isoleucine
Isoleucine	Ile	I		131.17	No charge, hydrophobic, isomer of leucine.
Proline	Pro	P		115.13	No charge, promotes turns, not hydrophobic

Aromatic Amino Acids				
Phenylalanine	Phe	F		165.19	No charge, absorbs UV, hydrophobic
Tyrosine	Tyr	Y		181.19	Weak charge, absorbs UV, hydrogen bonding, not hydrophilic.
Tryptophan	Trp	W		204.23	Largest amino acid, no charge, absorbs UV, hydrogen bonding, hydrophobic
Polar, Uncharged Amino Acids				
Serine	Ser	S		105.09	No charge, hydrogen bonding, hydrophilic
Threonine	Thr	T		119.12	No charge, hydrogen bonding, hydrophilic.
Asparagine	Asn	N		132.12	No charge, Amide of Asp, hydrogen bonding, hydrophilic
Glutamine	Gln	Q		146.14	No charge, amide of Glu, hydrogen bonding, hydrophilic.

Sulphur Containing Amino Acids					
Cysteine	Cys	C		121.16	Sulphur analog of Ser, weak charge, forms disulphide bonds, not hydrophilic.
Methionine	Met	M		149.21	Initiator of proteins, no charge, hydrophobic.
Charged Amino Acids					
Aspartic Acid	Asp	D		133.1	Acidic, Negative charge, hydrophilic.
Glutamic Acid	Glu	E		147.13	Acidic, negative charge, hydrophilic.
Histidine	His	H		155.15	Basic, weak positive charge, reactive, Imidizole in side chain,
Lysine	Lys	K		146.19	Basic, strong positive charge, reactive, hydrophilic, amine in side chain.
Arginine	Arg	R		174.2	Basic, strongest positive charge, hydrophilic, guandinium side chain.

References

[1]   http://www.ncbi.nlm.nih.gov/entrez/viewer.fcgi?db=protein&id=150954999

[2]   http://www.expasy.ch/cgi-bin/protparam

[3]   http://omlc.ogi.edu/spectra/PhotochemCAD/html/index.html

[Ahm95]   Ahmad, M. Lin. C.; Cashmore, A.R.; *Plant J.,* 8 (1995) 653.

[And05]   Anderson, S.; Dragnea, V.; Masuda, S.; Ybe, J.; Moffat K. and Bauer C.; *Biochemistry* 44 (2005) 7998.

[Aub00]   Aubert, C.; Vos, M. H.; Mathis, P.; Eker, A. P. M.; and Brettel, K. *Nature*, 405, (2000) 586.

[Bac94]   Baca, M.; Borgstahl, G.E, Boissinot, M.; Burke, P.M.; Williams, D.R.; Slater, K.A.; Getzoff, E.D.; *Biochemistry*, 33 (1994) 14369

[Bar09]   Barends, T.R.M.; Hartmann, E.; Griese, J.; Kirienko, N.V.; Ryjenkov, D.A.; Reinstein, J.; Shoeman, R.L.; Gomelsky, M.; Schlichting, I.; submitted for publication.

[Bar73]   Barrio, J. R.; Tolman, G. L.; Leonard, N. J.; Spencer, R. D. and Weber, G.; *Proc. Natl. Acad. Sci. USA,* 70, (1973), 941-943.

[Bat05]   Batschauer, A.; In *Handbook of Photosensory Receptors*, ed. WR Briggs, JL Spudich, pp. 211.Weinheim:Wiley-VCH, , 2005.

[Bej00]   Beja,, O.; Aravind, L; Koonin, E.V.; Suzuki, M.T.; Hadd, A.; Nguyen, L.P.; Jovanovich, S.B.; Gates, C.M.; Feldman, R.A.; Spudich, J. L. Spudich; E.N.;and DeLong, E. F.; *Science*, 289 (2000) 1902.

[Ber02]   Van den Berg, P. A. W.; Feenstra, K. A.; Mark, A. E.; Berendsen, H. J. C. and Visser, A. J. W. G.; *J. Phys. Chem. B,* 106 (2002) 8858.

[Ber07a]   Berndt, A.; Kottke, T.; Breitkreuz, H.; Dvorsky, R.; Hennig, S.; Alexander, M.; Wolf, E.; *J. Biol. Chem.* 282 (2007) 13011.

[Ber07b]   Berg, J.M.; Tymoczko, J.L.; Stryer, L.; *Biochemistry-ebook*, 6th Edn.; W. H. Freeman and Co., 2007.

[Ber89]   Beratan, D.N.; and Onuchic, *J.N.; Photosynthesis Res.;* 22 (1989) 173.

[Ber90]   Beratan, D.N.; Onuchic, J.N.; Betts, J.N.; Bowler, B. E.; Gray, H.B.; *J Am. Chem. Soc.;* 97 (1990) 7915.

[Ber91]   Beratan, D.N.; Betts, J.N.; Onuchic, *J.N.; Science* 252 (1991) 1285.

[Bir63]   Birks, J. B.; and Dyson, D. J.; The relations between the fluorescence and absorption properties of organic molecules, (1963), *Proc. Roy. Soc. London Ser A.* 275.

[Bor95]   Borgstahl, G. E. O.; Williams, D. R.; and Getzoff, E. D.; *Biochemistry,* 34 (1995) 6278.

[Bou07]   J.-P. Bouly, Schleicher, E.; Dionisio-Sese, M.; Vandenbussche, F.; Van Der Straeten, D.; Bakrim, N.; Meier, S.; Batschauer, A.; Galland, P.; Bittl, R.; Ahmad, M.; *J. Biol. Chem.,* 282 (2007) 9383.

[Bra02]   Braatsch, S.; Gomelsky, M., Kuphal S.; and Klug, G.; *Mol. Microbiol.,* 45 (2002) 827.

[Bre95]   van Brederode, M. E.; Gensch, T.; Hoff, W. D.; Hellingwerf, K. J.; and Braslavsky, S. E.*; Biophys. J.*; 68 (1995) 1101.

[Bri01]   Briggs W. R.; Beck C. F.; Cashmore A. R.; Christie J. M.; Hughes J.; Jarillo J.; Kagawa T.; Kanegae H.; Liscum E.; Nagatani A.; Okada, K. Salomon M.; Rüdiger W.; Sakai T.; Takano M.; Wada M. and Watson J. C.; *Plant Cell,*13 (2001) 993.

[Bri02]   Briggs W. R. and Christie J. M.; *Trends Plant Sci.*; 7 (2002) 204.

[Byr03]   Byrdin, M.; Eker, A. P. M.; Vos, M. H.; and Brettel, K.; *Proc. Natl. Acad.Sci. USA,* 100 (2003) 8676.

[Byr04]   Byrdin, M.; Sartor, V.; Eker, A. P.; Vos, M. H.; Aubert, C.; Brettel, K.; and Mathis, P. *Biochim. Biophys. Acta.*; 1655 (2004) 64.

[Car01]   Carell, T.; Burgdorf, L. T.; Kundu, L. M.; and Cichon, M. *Curr. Opin. Chem. Biol.;* 5 (2001) 491.

[Cas03]   Cashmore A.R.; *Cell,* 114 **(**2003) 537.

[Cas99]   Cashmore, A. R.; Jarillo, J. A.; Wu, Y. J.; and Liu, D.; *Science,* 284, (1999) 760.

[Cha95]   Chapman, S.K. , and Mount, A.R.; *Natural Product Reports*, (1995) 93.

[Che99]   Cheung, M. S.; Daizadeh, I.; Stuchebrukhov, A. A.; and Heelis, P. F., *Biophys. J.,* 76 (1999) 1241.

[Chr01]   Christie J. M. and Briggs W. R.; *J. Biol.Chem.,* 276 (2001) 11457.

[Chr05]   Christie JM, Briggs WR.; In *Handbook of Photosensory Receptors*, ed. WR Briggs, JL Spudich, pp. 277.Weinheim:Wiley-VCH, 2005.

[Chr07]   Christie, J.M.; *Annu. Rev. Plant Biol.*; 58 (2007) 21.

[Chr99]   Christie J. M.; Salomon M.; Nozue K.; Wada M. and Briggs W. R.; *Proc. Natl. Acad. Sci.USA*, 96 (1999) 8779.

[Cro02]   Crosson,, S. and Moffat, K.; *Plant Cell*, 14 (2002) 1067.

[Dai04]   Daiyasu, H.; Ishikawa, T.; Kuma, K. I.; Iwai, S.; Todo, T. and Toh, H.; *Genes Cells,* 9 (2004) 479.

[DeV80]   De Vault, D. *Q. Rev. Biophysics*, 13 (1980), 387.

[Dex53]   Dexter, D.L.; *J. Chem. Phys.;* 21, 836, (1953).

[Dmi91]   Dmitriev, V.G.; Gurzadyan, G.G.; Nikogosyan, N.N.; *Handbook of Nonlinear Optical Crystals*, Springer Verlag, Berlin, 1991.

[Dom08]   Domratcheva, T.; Grigorenko, B. L.; Schlichting, I.; Nemukhin, A. V.; *Biophys. J,.* 94 (2008) 3872.

[Dra05]   Dragnea, V.; Waegele, M.; Balascuta, S.; Bauer, C.; Dragnea, B.; *Biochemistry*; 44 (2005) 15978.

[Drö02]   Drössler, P, P.; Holzer, W.; Penzkofer, A. and Hegemann, P.; *Chem. Phys.,* 282 (2002) 429.

[Esp07]   Espagne, A.; Paik, D. H.; Changenet-Barret, P.; Plaza, p.; Martin, M. M.; Zewail, A. H.; *Photochem. and Photobiol. Sci.,* 6 (2007) 780.

[Fed03]   Fedorov, R.; Schlichting, I.; Hartmann, E.; Domratcheva, T.; Fuhrmann, M.; and Hegemann, P.; *Biophys. J.;* 84 (2003) 2474.

[Fle86]   Fleming, G. R. *Applications of Ultrafast Spectroscopy*, Oxford University Press, London, 1986.

[Fol01]   Folta, K. M. and Spalding E. P.; *Plant J.,* 26 (2001) 471.

[För59]   Förster, Th.; Discuss. *Faraday Soc*.; 27, 7 (1959)

[Fri88]   Friedrich, W.; *Vitamins*, (1988), Walter de Gruyter, Berlin.

[Fuk05a]   Fukushima, Y.; Okajima, K.; Ikeuchi, M.; and Itoh, S.; Photochem. Photobiol.; 83 (2007) 112.

[Fuk05b]   Fukushima, Y.; Okajima, K.; Shibata, Y.; Ikeuchi, M.; and Itoh, S.; *Biochemistry*, 44 (2005) 5149.

[Fuk07]   Fukushima, Y.; Okajima, K.; Ikeuchi, M.; Itoh, S.; *Photochem. Photobiol.,* 83 (2007) 112.

[Fuk08]   Fukushima, Y.; Murai, Y.; Okajima, K.; Ikeuchi, M.; Itoh, S.; *Biochemistry,* 47 (2008) 660.

[Gau05]   Gauden, M.; Yeremenko, S.; Laan, W.; van Stokkum, I. H. M.; Ihalainen, J. A.; van Grondelle, R.; Hellingwerf, K. J.; and Kennis J. T. M.; *Biochemistry,* 44, (2005) 3653.

[Gau06]   Gauden, M.; van Stokkum, I. H. M.; Key, J. M.; Lührs, D. C.; van Grondelle, R.; Hegemann, P.; Kennis, J. T. M.; *Proc. Natl. Acad. Sci.USA*, 103 (2006) 10895.

[Gau07]   Gauden, M.; Grinstead, J. S.**;** Laan, W. ; van Stokkum, I. H.M.; Avila-Perez, M.; Toh, K. C.; Boelens, R.; Kaptein, R.; van Grondelle, R.; Hellingwerf, K. J.; Kennis, J. T. M.; *Biochemistry,* 46 (2007) 7405.

[Gen97]   Genick, U. K.; http://www.scripps.edu/~ulrich/

[Ghe92]   Ghetti F; Checcucci G; Lenci F; *J Photochem Photobiol B,* 15 (1992) 185.

[Gil91]   Gilbert, A. and Baggott*,* J.; *Essential of Molecular Photochemistry*, 1st Edn.; Blackwell Scientific Publications, Oxford, 1991.

[Gom02]   Gomelsky, M. and Klug, G.; *Trends Biochem. Sci.;* 27, (2002) 497.

[Gom95]   Gomelsky, M. and Kaplan, S.; *J. Bacteriol.,* 177 (1995) 4609.

[Gom98]   Gomelsky, M. and Kaplan, S.; *J. Biol. Chem.,* 273 (1998) 35319.

[Gra96]   Gray, H. B.; Winkler, J. R.; *Annu. Rev. Biochem.*, 65 (1996) 537.

[Gri06a]   Grinstead, J. S.; Avila-Perez, M.; Hellingwerf, K. J.; Boelens, R.; Kaptein, R.; *J. Am. Chem. Soc.,* 128 (2006) 15066.

[Gri06b]   Grinstead, J. S.; Hsu, S. T. D.; Laan, W.; Bonvin, A. Hellingwerf, K. J.; Boelens, R.; Kaptein, R.; *ChemBioChem ,*7 (2006) 187.

[Gro02]   Groenhof, G.; Lensink, M.F.; Berendsen, H. J.; Snijders, J.G.; Mark. A.E.; *Proteins*, 48 (2002), 202.

[Hak04]   Haken, H. and Wolf, H.C.; *Molecular Physics and Elements of Quantum Chemistry. Introduction to Experiments and Theory*, 2nd Edn; Springer - Verlag, Berlin Heidelberg, 2004.

[Har03]   Harper A.M.; Neil L.C.; Gardner K.H.; *Science*, 301 (2003) 11541.

[Has04]   Hasegawa, K.; Masuda, S.; Ono, T.; *Biochemistry,* 43 (2004) 14979.

[Has05]   Hasegawa, K.; Masuda, S.; Ono, T.; *Plant Cell Physiol.,* 46 (2005) 136.

[Has06]   Hasegawa, K.; Masuda, S.; Ono, T.; *Biochem.,* 45 (2006) 3785.

[Hau99]   Haupt, W.; *Prog. Bot.* 60 (1999) 3

[Hen75]   Henderson, R. and Unwin; P.N.; *Nature,* 257 (1975) 28.

[Hit00]   Hitomi K, Okamoto K, Daiyasu H, Miyashita H, Iwai S, Toh H, Ishiura M, Todo T.; *Nucleic Acids Res*, 28 **(**2000) 2353.

[Hof94]   Hoff, W.D, Dux, P.; Hard, K, Devreese, B.; Nugteren-Roodzant, I.M.;
            Crielaard, W.; Boelens, R.; Kaptein, R.; van Beeumen, J.; Hellingwerf, K.J.;
            Biochemistry, 33 (1994) 13959.

[Hof99].   Hoff, W. D.; Xie, A.; Van Stokkum, I. H.; Tang, X. J.; Gural,J.; Kroon, A.
            R.;and Hellingwerf, K. J.; *Biochemistry*, 38 (1999) 1009.

[Hol02]   Holzer,W.; Penzkofer, A.; Fuhrmann, M. Hegemann, P.; *Photochem.
            Photobiol.*, 75 (2002) 479.

[Hol04]   Holzer, W.; Penzkofer, A.; Susdorf, T, Alvarez, M. Islam, S.D.M.; Hegemann,
            P.; *Chem Phys.;* 302 (2004) 105.

[Hol05]   Holzer, W.; Shirdel, J.; Zirak, P.; Penzkofer, A.; Hegemann, P.; Deutzmann, R.;
            Hochmuth, E.; *Chem. Phys.* 308 (2005) 69.

[Hol99]   Holzer, W.; Pichelmaier, M.; Penzkofer, A.; Bradley, D.D.C. and Blau, W.J.;
            Chem. Phys., 246 (1999) 445.

[Hor05]   van der Horst, M.A.; Hendriks, J.; Vreede, J.; Yeremenko, S.; Crielaard, W.;
            Hellingwerf, K.J. in: W.R. Briggs, J.L. Spudich (Eds.), *Handbook of
            Photosensory Receptors*, Wiley-VCH Verlag, Weinheim, Germany, 2005.

[Hua97]   Huala E.; Oeller P. W. Liscum E.; Han I.-S.;Larsen E. and Briggs W. R.;
            Science, 278 (1997) 2121.

[Iin01]   M. Iino, in: D.P. Ha¨der, M. Lebert (Eds.), *Photomovement,* Elsevier,
            Amsterdam, 2001, p. 659.

[Ima97]   Imamoto, Y.; Mihara, K.; Hisatomi, O.; Kataoka, M.; Tokunaga, F.; Bojkova,
            N.; and Yoshihara, K.; *J. Biol. Chem.*; 272 (1997) 12905.

[Ise02]   Iseki, M.; Matsunaga, S.; Murakami, A.; Ohno, K.; Shiga, K. Yoshida, K.;
            Sugai, M.; Takahashi, T.; Hori T.; and Watanabe, M.; *Nature,* 415 (2002)
            1047.

[Isl03a]   Islam, S. D. M.; Penzkofer, A. and Hegemann, P.; *Chem. Phys.* 291 (2003) 97.

[Isl03b]   Islam, S. D. M.; Susdorf, T.; Penzkofer, A. and Hegemann, P.; *Chem. Phys.*,
            295 (2003) 137.

[Jef 91]   Jeffery, G.A. and Saenger, W.; *Hydrogen Bonding in Biological Structures*;
            (Springer -Verlag, Berlin Heidelberg, 1991).

[Jen06]   Jenal, U; and Malone, J; Annu. Rev. Genet., 40 (2006) 385.

[Jun03]   Jung, K. H.; Trivedi, V.D.; Spudich, J. L.; *Mol. Microbiol.*, 47 (2003) 1513.

[Jun05]   Jung, A.; Domratcheva, T.; Tarutina, M.; Wu, Q.; Ko, W.; Shoeman, R.L.; Gomelsky, M.; Gardner, K.H.; Schlichting, I.; *Proc. Natl. Acad. Sci.USA*, 102 (2005) 12350.

[Jun06]   Jung, A.; Reinstein, J.; Domratcheva, T.; Shoeman, R. L.; Schlichting, I.; *J. Mol. Biol.,* 362 (2006) 717.

[Kag01].   Kagawa T.; Sakai T.; Suetsugu N.; Oikawa K.; Ishiguro S.; Kato T.; Tabata S.; Okada K. and Wada M.; *Science*, 291 (2001) 2138.

[Kag02]   Kagawa T. and Wada M.; *Plant Cell Physiol.*, 43 (2002) 367.

[Kag03]   Kagawa T.; *J. Plant Res.;* 116 (2003) 77.

[Kan97]   Kanai S, Kikuno R, Toh H, Ryo H, Todo T.; *J Mol Evol,* 45 (1997) 535.

[Kas02]   Kasahara M, Swartz TE, Olney MA, Onodera A, Mochizuki N,. *Plant Physiol.;* 129 (2002) 762.

[Kav93]   Kavarnos, G. J.; *Fundamentals of photoinduced electron transfer*, (1993), VCH Publishers Inc. New York.

[Ken03]   Kennis JTM, Crosson S, Gauden M, van Stokkum IHM, Moffat K, van Grondelle R.; *Biochemistry*, 42 (2003) 3385.

[Ken04]   Kennis JTM, van Stokkum NHM, Crosson S, Gauden M, Moffat K, van Grondelle R.; *J. Am. Chem. Soc.;* 126 (2004) 4512.

[Ken05]   Kennis J.T.M.; Alexandre, M.T.A.; In *Handbook of Photosensory Receptors*, ed. WR Briggs, JL Spudich, pp. 309.Weinheim:Wiley-VCH, 2005.

[Kit05]   Kita, A. Okajima, K. Morimoto, Y. Ikeuchi, M. Miki, K.; *J. Mol. Biol.*, 349 (2005) 1

[Kla07]   Klar, T.; Pokorny, R.; Moldt, J.; Batschauer, A. and Essen, L. O.; *J. Mol. Biol.*; 366 (2007) 954.

[Kor96]   Kort, R.; Vonk, H.; Xu, X.; Hoff, W. D.; Crielaard, W.; and Hellingwerf, K. J.; *FEBS Lett.;* 382 (1996) 73

[Kot03]   Kottke T, Heberle J, Hehn D, Dick B, Hegemann P.; *Biophys. J,* 84 (2003) 1192.

[Kra03]   Kraft, B. J.; Masuda, S.; Kikuchi, J.; Dragnea, V.; Tollin, G.; Zaleski, J. M.; Bauer, C. E.; *Biochemistry*; 42 (2003) 6726.

[Kre02]   Krebs, R. A.; Alexiev, U.; Partha, R.; Devita, A. M.; Braiman, M. S.; *BMC Physiology*, 2 (2002) 5

[Laa03]   Laan, W.; van der Horst, M. A.; van Stokkum, I. H.; Hellingwerf, K. J.; *Photochem. Photobiol.,* 78 (2003) 290.

[Laa06]   Laan, W.; Gauden, M.; Yeremenko, S.; Van Grondelle, R.; Kennis, J. T. M.; Hellingwerf, K. J.; *Biochemistry,.* 45 (2006) 51.

[Lak99]   Lakowicz J. R.; *Principles of Fluorescence Spectroscopy*, 2nd Edn; (KluwerAcademic/Plenum Publishers, New York, 1999).

[Lin03]   Lin, C. and Shalitin, D.; *Annu. Rev. Plant. Biol.,* 54 (2003) 469.

[Lin95]   Lin, C.; Robertson, D. E.; Ahmad, M.; Raibekas, A. A.; Jorns, M. S.; Dutton, P. L. and Cashmore, A. R.; *Science,* 269 (1995) 968.

[Lis02]   Liscum E. (2002), Phototropism: Mechanisms and Outcomes ,In C. R. Somerville and E. M. Meyerowitz, eds, *The Arabidopsis Book.* American Society of Plant Biologists, Rockville, MD, doi/10.1199/tab.0074/, http://www/aspb.org.org/ publications/arabidopsis/

[Los07]   Losi, A.; *Photochem. and Photobiol.;* 83 (2007) 1.

[Los08]   Losi, A.;Gärtner, W; *Proc. Natl. Acad. Sci.USA*, 105 (2008) 7.

[Mah75]   Mahr, H.; Hirsch, M.D.; *Opt. Commun.*; 13 (1975) 96.

[Mar56]   Markus, R.A.; *J. Chem Phys,* 24 (1956) 966.

[Mar85]   Markus, R.A.; and Sutin, N.; *Biochim. Biophys. Acta.;* 811 (1985), 265.

[Mas00]   Massay, V.; *Biochem. Soc. Trans*., 28 (2000) 283.

[Mas02]   Masuda, S. and Bauer, C. E.; *Cell*, 110 (2002) 613.

[Mas04a]   Masuda, S.; Hasegawa, K.; Ishii, A.; Ono, T.; *Biochemistry,* 43 (2004) 5304.

[Mas04b]   Masuda, S.; Ono, T.; *FEBS Lett.* 577 (2004) 255.

[Mas05a]   Masuda, S.; K. Hasegawa and T. A. Ono, *FEBS Lett.* 579 (2005) 4329.

[Mas05b]   Masuda, S.; Hasegawa, K.; Ono, T. A.; *Plant Cell Physiol.,* 46 (2005) 1894.

[Mas05c]   Masuda, S.; Hasegawa, K.; Ono, T.; *Biochem*istry, 44 (2005) 1215.

[Mas05d]   Masuda, S.; Ono, T.; in: *Photosynthesis: Fundamental Aspects to Global Perspectives*, Vol. 2, edited by A. van der Est and D. Bruce, Allen Press, Lawrence, KS, (2005) pp. 700.

[Mas07]   Masuda, S.; Tomida, Y.; Ohta, H.; Takamiya, K. I.; *J. Mol. Biol.,* 368 (2007) 1223.

[Mas95]   Massey, V. *Faseb J*.; 9 (1995) 473.

[Mat00]   Mataga, N.; Chosrowjan, H.; Shibata, Y.; Tanaka, F.; Nishina, Y.; Shiga, K.; *J. Phys. Chem. B* 104 (2000) 10667.

[Mat07]   Mathes, T.; Disseration, Humboldt University, Berlin, 2007.

[Mey85]   Meyer, T.E.*; Biochim. Biophys. Acta*, 806 (1985) 175.

[Mil68]   Miles, D. W. and Urry, D. W.; *Biochemistry,* 7 (1968) 2791.

[Mos88]   Moser, C. C.; Keske, J. M.; Warcke, K.; Farid, R. S.; Dutton, P. L.; *Nature,* 355 (1988) 796.

[Mül70]   Müller, F.; Hemmerich, P. Ehrenberg, A.; Palmer, G.; and Massey, V.; *Eur. J. Biochem.;* 14 (1970) 185.

[Mül72]   Müller, F.; Brüstlein, M.; Hemmerich, P.; Massey, V. and Walker, W.H.; *Eur. J. Biochem.;* 25 (1972) 573.

[Mül87]   Müller, F.; *Free Radical Biology and Medicine*, 3 (1987) 215.

[Mül91]   Müller, F.; *Chemistry and Biochemistry of Flavoenzymes*, (1991), (CRC Press, Inc), USA

[Nag03]   Nagel, G.; Szellas, T.; Huhn, W.; Kateriya, S.; Adeishvili, N.; Berthold, P.; Ollig, D.; Hegemann, P.; Bamberg, E.;, *Proc. Natl. Acad. Sci. U.S.A.,* 100 (2003) 13940.

[Nam91]   Nambu, J.R.; Lewis, J.R.; Wharton, K. A.; Crews, S.T.; *Cell*, 67 (1991) 1157.

[Nel04]   Nelson, D.L.; Cox, M.M.; *Lehninger Principles of Biochemistry ebook*, 4th Edn. W. H. Freeman and Co., 2004.

[Nte03]   Ntefidou, M.; Iseki, M, Watanabe, M.; Lebert, M.; Hader, D.P.; *Plant Physiol.;* 133 (2003) 1517.

[Oba08]   Obanayama, K.; Kobayashi, H.; Fukushima, K.; Sakurai, M.; *Photochem. Photobiol.,* 84 (2008) 1003.

[Ohi01]   Ohishi, S.; Shimizu, N.; Mihara, K.; Imamoto, Y.; and Kataoka, M.; *Biochemistry,* 40 (2001) 2854..

[Oka05]   Okajima, K.; Yoshihara, S.; Fukushima, Y. Geng, X.; Katayama, M.; Higashi, S.; Watanabe, M.; Sato, S. Tabata, S.; Shibata, Y.; Itoh, S.; Ikeuchi, M.; *Biochemistry,* 137(2005) 741.

[Oka06]   Okajima, K.; Fukushima, Y.; Suzuki, H.; Kita, A.; Ochiai, Y.; Katayama, M.; Shibata, Y.; Miki, K.; Noguchi, T.; Itoh, S.; Ikeuchi, M.; *J. Mol. Biol.* 363 (2006) 10.

[Orr03]   Orrit, M.; *Science,* 302 (2003) 239.

[Özt08]   Öztürk, N.; Song, S.H.; Sleby, C.P.; Sancar, A.; *J. Biol. Chem.;* 283 (2008) 3256.

[Par05]   Partch, C. L.; Sancar, A.; *Photochemistry and Photobiology*, 81 (2005) 1291.

[Pel98]   Pellequer, J.L.; Wager-Smith, K.A.; Kay, S.A.; Getzoff, E.D.; *Proc. Natl. Acad. Sci. USA,* 95 (1998) 5884.

[Pen07]	Penzkofer, A.; Shirdel, J.; Zirak, P.; Breitkreuz, H.; Wolf, E.; *Chem. Phys.* 342 (2007) 55.
[Pen87]	Penzkofer, A. and Leupacher, W.; *J. Luminescence,* 37, (1987), 61.
[Pen88]	Penzkofer, A.; *Appl. Phys. B*, 46 (1988) 43.
[Pok05]	Pokorny, R.; Klar, T.; Essen, L. O.; and Batschauer, A.; *Acta Cryst. F,* 61 (2005) 935.
[Rag04]	Ragni, M.; D'Alcala, M. R. ; *J Plankton Res.,* 26 (2004)433.
[Raj04]	Rajagopal, S.; Kay, J.M.; Purcell, E.B.; Boerema, D.J.; Moffat, K.; *Photochem. Photobiol.,* 80 (2004) 542.
[Rid07]	Ridge, K. D.; Palczewski, K. ; *J. Biol. Chem.,* 282 (2007) 9297.
[Rub98]	Rubinstenn, G.; Vuister, G. W.; Mulder, F. A.; Düx, P. E.;Boelens, R.;Hellingwerf, K. J.; and Kaptein, R.; *Nat.Struct. Biol.;* 5 (1998) 568.
[Sad08]	Sadeghian, K.; Bocola, M.; Schütz, M.; *J. Am. Chem. Soc.,* 130 (2008)12501.
[Sak01]	Sakai, T.; Kagawa, T.; Kasahara, M.; Swartz, T.E.; Christie, J.M.; Briggs, W.R.; Wada, M. and Okada, K.; *Proc. Natl Acad. Sci.USA*, 98 (2001) 6969.
[Sak02]	Sakamoto K. and Briggs W. R.; *Plant Cell*, 14 (2002) 1723.
[Sal00]	Salomon M, Christie JM, Knieb E, Lempert U, Briggs WR.; *Biochemistry,* 39 (2000) 9401
[Sal01]	Salomon,, M.; Eisenreich, W.; Durr, H.; Schleicher, E.; Knieb.; E; Massey, V.; Rudiger, W; Muller, F; Bacher, A.; and Richter, G.; *Proc. Natl. Acad. Sci. U.S.A*. 98 (2001) 12357.
[San00]	Sancar, A; *Annu. Rev. Biochem.,* 69 (2000) 31.
[San03]	Sancar, A.; *Chem Rev.;* 103 (2003) 2203.
[San94]	Sancar, A.; *Biochem.;* 33 (1994) 2.
[Sch05]	Schmidt, A. J.; Ryjenkov, D. A.; Gomelsky, M.; *J. Bacterol.,* 187 (2005) 4774.
[Sch89]	Schmidt, J.; Penzkofer, A.; *J. Chem. Phys.* 91 (1989) 1403.
[Sel06]	Selby, C. P.; and Sancar, A. *Proc. Natl. Acad. Sci. U. S. A.;* 103 (2006) 17696.
[Sha88]	Shah, J.; *IEEE J. of Quant. Electronics*, 24, 2 (1988) 276.
[Shi07]	Shirdel, J.; Penzkofer, A.; Shen, Z.; Procházka, R.; Daub, J.; *Chem. Phys.,* 337 (2007) 99.
[Shi08]	Shirdel, J. Zirak, P.; Penzkofer, A.; Breitkreuz, H. Wolf, E.; *Chemical Physics*, 352, (2008) 35
[Sin02]	Sineshchekov, O. A.; Jung, K. H.; and Spudich, J. L.; *Proc. Natl. Acad. Sci. U.S.A.;* 99 (2002) 8689.

[Son06]   Song, S. H.; Dick, B.; Penzkofer, A.; Pokorny, R.; Batschauer, A.; and Essen, L. O.; *J. Photochem. Photobiol.; B: Biol.;* 85 (2006) 1.

[Son07]   Song, S.-H.; Dick, B.; Penzkofer, A.; *Chem. Phys.,* 332 (2007) 55.

[Spe96]   Speiser, S.; *Chem. Rev.*, 96 (1996) 1953.

[Spu00]   Spudich, J.L.; Yan, C.; Jung, K.H. and Spudich, E.N.; *Annu. Rev. Cell. Div. Biol.* 16, (2000) 365.

[Ste07]   Stelling, A. L.; Ronayne, K. L.; Nappa, J.; Tonge, P. J.; Meech, S. R.; *J. Am. Chem. Soc.;* 129 (2007) 15556.

[Str62]   Strickler, S.J. and Berg, R. A.; *J. Chem. Phys.* 37, (1962), 814.

[Swa01]   Swartz T.E.; Corchnoy S.B.; Christie J.M.; Lewis J.W.; Szundi I.; *J. Biol. Chem.;* 276 (2001) 36493

[Tak07]   Takahashi, R.; Okajima, K.; Suzuki, H.; Nakamura, H.; Ikeuchi, M.; Noguchi, T.; *Biochemistry,* 46 (2007) 6459.

[Tay99]   Taylor B.L.; Zhulin I.B.; Microbiol.; *Mol. Biol. Rev.*; 63 (1999) 479.

[Toh08]   Toh, K. C.; van Stokkum, I. H. M.; Hendriks, J.; Alexandre, M. T. A.; Arents, J. C. ; Perez, M. A.; van Grondelle, R.; Hellingwerf, K. J.; Kennis, J. T. M.; *Biophys. J.,* 95 (2008) 312.

[Tya08]   Tyagi, A.; Penzkofer, A.; Griese, J.; Schlichting, I.; Kirienko, N. V.; Gomelsky, M.; *Chem. Phys.,* 354 (2008) 130.

[Unn05]   Unno, M.; Sano, R.; Masuda, S.: Ono, T.; Yamaguchi, S.; *J. Phys. Chem. B,* 109 (2005) 12620.

[Unn06]   Unno, M.; Masuda, S.; Ono, T.; Yamauchi, S.; *J. Am. Chem. Soc.* 128 (2006) 5638.

[Val02]   Valeur, B.; *Molecular Fluorescence. Principles and Applications*, Wiley-VCH, Weinheim, 2002.

[Vis84]   Visser, A.J.W.G.; *Photochem. Photobiol.,* 40 (1984) 703.

[Wad03]   Wada M.; Kagawa T. and Sato Y.; *Annu.Rev. Plant Biol.*; 54 (2003) 455.

[Wan02]   Wang, H. and Deng, X. W.; (2002), Phytochrome Signaling Mechanism In C. R. Somerville and E. M. Meyerowitz, eds, *The Arabidopsis Book*. American Society of Plant Biologists, Rockville, MD, doi/10.1199/tab.0074/, http://www/aspb.org.org/ publications/arabidopsis/

[Web50]   Weber, G.; *Biochem. J.*, 47 (1950) 114.

[Whi53]   Whitby, L. G.; *Biochem. J.,* 54 (1953) 437.

[Wor03]   Worthington, E. N.; Kavakli, I. H.; Berrocal-Tito, G.; Bondo, B. E. and Sancar, A.; *J. Biol. Chem.;* 278 (2003) 39143.

[Xia00]   Xiao, W.; Brown, L.S.; Needlman; R.; Lanyi, J.K.; and Shin, Y.K.; *J. Mol. Biol.* 304 (2000) 715.

[Xie96]   Xie, A.; Hoff.; W. D.; Kroon, A. R.; and Hellingwerf, K. J.; *Biochemistry*, 35 (1996), 14671.

[Yan91]   Yan, B.; Takahashi, T.; Johnson, R.; and Spudich, J.L.; *Biochemistry,* 30 (1991) 10686.

[Yeh98]   Yeh.; K.C. and Lgarias, J.C.; *Proc. Natl. Acad. Sci. U.S.A.;* 95 (1998) 13976.

[Yod01]   Yoda, M.; Houjou, H.; Inoue, Y.; Sakurai, M.; *J. Phys. Chem. B,* 105 (2001), 9887.

[Yua06]   Yuan, H.; Anderson, S.; Masuda, S.; Dragnea, V.; Moffat, K.; Bauer, C.; *Biochemistry;* 45 (2006) 12687.

[Zir05]   Zirak, P.; Penzkofer, A.; Schiereis, T.; Hegemann, P.; Jung, A.; Schlichting, I.; *Chem. Phys.;* 315 (2005) 142.

[Zir06]   Zirak, P.; Penzkofer, A.; Schiereis, T.; Hegemann, P.; Jung, A.; Schlichting, I.; *J. Photochem. Photobiol. B: Biol.,* 180 (2006) 180.

[Zir07a]   Zirak, P.; Penzkofer, A.; Lehmpfuhl, C.; Mathes T.; and Hegemann, P.; *J. Photochem. Photobiol. B: Biol.,* 86 (2007) 22.

[Zir07b]   Zirak, P.; Penzkofer, A.; Hegemann, P.; Mathes, T.; *Chem. Phys.,* 335 (2007) 15.

[Zon01]   Zong, D.; Zeweil, A. H.; *Proc. Natl. Acad. Sci.USA*, 98 (2001) 11867.

Acknowledgement

This thesis owes its existence to the help, support, and inspiration of many people. It is a pleasure to convey my gratitude to them all in my humble acknowledgment.

In the first place I would like to express my gratitude to Prof. Dr. Alfons Penzkofer for giving me an opportunity to work in his lab under his guidance. His patience, motivation, immense knowledge and kind hearted advice from the early stages of this research have helped me to finish this work. I am indebted to him more than he knows.

Special thanks to Prof. Ilme Schlichting and Prof Mark Gomelsky for providing the biological samples and their helpful advices.

I gratefully acknowledge my colleagues in the lab: Thomas Susdorf for helping me during the early stages of research in lab and working with the laser, Sang Hun Song for being a very good friend, Javid Shirdel for help in working over Tracor system, Peyman Zirak for his help in handling the proteins and many useful discussions, Ashu Bansal for his help since my early days in Regensburg, Anton Sparrer, Martin Putschögl and Evgenia Slysureva for their friendship and providing a very nice environment for working. I would also thank David del Agua from Spain who brought with him some samples and lots of enthusiasm which made working in lab with him a wonderful experience.

Thanks are also due to all the members of work groups of Prof. F. Gießibl and Prof. J. Repp who have been extremely helpful and cooperative during the entire period.

Many thanks to the secretaries of our lehrstuhl, Mrs König and Mrs. Schäffer for their indispensable help in many things despite having a lot to do all the time. I am also thankful to Anja Merkel and her colleagues in mechanical workshop for always providing technical help. Mr. Riedl and his colleagues in electronics workshop are also gratefully acknowledged for their help.

I would also like to thank many friends: Carolina Cano, Keyarash Sadeghian, Siri and Hari Nanduri, Sofia and Deepak Chhabra, Lakshmi and Deepu, Manoj Bansal, Sanjeev Singh, Prashant Chauhan and Kanak Pal for some great time and providing lots of advices and help whenever needed.

I also acknowledge the funding from DFG in Graduate College "Sensory Photoreceptors in natural and artificial systems" of which I was a part first as a collegiate and then as a stipendiate. All the ring lectures and guest lectures which were very informative are also gratefully acknowledged.

I am thankful to my sister and brother-in-law who have taken care of lots of things in India in my absence. I would also like to thank my in-laws for the immense help they have provided all the time.

I am indebted to my wife, Bhawana, whose dedication, love and persistent confidence in me encouraged me to give my best. I owe her for her unselfish support and letting her own ambitions wait for the sake of mine. Thank you, Bhawana, for everything. I also thank our adorable son, Abhay, who always made me feel relaxed after the day's work by his many stories and news from the krabbelstube and of late from kindergarten.

I would like to dedicate this work to my parents, none of whom could live long enough to see this day.

Finally, I thank everybody who was important for the successful realization of thesis, as well as expressing my apology that I could not mention personally one by one.